SYNTHESIS, CHARACTERIZATION AND EVALUATION OF HIERARCHICAL DEALUMINATED FAU-TYPE Y ZEOLITES IN CATALYTIC AND HEAVY METAL IONS ADSORPTION STUDIES

BY

KAZEEM OLUDARE SULAIMAN

A Thesis Presented to the

DEANSHIP OF GRADUATE STUDIES

KING FAHD UNIVERSITY OF PETROLEUM & MINERALS

DHAHRAN, SAUDI ARABIA

In Partial Fulfillment of the
Requirements for the Degree of

MASTER OF SCIENCE

In

CHEMISTRY

MAY 2015

KING FAHD UNIVERSITY OF PETROLEUM & MINERALS

DHAHRAN- 31261, SAUDI ARABIA

DEANSHIP OF GRADUATE STUDIES

This thesis, written by **KAZEEM OLUDARE SULAIMAN** under the direction his thesis advisor and approved by his thesis committee, has been presented and accepted by the Dean of Graduate Studies, in partial fulfillment of the requirements for the degree of **MASTER OF SCIENCE IN CHEMISTRY.**

Dr. Khalid R. Alhooshani
(Advisor)

Dr. Abdulaziz Alsaadi
Department Chairman

Dr. Nabil O. Al-Yassir
(Member)

Dr. Salam A. Zummo
Dean of Graduate Studies

Dr. Abdalla M. Abulkibash
(Member)

17/5/15

Date

Dedication

The success of this research effort is dedicated to my family members (The Sulaimans) for their unflinching supports in all ramifications, throughout my stay out of Nigeria and my better half whose prayer and encouragement I found instrumental to this resounding success.

ACKNOWLEDGMENTS

In the name of Allah, the most gracious, the most compassionate and merciful. All praise is due to the Almighty Allah (SWT) for giving me sound health, disposition and patience to successfully saddle this challenging stage of my academic pursuit. Alhamdulilah!

I sincerely appreciate the scholarship award received from KFUPM through the Ministry of Higher Education, Kingdom of Saudi Arabia to pursue this master degree. Also, I am beholden to the King Abdulaziz City for Science and Technology (KACST) through Science and Technology Unit at KFUPM for accepting and funding my research assistantship in the Project No: 12-PET2395-04 as part of National Science, Technology, and Innovation Plan (NSTIP).

Special thanks to my thesis committee in persons of Dr K. Alhooshani, Dr N. Al-Yassir, and Dr A. Abulkibash for their inspiring guidance and excellence cooperation in giving professional touch to this work. The timely advice, guidance, encouragement, and understanding I received from Dr K. Alhooshani poised me to go this far and thus deserve my deepest gratitude. I am as well very grateful to Dr N. Al-Yassir whose knowledge of material chemistry facilitated major landmarks achieved in this work.

While I acknowledge the support from staff and faculty members of the chemistry department, I am also indebted to Center of Research Excellence in Refining and Petrochemical (CRP), Research Institute, KFUPM for providing enabling environment to conduct large part of this research work.

My heartfelt gratitude goes to my parents, siblings, wife, in-laws, cousins, and friends, too numerous to mention, both at home and in diasporas, for all kinds of support I always receive from them. To my good people from great nation, Nigeria, I owe you a lot for making my stay at Saudi not completely different from home. Several activities by NCUPM make life at KFUPM more conducive for learning. Finally, I acknowledge the cheerful moments I experienced with people from other countries. You are all indispensable components of whatever I can refer to as my academic achievements, especially the international conference presentations and award received. Thanks to you all.

TABLE OF CONTENTS

LIST OF TABLES

LIST OF FIGURES

LIST OF ABBREVIATIONS

AA-µ-SPE	:	Agitation Assisted Micro Solid Phase Extraction
AT-SDUSY	:	Alkaline Treated (TB+Na) SDUSY zeolite (Si/Al = 40)
BET	:	Brunauer-Emmett-Teller
BJH	:	Barret-Joyner-Halenda
CEC	:	Cation Exchange Capacity
DSC-TGA	:	Differential Scanning Calorimetry - Thermogravimetry Analysis
FAU	:	Faujasite
FTIR	:	Fourier Transform Infra-red Spectroscopy
LDPE	:	Low Density Poly Ethylene
LTA	:	Linde Type A
NMR	:	Nuclear Magnetic Resonance
PDA	:	Pore Directing Agent
SDUSY	**:**	Super Dealuminated UltraStable Y zeolite
SEM	:	Scanning Electron Microscopy
TBAOH	:	Tetrabutyl ammonium hydroxide
TEAOH	:	Tetraethyl ammonium hydroxide
TEM	:	Transmission Electron Microscopy
TMAOH	:	Tetramethyl ammonium hydroxide
TPAOH	:	Tetrapropyl ammonium hydroxide
XRD	:	X-ray Diffractometer
ZSM-5	:	Zeolite Socony Mobil-5 (ZSM-5)

ABSTRACT (ENGLISH)

Full Name : [KAZEEM OLUDARE SULAIMAN]

Thesis Title : [SYNTHESIS, CHARACTERIZATION AND EVALUATION OF HIERARCHICAL DEALUMINATED FAU-TYPE Y ZEOLITES IN CATALYTIC AND HEAVY METAL IONS ADSORPTION STUDIES]

Major Field : [CHEMISTRY]

Date of Degree : [MAY, 2015]

Zeolites possess multidimensional network of micropores of molecular dimensions with solid acidity, ion-exchange capacity and unequaled shape selectivity. These unique properties are undermined by diffusion limitation and rapid deactivation, which thus necessitate the strategic tuning of the conventional zeolite structures to fully explore their potentials in high volume processes; separation and catalysis. To this end, introducing well accessible intracrystalline mesoporosity by experimentally simple, economical and effective method, alkaline treatment emerged as an alternative solution but with comparatively limited adoption for silica-rich Y-zeolites, known for many industrial applications. This study subjected dealuminated faujasite-type Y zeolite (Si/Al =15-40) to various alkaline treatments using mono-and binary mixture of inorganic and/or organic base(s). Hierarchically structured zeolites of different degree of mesoporosity, with preserved intrinsic properties, were obtained using quaternary ammonium cations either as desilicating and/or pore directing agents. The effective cationic diameters and steric hinderance of these cations played significant role in the kinetic dissolution of silicon from the zeolite structure. The novel binary organic mixture strategy bypassed the time

consuming ion-exchange step in the common alkaline treatment procedures and showed superior catalytic performance both in the pyrolysis of low-density polyethylene and Friedel Craft alkylation of toluene with benzyl alcohol. Furthermore, the alkaline treatment enhanced the cation exchange capacity of the studied zeolite type with better adsorption capacity in heavy metal ions removal using simple, fast and efficient AA-µ-SPE method. The adsorption was favorable and endothermic with data fitted to the pseudo second order kinetics and Freundlich isotherm pattern.

ABSTRACT (ARABIC)

ملخص الرسالة

الاسم الكامل: قاسم اولدار سليمان

عنوان الرسالة: تحضير، توصيف وتقييم الزيوليت الهرمى منزوع الالمونيوم FAU من النوع Y فى دراسات الحفز و إدمصاص المعادن الثقيلة

التخصص: كيمياء

تاريخ الدرجة العلمية: مايو,2015

تتضمن المواد الزيولايتية متعددة الأبعاد شبكة من المسامات صغيرة الحجم ذات ابعاد جزيئية بالإضافة إلى حموضية صلبة, سعة تبادل أيوني و أنتقائية متفاوتة بتغير شكل وأبعاد المواد المتفاعلة. هذه الخواص الفريدة تُقَوض بمحدودية الإنتشار وسرعة فقدان الفاعلية, مما يستوجب تعديل بنية المواد الزيولايتية الشائعة لإستكشاف إمكانياتها بدقة في العمليات ذات السعة العالية, عمليات الفصل والمحفزات. تحقيقا لهذه الغاية, لإستقدام بلورات داخلية يمكن الوصول إليها بفاعلية ذات مسامات كبيرة عن طريق تجارب معملية مبسطة, بطرق ذات كفاءة إقتصادية, ظهرت المعالجة القلوية كحل بديل ولكن بمحدودية في الزيولايت من نوع Y الغني بالسيليكون ذو الأستخدامات الصناعية المتعددة. في هذه الدراسة تم معالجة الزيولايت من نوع Fujasite Y ذو نسبة سيليكون إلى ألمنيوم = 15-40 بطرق معالجة قلوية مختلفة وباستخدام خليط أحادي أو ثنائي مكون من قواعد عضوية أو غير عضوية. تم الحصول على مواد زولايتية هرمية ذات مسامات كبيرة بدرجات متفاوتة مع حفظ الخواص الجوهرية باستخدام كاتيونات أمونيوم رباعية كعوامل لتوجيه المسامات أو لإنتزاع السيليكون. الأبعاد الفعالة للكاتيونات أثرت بطريقة ملاحظة على إنتزاع السيليكون من بنية الزيولايت. الخليط العضوي الثنائي تجاوز عملية التبادل الأيوني المستهلكة للوقت في طرق المعالجة القلوية التقليدية كما أنها اظهرت نتائج متفوقة في أدائها كمحفزات في التحلل الحراري للبولي أيثلين ذو الكثافة المنخفضة وكذلك في تفاعل فريدل كرافت للتولوين مع الكحول البنزيلي. أيضا, المعالجة القلوية حسنَّت سعة التبادل الكاتيوني للمواد الزيولايتية تحت الدراسة مع سعة إمتصاص أعلى في إزالة أيونات المعادن الثقيلة بطريقة مبسطة, ذات سرعة وكفاءة عاليتين.

CHAPTER 1

INTRODUCTION

1.1 Background Information

The continuous increase in population growth alongside with the energy demand and industrial development create a wide range of environmental and health concerns that thus call for the review of operational processes, industrial effluent disposal, as well as the provision of analytical solution to the menace. Undoubtedly, energy generation and industrial activities contribute significantly to the environmental water contamination. Several toxic metals get to the environment as industrial waste causing soil and water pollution. For instance, lead (Pb) gets into water bodies from acid mine drainage release and into the atmosphere through fuel combustion [1-4], and its accumulation in living organisms causes numerous disease and disorders [5]. As a result, certain acceptable limits were set for different contaminants, for example, 15 ppb and 50 ppb of Pb were set to be safe for drinking water by USEPA and WHO respectively [6,7].

With the existence of numerous approaches for removing the dissolved heavy metals in water, the research trend focuses on the development of alternative cheap and versatile materials as potential sorbents for selective removal of any of the heavy metals from water matrix. Meanwhile, the relatively high cost of producing and regenerating spent

carbon in developing countries allows the search for better ion-exchanger in water treatment [8,9].

The ion-exchange is a cost-effective method of removing heavy metal contaminants from water by exchanging them via a reversible reaction with ions (e.g. H^+ and Na^+) present in the exchange media (e.g. zeolites, a low-cost ion-exchanger) [10,11]. Zeolites are such microporous materials with proven record of water purification, alongside catalysis, owing to their ion-exchange properties [12]. About half of the total volume of zeolite framework comprises of cavities and channels that can hold cations such as Mg^{2+}, Ca^{2+}, K^+ and H_2O molecules with high degree of mobility and exchange with one another [13]. Meanwhile, the intra-crystalline diffusivity challenge of the conventional zeolites limits their efficiency in high volume processes; catalytic and adsorption inclusive [14].

To overcome this problem, the modification of the conventional zeolite to the hierarchical form becomes a necessity as the quality of pore structure, particle size, and total surface area are also used to evaluate the adsorbent in any of the solid phase extraction method. As a matter of fact, the introduction of modification of zeolite structure, by preserving their intrinsic properties such as crystallinity, high surface area, acidity, shape selectivity and ion-exchange capacity by reversible process, amongst other, in the present millennium has led to a paradigm shift in separation, adsorption processes and catalysis [15].

1.2 Statements of the problem

Heavy metals, with consequent health hazard, constitute serious environmental pollutants, especially in the oil producing area. And due to their low concentration in water, many materials are to be investigated for excellent sorption capacity and efficiency in the solid phase extraction of heavy metal ions (adsorption by ion-exchange) from water bodies to improve the portability of the water for man's use. Zeolites are found to be low cost ion-exchanger and their regeneration when used as adsorbent make them alternative to activated carbon, especially in the developing countries. However, zeolites in their conventional form are being under-utilized and their full potential can be attained by post-synthetic modification to improve the surface area, pore structures while preserving all the intrinsic properties.

Consequently, it becomes strategic to identify, design and develop hierarchical zeolite materials that can simultaneously serve the dual purpose of adequately removing the heavy metals ions to improve the water quality and catalyze chemical reactions in fine chemical production.

1.3 Objectives of the study

The general objective is to design and develop novel and efficient faujasite Y zeolite-based solid materials suitable for the catalysis of chemical reactions in the fine chemical production and for heavy metal ions extraction from water in the adsorption process of separation science. This would be achieved with the following specific objectives:

- ❖ To study the chemistry of the post synthesis and to identify the optimum alkaline treatment conditions (duration, temperature and concentration);
- ❖ To create substantial intracrystalline mesoporosity in dealuminated Y zeolites upon quaternary ammonium hydroxides treatment while largely preserving the microporosity, crystallinity and subsequently acidity;
- ❖ To investigate the novelty of using mixture of organic ammonium bases as pore-growth agents in the synthesis of the hierarchical dealuminated Y zeolites;
- ❖ To perform extensive characterization in evaluating the physico-chemical properties using state-of-the-art spectroscopic and imaging techniques;
- ❖ To evaluate the potential application of the new hierarchical dealuminated Y zeolites as sorbent materials for removal of heavy metal ions and as catalyst in simple chemical reaction.

1.4 Significance of the study

The need for hierarchical form of dealuminated Y zeolites is applicable to both separation science and catalysis as it proffers solution to overcome the diffusivity problems of using conventional zeolites either as an ion exchanger media for the removal of heavy metal ions in water treatment or catalytic active sites in fine chemical production.

1.5 Scheme of the research work

The research pursuit has four major schemes as highlighted below:

- Post-synthetic modification of dealuminated Y zeolite materials using a wide range of treatment conditions
- Extensive characterization to reveal the pysico-chemical properties of the modified zeolite materials as compared to the unmodified one.
- Evaluation of the obtained solid materials in catalytic processes: Friedel Craft Alkylation and LDPE Pyrolysis.
- Comparative studies of parent and modified zeolite in adsorption process; heavy metal ion removal using agitation assisted micro-solid phase extraction method.

1.6 Scheme of the research report writing

The thesis report writing has been structured into five chapters to ease the reading and understanding, with references, appendices and author's resume at the later end as follows:

Chapter 1 described the water pollution problem, the need for hierarchical zeolite in catalysis and adsorption process, highlighted the general and specific research objectives, followed by the statement of problem and significance of this study, as well as the scheme of the research work and report writing.

Chapter 2 gave an overview about the zeolite structures, properties, synthesis and various applications as found in the literatures.

Chapter 3 discussed comprehensively the design, synthesis, characterizations and catalytic evaluation of modified superdealuminated Faujasite Y-zeolite based on quaternary ammonium hydroxide alkaline treatment.

Chapter 4 discussed the application of zeolites in water treatment using agitation assisted micro-solid phase extraction hyphenated with inductively coupled plasma optical emission spectroscopy (AA-µ-SPE-ICP-OES) to investigate the potential ability of the alkaline treated dealuminated Faujasite Y-zeolites in the removal of heavy metals from water.

Chapter 5 gave conclusions drawn from this work and recommendations for further works.

CHAPTER 2

ZEOLITES AS SUPERB SOLID MATERIALS FOR CATALYTIC AND ADSORPTION STUDIES

2.1 Background Information

The word zeolite (Greek: boiling stone) coined by Alex Cronstedt, a Swedish mineralogist, in 1756, can be traced back to the early observation of release of water when the hydrated aluminium silicates compound was heated. These silicates, called zeolites, are characterized by complex three-dimensional, less dense structures with large, cage-like cavities that can accommodate small ions and molecules, which can also be removed without destroying the aluminosilicate framework [16-18]. The zeolite framework comprises of tetrahedral TO_4 building units (T=Si, Al, etc.) linking to each other by oxygen atoms distribution to form the 3-D crystalline spongy skeletons [19,20], and the overall negative charge of the framework is balanced by the cations housed in the cage-like cavity [18].

The T-O-T links (Fig. 2.1) result in a diversity of rings, which are dependable for zeolites' cages and channels of different window sizes [19]. The window sizes are in the range of 0.3-1.5 nm. For example, FER zeolite has 2-D channels, 10 oxygen ring channels with 0.54 nm×0.42 nm windows and 8 oxygen ring channels with 3.5 nm×4.8 nm openings, FAU type zeolite has 3-D 0.74 nm channels with 12 oxygen membered ring windows and supercages of 1-2 nm of diameter (Fig.2.2) [20].

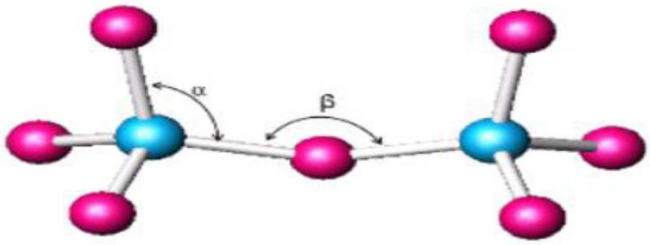

Figure 2.1 TO_4 tetrahedral where α is the O-T-O bond angle and β is the T-O-T bond angle (T= Si or Al) [18].

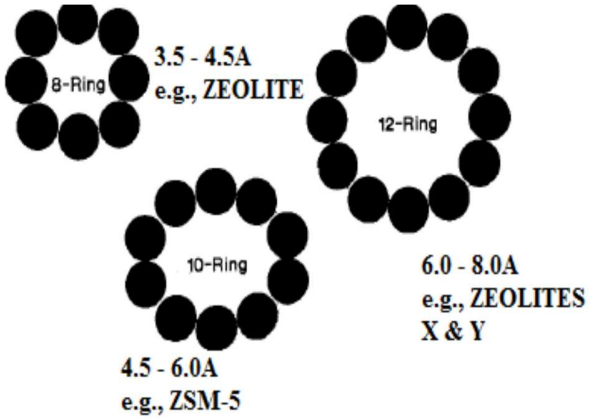

Figure 2.2 Schematic representations of typical zeolite windows; pore sizes oxygen packing.

The general structural formula that represents the mineral compositions of zeolites is given in equation 2.1 as:

$$(A^{z+})_{y/z}(B^{3+})_y(Si)_xO_{2(x+y)} \cdot nH_2O \qquad (2.1)$$

where A represents interchannel cations (such as Na^+, K^+, Ca^{2+}, Ba^{2+}, Sr^{2+}, Mg^{2+} and Fe^{2+}), B are tetrahedral coordinated trivalent cations in the zeolite framework (Al^{3+} and Fe^{3+}), z is the charge on the interchannel cations, n is the number of moles of interchannel molecular water, and x and y are the stoichiometric coefficients for trivalent cations and Si^{4+} in tetrahedral sites, respectively. The quantities 2(x+y) and y/z represent the stoichiometries of the interchannel cations and framework oxygens, respectively,

necessary for maintaining charge balance in the tectosilicate lattices of zeolites [22]. The water molecules within the structural channels can be exchanged like cations in the cavities without disrupting framework bonds [23].

2.2 Classification of zeolites

2.2.1 Based on framework topology

Huge numbers of zeolite frameworks are possible on theoretical ground, due to the connectivity of the SiO_4 or AlO_4 tetrahedra [24]. The variation of gel composition, temperature, and crystallization time gives rise to synthetic zeolites with different framework topology. The number of Si or Al atoms on the smallest possible cross-section, for example 8, 10, or 12 membered rings is used to express the pore sizes, which are used to classify the zeolites, together with the composition [24]. The classification of zeolites structures on the basis of their framework topologies, with distinct framework receiving a three-letter code (e.g. MFI, MOR, BEA, AST, FER, STF, LTA, FAU, etc), is popular among the three widely used broad classification schemes [25]. The other two are based on either secondary building units" (SBU) and/or context of how the zeolites were discovered [19,26].

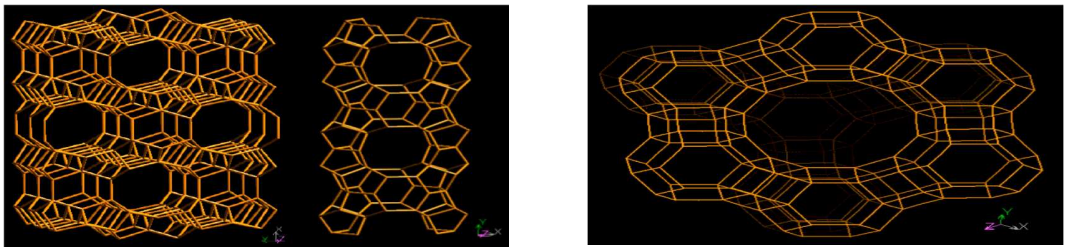

Figure 2.3 The zeolite framework (Left: FER type viewed along [001] and [010]; Right: FAU type zeolite supercage, viewed along [111]).

2.2.2 Based on the secondary building unit (SBU)

Zeolites can be categorized into seven groups based on their secondary building unit (SBU) [27,28] as summarized in the table below:

Table 2.1 Zeolite Structure classified by their Secondary Building Unit (SBU).

Group	Secondary Building Units	Examples
1	S4R	Analcime, Harmotome
2	S6R	Levynite, Sodalite Hydrate
3	D4R	Zeolite A, ZK-4
4	D6R	Faujasite, Zeolite X
5	4-1	Natrolite, Mesolite
6	5-1	Mordenite, Bikitaite
7	4-4-1	Heulandite, Clinoptlilolite

2.2.3 Based on production: Natural and Synthetic Zeolites

Natural zeolites are formed when ash layers and volcanic rocks chemically combine with alkaline ground water and the annual production of natural zeolite globally is approximately 3 million tonnes, with countries like China, South Korea, Japan, Jordan, Turkey, and USA taking leads in that order, in the year 2010 [29]. They are being tapped by open pit mining technique and are readily available at low cost but they are rarely pure and are contaminated to varying degrees by other minerals, quartz, metals, or even other zeolites. Natural zeolites have a lesser range of properties and smaller cavities than synthetic types. Consequently, natural zeolites are excluded from many important commercial applications where uniformity and purity are essential [30].

Firstly produced in the 1950s, the annual production of synthetic zeolites currently exceeds 12,000 tons globally. In fact, hundreds of different synthetic zeolites have been reported and a particular type produced depends on starting material composition and the reaction conditions that are not limited to acidity, temperature, and water pressure. For example, the notable method involves mixing sodium, aluminum, and silica chemicals with steam to form an amorphous, non-crystalline, water-rich solid, called gel. The gel is aged, then heated to about 90°C. Another technique uses kaolin clay that has been heated in a furnace until it begins to melt, then chilled and ground to powder. This powder is mixed with sodium salts and water, aged, and heated [16-18].

2.2.4 Based on pore sizes

According to the International Union of Pure and Applied Chemistry (IUPAC), pores can be classified with respect to pore diameters (pd) as either

1- Micropores: $pd \leq 2nm$,

2-Mesopores: $2nm < pd \leq 50$ nm, or

3-Macropores: $pd > 50$ nm. [31]

2.2.5 Based on Si/Al ratio

The Si/Al ratio in the zeolite framework structures can be used to classify them as to whether low silica, intermediate silica or high silica zeolites.

1- Low-silica zeolites have ratio Si/Al ratio ≤ 2. The famous commercial adsorbents, Zeolite A and X, are typical examples of low silica zeolites. They have water and polar molecule selective surface and thus commonly used for purification and drying [32].

2- Intermediate silica zeolites have Si/Al ratio ranging from 2.0 to ~5.0. Zeolite-Y and mordenite widely used for catalysis applications are common examples [33].

3- High silica zeolites have Si/Al ratio > 5. Beta and ZSM-5 (founded by the Mobil Research and Development Laboratory in early 1970's) have Si/Al ratios from ten to more than hundred, and have homogenous surface with organophilic-hydrophobic selectivity [33].

2.3 Brief description of some commercial zeolites

2.3.1 Zeolite Socony Mobil-5 (ZSM-5)

ZSM-5 (Zeolite Socony Mobil–5) is a synthetic zeolite with low water content and low aluminium content framework. It has 5-1 SBUs joined by oxygen bridges to other identical ring, forming pentasil chains. ZSM-5 has a 3-D pore structure surrounded by 10 oxygen windows. Its Si/Al ratio ranges from 7 to infinity [34]. 0.10cm^3g^{-1} void volume, pore size of (0.54 x 0.56) nm and (0.55 x0.51) nm are known with ZSM-5 [35]. ZSM-5 is being used as a heterogeneous catalyst for isomerization of hydrocarbons in the petroleum industry [36].

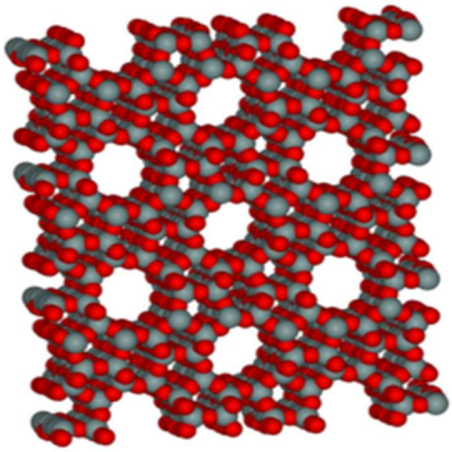

Figure 2.4 Microporous molecular structure of ZSM-5 zeolite [37].

2.3.2 Zeolite A (LTA)

Zeolite-A, also known as Linde Type A (LTA) zeolite, has a 3-D pore system that allows molecules to diffuse in space in all directions by moving across the 8-ring windows connecting the cavities. Its pore sizes range from 0.35 to 0.45nm [34]. Zeolite-A is industrially useful for removal of Ca^{2+} and Mg^{2+} in water hardness treatment.

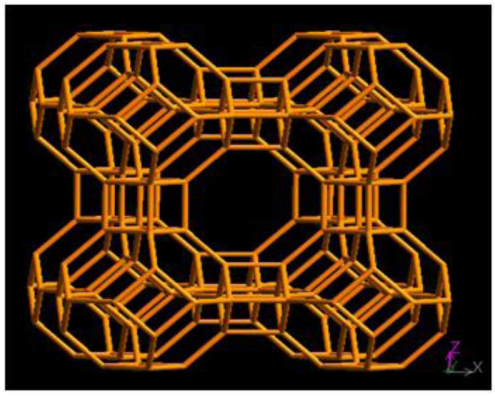

Figure 2.5 The microporous molecular structure of a zeolite A [38].

2.3.3 Zeolite X and Y (Faujasite)

Both zeolites X and Y have the FAU type framework with a double 6-ring and large pores in the range of 0.6-0.8nm, but differ in composition and properties. X has a Si/Al ratio≈1.25 while Y ≈1.5-2.3 [39]. Unlike zeolite-X that is majorly used for gas drying and as adsorbent, zeolite-Y is mostly used as a solid-acid catalyst or for ion exchange applications [40].

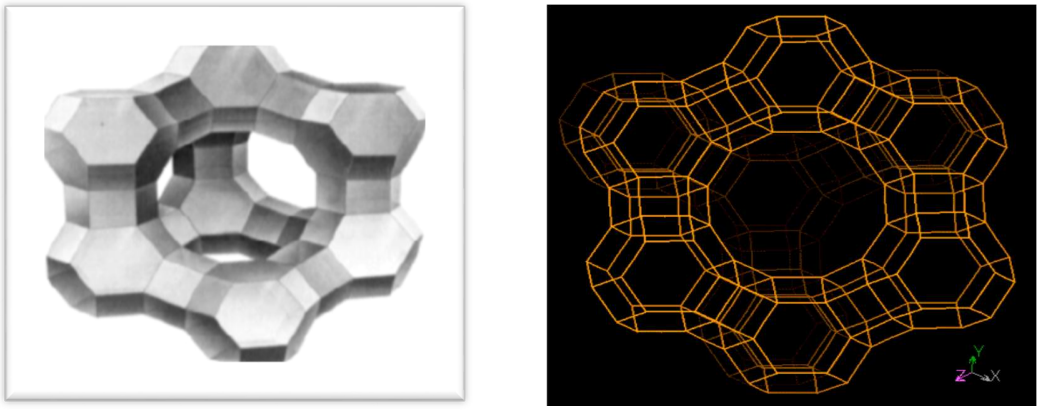

Figure 2.6 Zeolite X (left) and Y (right) Faujasite (FAU) [40].

2.4 Industrial applications of zeolites

The wide application of zeolite in several industrial processes can be attributed to their unique structural, chemical and physical properties. For instance, they can be used as molecular sieves, ion-exchange materials, superb solid catalyst as well as for adsorption studies.

2.4.1 Zeolites as molecular sieves

Molecular sieves are porous solids containing pores with a diameter of 0.3 to 1.3 nm. The cavities and channels in zeolite structure (an example of porous solid) enable them to retain water molecules within their structure. Releasing the water molecules from these voids via thermal heat application permits other molecules to be sorbed. Molecules whose sizes exceed the pores diameter range are restricted from passing through them, that is, acting as molecular sieves. The adsorption characteristics and the pore size can be amended by cations exchange. For example, exchange of sodium ions with potassium

ions decreases the pore size to 3Å (and so called 3A molecular sieves) but exchange with calcium ions increases the pore size to 5Å (and so called 5A molecular sieves) [41].

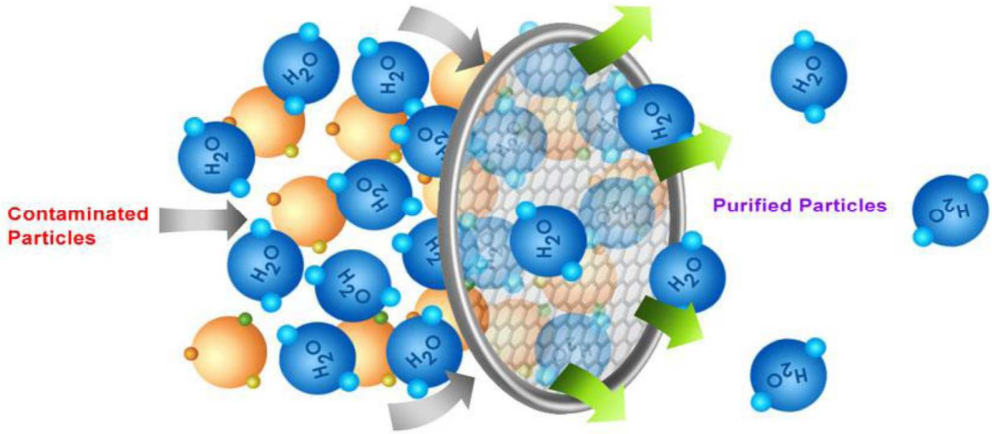

Figure 2.7 Illustration of molecular sieving [42].

2.4.2 Zeolites as ion exchange media

The cations, present within the zeolite framework to balance the net charges of Al^{3+} and Si^{4+}, are facile and can easily be exchanged with other cations like Pb^{2+}, Cd^{2+}, Cu^{2+}, Cr^{3+}, etc. Remarkably, zeolites are good ion exchange media in the process of water softening [43].

Cation exchange is an equilibrium process which extent is determined by factors such as: density charge and diameter of the cation being exchanged; the morphology features of the zeolite species and its Si/Al ratio; prior modification treatment of the zeolite; the cation concentration in the solution; cation position in the zeolite species; and temperature [27, 44]. The Cation Exchange Capacity (CEC) of zeolite increases with the decrease in Si/Al ratio and vice versa. An increase in Si/Al ratio of zeolite gives a

decrease in the framework charge which results to decrease in the numbers of cations that can be exchanged, meaning a drop in the CEC [27,44].

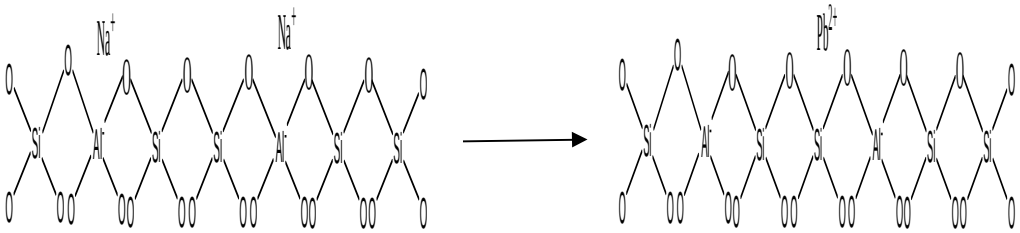

Figure 2.8 Schematic of zeolite ion exchange; Na^+ is exchanged for Pb^{2+}.

2.4.3 Zeolites as efficient solid catalysts

When the cations are protons H^+, zeolites serve as superb solid acid catalyst, artistic with high selectivity and stability maintenance, during chemical reactions [34]. Requirement of the adequately large pores to enable molecular transport to and from the zeolite active site, encourages the tuning of the zeolite frameworks to enhance the active sites accessibility and thermal stability. Section 2.4 elaborated on zeolite in catalysis as related to this research work while the modification, characterization and catalytic evaluation of a particular superdealuminated ultrastable Y-zeolite were extensively investigated and discussed in chapter 3.

2.4.4 Zeolites as excellent sorbent material in adsorption studies

Zeolites are highly sought after sorbent material, due to their high internal surface area while in dehydrated form, for adsorption studies [27,46]. Different types of materials can be exceptionally adsorbed by zeolite, in the absence of steric hindrance. There exists an

electric field within the zeolite cavity and the polarization of this electric field by the interaction with polar molecule like water makes the non-polar molecules strongly adsorbed. The reversibility of electrostatic field-, polarizability- and molecular sieve-based adsorption studies enables the reusability of zeolite and remarks zeolites as cost-effective adsorption media. It is noteworthy that high cost of production and regeneration of spent activated carbon makes it less economical, in spite of its widely use, than zeolite as adsorbent medium for the heavy metals removal from water [47].

2.5 Zeolites in catalysis

The zeolites have their wide application as catalysts (about 55% in 2008) [48] in various reactions in oil refining, petrochemicals, and fine chemical industries [49,50]. The replacement of the cations with H^+ gives strong Bronsted acid and the strong acidity and uniform micropores are great assets enabling the efficient catalytic role of zeolites in several chemical conversions. The micropores impose confinement on the mass transport to and from the acid site, which gives product selectivity [51-53]. This is an explainable success in a way as solid catalysts but these features impose serious access and diffusion limitations on the extensive use of zeolite without tuning both acidity and micropore size. This diffusivity challenge is borne out of the fact that only section of the micropore around the external surface of the zeolites is being used in most catalytic reactions. This under-exploitation of the zeolite volume can be reverted by preparing hierarchical zeolites with intracrystalline pores via post-synthetic modification strategies [54]. These hierarchical zeolites merge the intrinsic microporosity with the inter- and intra-crystalline

mesopore network to amend the diffusional limitation of the conventional zeolites, such that the introduced mesopores enable access to the catalytically active sites in the micropores [54-58].

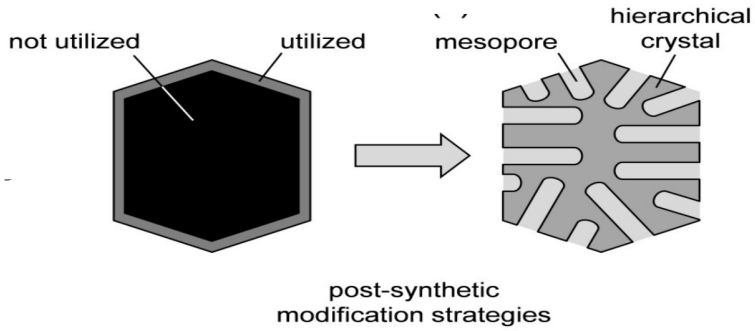

Figure 2.9 The illustration of increase in zeolite surface area by post-synthetic strategies.

2.5.1 Synthetic routes of hierarchical zeolites

Post-synthetic modifications entail several approaches that are broadly grouped into bottom-up and top-down routes. While the former involves modification of the synthesis protocol to give nanosized zeolite crystals [59] or that with a secondary mesopore template [55,60], the latter involves the delamination or demetallation (i.e. extraction of framework atoms) via post-synthetic treatment(s) of formerly developed zeolites with irradiation [61,62] and/or strong oxidizing reagents [62], swelling agents [63,64], acid [65], base (desilication) [56] or steam [66].

Both routes give desirable mesoporosity and improved catalytic performance but many bottom-up methods are characterized with large amounts of expensive and unavailable templates or not easily separable crystals from the mother liquor [57], and thus prove

difficult to be amended into industrial scale unlike top-down approaches that are more readily employed at this scale [54,57,65,67]. This thus explains the much adoption of top-down approaches in widening the micropore channels [68] and generating intracrystalline mesopores in the zeolite crystals [55,56] in order to improve the accessibility of the active sites in conventional zeolites.

2.5.2 Desilication approach

It is a top-down, non-templating, scalable, tunable, economical, experimentally simple and effective alkaline mediated method of introducing interconnected and well accessible (from the external surface of the zeolite) mesopores by selectively leaching the framework silicon [54,57,67-69]. Mesoporous zeolites synthesized by this base leaching method have been reported, both in patents and open literatures, to be of good activity, selectivity and lifetime in catalyzing several reactions that are not limited to methanol-to-hydrocarbons, pyrolysis, cracking, isomerization, aromatization, alkylation, acylation, among others [54,70].

Later, aqueous sodium carbonate mediated alkaline treatment of ZSM-5, X, and Y zeolites reportedly gave an increased Al content and enhanced ion-exchange capacity without drastic change in the zeolite structures [71]. Subsequently, a more insightful study on the potential of mesoporous MFI through desilication led to the establishment of the optimal molar Si/Al window of 25-50 under treatment condition (0.2 M of NaOH, 65°C, 30 min) for the successful introduction of intracrystalline mesopores [72]. This fixed window served as a major setback for this approach as there would be excessive Si

dissolution at higher molar Si/Al ratios and limited extra mesoporosity at lower ratios [54,57].

Efforts to comprehend the desilication mechanism can be traced down to Cižmek *et al.* [73] that established the uncommon influence of aluminum on the dissolution kinetics. Furthermore, the Al in the zeolite framework was seen as 'pore-directing agent' (PDA) owing to its role in controlling the Si dissolution [74] and the selective silicon extraction was credited to the re-alumination of extracted framework Al on the external surface of the zeolite giving rise to disordered mesopores formation [75].

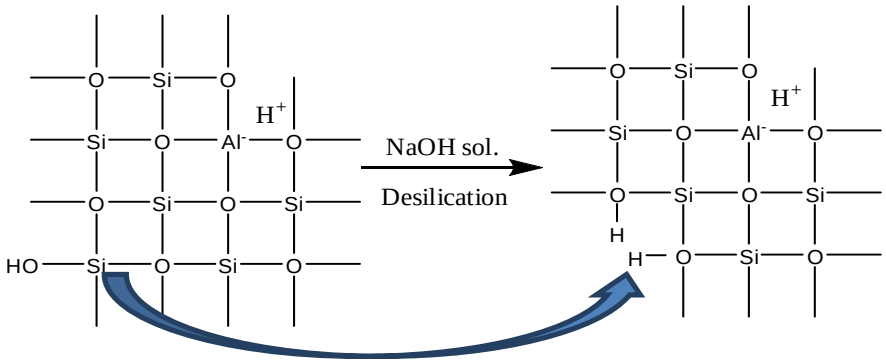

Figure 2.10 Schematic representation of desilication effect on zeolite framework.

The surface-deposited aluminium during the alkaline treatment of zeolite is mostly Lewis acidic [76-78]. This pore directing role of the framework Al (**internal PDAs**) can be competed with the presence (individual role) of quaternary ammonium cations (**external PDAs**), which form a protective layer on zeolites external surface by binding to the silica surface and thus influence the process of pore formation [79,80]. So, it becomes necessary to assess the acidity and coordination of the re-aluminated species during alkaline treatment, using infrared spectroscopy and nuclear magnetic resonance. The well controlled growth of intracrystalline mesoporosity in all-silica zeolites can be achieved

with the inclusion of quaternary ammonium cations or metal-cation complexes in desilicating solution [81].

2.5.3 Y-zeolites and their hierarchical analogues

Y-zeolite of Faujasite family is a leading catalyst used in several industrial processes ranging from hydrocracking and fluid catalytic cracking (FCC) process to aliphatic alkylation reactions [82]. The pristine Y-zeolite has high Al content in its framework and this makes it unstable when in H-form [83]. However, the stabilization can be induced by modifications like steaming [24,48-50] and framework dealumination [21,47]. These form ultra-stable derivatives, USY zeolites, which are indispensable catalysts in FCC [51]. Further framework dealumination of the USY gives different series of USY derivatives depending on the extent of dealumination: USY (steamed; Si/Al = 2.6); VSUSY (steamed and dealuminated; Si/Al = 6); SDUSY (severely steamed and dealuminated; Si/Al = 15-40) [81].

In addition to the induced stability, steaming gives mesopores in form of cavities [54] while dealumination gives a secondary network of mesopores [24,53,68]. In spite of these, the bulky nature of the probe molecules in several industrial processes further necessitates the synthesis of the hierarchical analogues of the USY, commonly by desilication (alkaline treatment). Bearing in mind that the FAU topology in USY zeolites is highly sensitive to alkaline media, due to their relatively high surface area, large tightly interconnected micropores, and low framework density, it becomes a good idea to include external pore directing agent to obtain substantial mesoporosity and preserve the intrinsic

zeolite properties, in the case of severely dealuminated USY zeolites [52,83]. The catalytic cracking of vacuum gas oil, the pyrolysis of polyethylene, and the alkylation of benzyl alcohol with toluene are few of model reactions that evidently show the superiority of hierarchical USY [83].

2.6 Adsorption process

Adsorption is such a mass transfer process that is popular for wastewater treatment and air pollution control, perhaps due to its efficient and economical process [84]. It entails the removal of contaminant by adsorbing it on the adsorbent's surface through chemical or physical bonding. While the "adsorbate" is the material to be adsorbed, the "adsorbent" is the porous solid material onto which the adsorbate is adsorbed. For example, in chapter four of this report, heavy metal ions are the "adsorbates" and the zeolites are the "adsorbents". The important advantages of the adsorption process as treatment methods include, but not limited to the following: safety and ease of operational technique; absence of chemical additives that can give sludge formation; removal of a wide spectrum of constituents at very low concentration; regeneration and reusability of the adsorbent; and suitability for batch and continuous operations [85].

2.6.1 Types of adsorption process

There are the two general types of adsorption based on the nature of the bonding between the adsorbate and the adsorbent, namely chemical (chemisorptions) and physical (physisorption) [75].

2.6.1.1 Chemisorption

The chemical adsorption involves formation of a single layer of adsorbate chemically bonded to the adsorbent surface. So, it requires much stronger forces of comparable magnitude with those in chemical compounds [87]. By its chemical bonding nature, the chemisorption is irreversible with characteristic high enthalpy (> 200 KJ/mole) [88].

2.6.1.2 Physisorption

Physical adsorption involves the electrostatic attraction between the adsorbate and the adsorbent surface; an important mechanism for heavy metals removal. Although it generally occurs at low temperatures, it requires adequate energy to be given to overcome the attractive forces [89]. It can form a single or multiple layers of adsorbate on the adsorbent surface with relatively low enthalpy of adsorption (activation energy <40 KJ/mole), meaning that the adsorbate is held weakly to the adsorbent [90,91].

2.6.2 Factors affecting physical adsorption

Many factors such as surface area of adsorbent, nature of the adsorbate, pH of the solution, temperature, and presence of inorganic salts determine the amount of adsorbate that can be adsorbed on the adsorbent's surface [92].

2.6.2.1 Adsorbent's surface area

There exists a strong positive correlation between the quantitative adsorption and the surface area of the adsorbent. That is, the larger the surface areas, the better the adsorption provided that other factors remain constant.

2.6.2.2 Nature of adsorbate

For inorganic ions, the degree of ionization of the solute is crucial to the adsorption process. A weakly dissociated HgCl adsorbs well but a strongly dissociated NaCl does not adsorb at all. In the case of organic sorbent, the large molecule and low aqueous solubility favor the adsorption process, with the exception of the scenario where the molecule is so large to cause blockage of the pores of the adsorbents [92].

2.6.2.3 pH of the solution

Increase in pH of the solution enhances the adsorption process of similarly charged adsorbate species, but mutual electrical repulsion prevents multi-layer adsorption form. Meanwhile, neutral adsorbate species can have multi-layer and thus maximized adsorption. Obviously, basic species adsorb better at high pH but the acidic species adsorb better at low pH. The actual extent of adsorption differs for different metals for different pH and this is because different chemical species of a metal occur with pH changes and will have different charges and adsorption at solid–liquid interfaces [92,93].

2.6.2.4 Temperature

In general, temperature has inverse relationship with the quantity of adsorption because the adsorbed molecules break away from the surface of adsorbent surface due to great energy at high temperature [92].

2.6.2.5 Effect of inorganic salts

The presence of inorganic salts like sodium chloride in the system can promote adsorption due to their ability to fit in between adsorbed species and thus screening the repulsive forces on the surface and also hold an opposite charge to the adsorbent [92].

2.6.3 Adsorption Isotherm Models; Langmuir, Freundlich and Temkin

Adsorption process is often described using isotherm which represents the equilibrium state between the quantity of adsorbate ions per unit weight of adsorbent (q_e) and the equilibrium concentration of the adsorbate remaining in solution (C_e) at a given temperature. This study employed the three popular isotherm models (Langmuir, Freundlich and Temkin models) to fit the experimental data for the adsorption study.

2.6.3.1 Langmuir model

The Langmuir model isotherm, pioneered by Irving Langmuir in 1918, is an empirical isotherm that quantifies sorption on localized adsorption sites as derived from a proposed kinetic mechanism. Although it can be used to describe both physi- and chemi-sorption, yet it is only valid for single-layer adsorption [94-96]. The Langmuir model hypotheses can be summarized as follows [97,98]:

1) Highest adsorption corresponds to a saturated monolayer of adsorbate molecules on the solid surface. By extension, maximum adsorption occurs on a monolayer only at the defined sites of the adsorbent and no others, and that all sites are equal on the uniform surface of adsorbent.

2) All adsorption is formed through the same system and the adsorption energy is constant without transmigration of adjacent adsorbed molecules, that is, no interaction between the adsorbed molecules

The Langmuir model equation (equation 2.2) can be linearized to give equation 2.3 [99].

$$q_e = \frac{K_L\, b\, C_e}{1 + b\, C_e} \tag{2.2}$$

$$\frac{1}{q_e} = \frac{1}{C_e} \cdot \frac{1}{b\, K_L} + \frac{1}{K_L} \tag{2.3}$$

where q_e is the equilibrium ion uptake ($mg.g^{-1}$), *Ce* represents the equilibrium concentration ($mg.L^{-1}$), *b* is the sorption equilibrium constant ($L.mg^{-1}$) and K_L *is* the maximum adsorption capacity ($mg.g^{-1}$).

Weber and Chakravorti (1974) described a dimensionless constant, R_L, (see equation 2.4) as separation factor to characterize Langmuir isotherm pattern [100,101]. $R_L > 1$ unfavourable isotherm type, $R_L = 0$; Linear isotherm, $0<R_L<1$; favourable isotherm and $R_L<0$ irreversible.

$$R_L = \frac{1}{1 + b\, C_o} \tag{2.4}$$

where *Co* is the highest initial concentration of element ($mg.L^{-1}$).

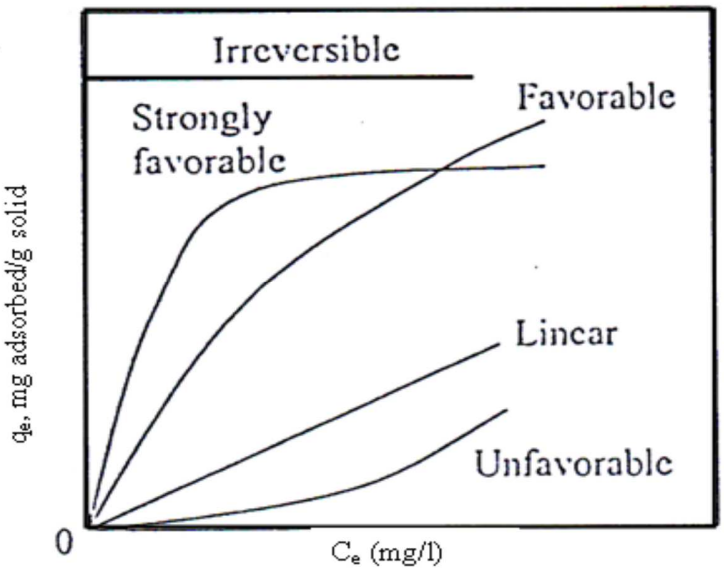

Figure 2.11 Graphical representation of Langmuir isotherm separation factor [102].

2.6.3.2 Freundlich model

Freundlich and Küster in 1907 founded an empirical equation that described sorption isotherm in terms of sorbate concentration, as mathematically expressed in equation 2.5 [102-104], with its logarithmic form in equation 2.6. The Freundlich model, as fondly called, can be used for multilayer sorption and for non-ideal sorption on heterogeneous surfaces, unlike the Langmuir model [105].

$$q_e = K_F (C_e)^{1/n} \tag{2.5}$$

$$\log q_e = \log K_F + \left(\frac{1}{n}\right) \log C_e \tag{2.6}$$

where n and K_F are Freundlich isotherm constants related to adsorption intensity and adsorption capacity respectively.

2.6.3.3 Temkin isotherm model

Temkin adsorption isotherm represents the amount of energy required for the absorption by one layer on the adsorbent's surface [106]. Its linear form can be written as:

$$\ln q_e = \left(\frac{RT}{b_T}\right) \ln K_T + \left(\frac{RT}{b_T}\right) \ln C_e \quad (2.7)$$

where b_T is the Temkin constant related to the sorption heat in kJ/mol, k_T is the binding energy constant at equilibrium; an equivalence of maximum binding energy (L/g), R is the universal gas constant (0.008314J/mol-K) and T is the absolute temperature in Kelvin.

2.6.4 Adsorption kinetics

Kinetics describes the speed and factors influencing the reaction rate. Both physical and chemical characteristics of the adsorbent as well as the entire system conditions determine the nature of the sorption process [107]. The commonly used kinetic expressions to elucidate the kinetics of the solid-liquid adsorption processes are pseudo-first order, pseudo-second order, and intraparticle diffusion models [108].

2.6.4.1 Lagergren pseudo first-order kinetics

This is a common model for understanding the mechanism of the solid-liquid system [109]. It represents well the experimental kinetic data where the probable adsorbate interactions were anticipated to be insignificant [107] and not for the entire sorption

period [110]. More often than not, it fails to correctly predict the q_e theoretically [109]. It is expressed as follows:

$$\log(q_e - q_t) = \log q_e - \left(\frac{K_1}{2.303}\right) t \quad (2.8)$$

where K_1 is the rate constant (min^{-1}), q_e is the amount of adsorbed at equilibrium (mg/g), q_t is the amount adsorbed at time t (mg/g), h is the initial sorption rate (mg/g.min).

2.6.4.2 Pseudo second-order kinetics

This adequately elucidates the kinetics of the most of sorption systems so well for the entire sorption period, unlike pseudo first-order. It was found to show a better fit towards the sorption of heavy metals [111,112]. Its mathematical expression is as follows:

$$\frac{t}{q_t} = \frac{1}{h} + \frac{t}{q_e} \quad (2.9)$$

$$h = K_2 q_e^2 \quad (2.10)$$

where K_2 is the rate constant (g/mg.min), q_e is the amount of adsorbed at equilibrium (mg/g), q_t is the amount adsorbed at time t (mg/g), h is the initial sorption rate (mg/g.min).

2.6.4.3 Intra-particle diffusion kinetic model

The Morris-Weber model is an intensive description of the intra-particle diffusion of the adsorbate from the solution into the adsorbent pores. It predicts the intra-particle diffusion as the limiting step of the adsorption process [113]. The Morris-Weber equation can be written as:

$$q_t = K_{id} t^{\frac{1}{2}} + c \quad (2.11)$$

where K_{id} is the rate constant of the intraparticle transport (mg/g.min$^{1/2}$), q_t is the amount adsorbed at time t (mg/g).

CHAPTER 3

QUARTERNARY AMMONIUM CATIONS BASED SYNTHESIS OF HIERARCHICAL DEALUMINATED Y-ZEOLITES FOR CATALYTIC EVALUATIONS

3.1 Background Information

Several chemical processes in the oil refining and petrochemical sectors are exclusively catalyzed by zeolites [114]. These crystalline aluminosilicates possess unique properties, such as solid acidity, ion-exchange capacity, and unequaled shape selectivity, due to the presence of multidimensional network of micropores of molecular dimensions (the so-called “micro-reactor” of 0.25-1 nm in size) [114,115]. On the contrary, the sole presence of these micropores imposes transport/diffusion limitations and provokes rapid deactivation, thus negatively impacts the catalyst activity and lifetime, particularly in processing and synthesizing large molecules used as fine chemicals, (i.e. under-utilization of zeolite potential). To alleviate this, various strategies of distinctively two different routes have been reported to improve the pore accessibility [116-130]. The first approach focuses on increasing the effective diffusivity in the micropores by synthesizing wide-pore and large-cavity zeolites (i.e. ITQ-21 with 1.18-nm-wide cavities) [116,117]. The other method aims at shortening the micropore diffusion path length by integrating the inherent micropores with a secondary network of inter or intra-crystalline mesopores,

resulting in hierarchical zeolites [118-119]. This facilitates the accessibility of the micropores by substantially increase the external surface area.

These zeolites can be obtained in the form of nanosized [120,121], composites [122,123], delaminated [124,125], and mesoporous crystals [55,56,126-130]; via templated and nontemplated bottom-up and top-down routes. However, mesoporous crystals obtained by top-down routes (viz. post-synthetic demetallation (removal of framework atoms)) have received more attention. Most bottom-up routes involve costly and environmentally harmful templates as mesopore directing agents, and thus cannot be easily implemented at an industrial scale [130]. On the contrary, demetallation such as dealumination (steaming, acid leaching) [128,129], desilication (base leaching) [56,130,133], and detitanation (H_2O_2 treatment under irradiation) [134]) are experimentally simple and cost-effective, and yield superior active catalysts.

Among these strategies, the preferential extraction of Si from zeolite framework in an alkaline medium (i.e desilication) stands out to be the simplest and most economical way for effectively introducing well-interconnected and accessible mesopores. The importance and implications of desilication on mesoporosity, diffusion, and catalysis have been comprehensively reviewed by Groen *et al.* [56] and recently by Verboekend and Perez-Ramirez [130]. Since the 90s, several studies have examined many facets of desilication such as concentration of alkaline medium (e.g. NaOH, Na_2CO_3, LiOH, and/or alkylammonium hydroxides), temperature, and duration) over broad variety of zeolite structures. Groen *et al*. [74] pioneering work laid down the basis for mesopore formation by desilication, showed that Si/Al window of 25-50 is the optimum for mesopore formation in MFI, and considered framework Al as inherent “pore-directing agent

(PDA)". This contribution was subsequently applied to other zeolite topologies like MTW, MWW, MOR, and TON [56,130]. Groen *et al.* [135] pointed out later that the relatively low stability of framework Al in BEA, compared to MFI, is also detrimental for the mesopore formation by desilication, since Al cannot optimally exert its pore-directing role. Verboekend and Perez-Ramirez [136] demonstrated that desilication in the presence of external PDA (i.e. metal-cation complexes or quaternary ammonium cations) facilitates the formation of mesoporosity in silicalite-1. This proves that framework Al is not the only prerequisite for the introduction of mesoporosity. Consequently, the effective introduction of mesopores largely depends on three factors: the zeolite, the treatment conditions, and the PDA [136].

Introduction of mesoporosity in zeolites of FAU topology such as Y and ultra-stable derivative (USY) (Si/Al~ 2.5) upon desilication remains relatively unexplored, compared to other industrially used zeolites [137-140]. This is despite the fact that these zeolite types are widely used in oil refining and petrochemical industries (i.e. fluid catalytic cracking, hydrocracking, and alkylation). The crucial stabilization of zeolite Y by dealumination via steaming and acid leaching generates mesoporosity [141], but the introduced mesopores (>20 nm in diameter) are present as cavities, and thus, they do not significantly influence the diffusion of molecules. Qin *et al*. [137] reported the preparation of hierarchical zeolite Y by sequential severe NaOH desilication and ammonium hexafluorsilicate dealumination, but of limited mesoporosity (S_{meso} = 61 m^2g^{-1}, compared to 18 m^2g^{-1} for pristine Y). Their further attempt in synthesizing hierarchical USY also resulted in limited mesoporosity (S_{meso} increased to 69 m^2g^{-1} up from 52 m^2g^{-1}) [135]. de Jong *et al*. [66] managed to synthesize USY of trimodal mesoporosity (S_{meso} =

443 m^2g^{-1}, compared to 213 m^2g^{-1}) upon mild treatment (0.05-0.1 M NaOH, 25 °C, 15 min) of severely steamed and acid-leached USY, but the obtained USY exhibited strong amorphization with damaged microporosity (from 0.21 cm^3g^{-1} to 0.07 cm^3g^{-1}).

Remarkably, Perez-Ramirez group [83] succeeded in developing a wide family of hierarchical Y and USY zeolites, by establishing strategic blend of post-synthetic modifications that include desilication and acid treatments. They reported hierarchical Y zeolite (S_{meso} = 292 m^2g^{-1} up from 22 m^2g^{-1}) upon sequential mild dealumination (H_4EDTA)-desilication (NaOH)-acid wash (Na_2H_2EDTA) treatments of Y (Si/Al = 2). Hierarchical USY zeolites of large mesoporsity (S_{meso} up to 500 m^2g^{-1}) and well-preserved crystallinity were also obtained upon treatment of severely steamed and dealuminated USY (Si/Al = 15-30) using solution of NaOH and pore directing agent (TPAOH).

In continuous efforts to overcome the main challenges of introducing intracrystalline mesoporosity in USY zeolites, Verboekend and Perez-Ramirez [136] showed that besides the location and concentration, the affinity of PDAs to the zeolite surface as well as their nature, plays a critical role in the mesopore generation in silica-rich zeolites (Silicalite-1). They compared the role of TMAOH and TPAOH in the mesopore formation for silica-rich zeolites, and found that the dissolution process and subsequently mesoporosity are reduced drastically in the case of TMAOH due to the strong affinity of TMA^+ to the zeolite external surface. The beneficial role of TPAOH on mesoporosity was also reported for FAU-type zeolites [83,139,140].

To further build on this landmark, this work focuses on the inclusion of more effective PDAs than those previously reported. Herein, for the very first time, to the best knowledge of available information, the effects of tetrabutylammonium hydroxide (TBAOH) as a desilicating agent and/or PDA and novel binary mixture of organic templates based strategy on the formation of substantial intracrystalline mesoporosity in USY zeolite of different steaming-dealumination degrees (Si/Al=15-40) are reported, with highlights on the comparison with other less bulky tetraalkylammonium hydroxides (TMAOH, TEAOH and TPAOH) in the range of 0.01-1.0 M over broad range of desilication conditions, as well as the correlations between the inclusion of TBAOH, the generated mesoporosity, and the level of steaming-dealumination of USY zeolite.

3.2 Materials

The USY zeolites exploited in this study were supplied by Zeolyst International and were found to be derivatives of the same pristine NaY zeolite (CBV100) subjected to different degree of steaming-dealumination treatments. The resulting five different USY zeolites are: (i) mildly steamed CBV500 (USY, NH_4-form, Si/Al = 2.6), noted as USY; (ii) steamed CBV712 (very stable USY "VUSY", NH_4-form, Si/Al = 6), noted as VSUSY; (iii) severely steamed + dealuminated CBV720, CBV760 and CBV901 (super dealuminated USY "SDUSY", H-form, Si/Al = 15, 30 and 40, respectively). The latter samples were coded SDUSY15, SDUSY30 and SDUSY40, respectively and got the attention of this research work. Prior to post-synthetic treatments, the as-received SDUSYs were air-calcined at 550°C for 6 h (3°C/min) to ascertain their H-forms.

Reagents used for post-treatments included NaOH (97+%, Aldrich), sodium carbonate anhydrous (Panreac), TMAOH (25 wt.% in H_2O, Sigma-Aldrich), TEAOH (35 wt.% in H_2O, Aldrich), TPAOH (20 wt.% in H_2O, Fluka), and TBAOH (40 wt.% in H_2O, Sigma-Aldrich). They were all used as purchased without further modifications.

3.3 Post-Synthetic Alkaline Treatments

Alkaline treatment of the calcined SDUSY zeolites was carried out in aqueous solutions of 0.01-1.0 M pure or mixture of inorganic and organic hydroxides at different temperatures and durations under atmospheric pressure. The alkaline solutions used in this study included NaOH, Na_2CO_3, and four different tetraalkylammonium hydroxides (TMAOH, TEAOH, TPAOH and TBAOH) Typically, 50 ml of the alkaline solution (i.e. NaOH, TBAOH, or NaOH + TBAOH) was heated up to 65°C (or 85-100°C) in a flask connected to a reflux using a oil bath, followed by the addition of 1.5 g of USY zeolite (Si/Al = 15-40) to the heated solution, and continuous stirring of the solution at that temperature for a period of 2 hrs (or 0.30 - 24 hrs). When the reaction time reached, the zeolite suspension was cooled down immediately using an ice bath, and then was isolated by suction filtration. The filtrate was collected for elemental analysis while the solid product was washed painstakingly with deionized water until the pH is neutral (400 ml of water was adequate). The obtained wet solid was then dried at room temperature, followed by drying at 110°C for 10 hrs minimum. Afterwards, the dried sample was calcined at 550°C in static air (holding time 6 hrs, 3°C/min). Depending on the alkaline medium used and thus the need, some selected alkaline treated zeolite samples were transformed into ammonium form by two-fold ion-exchange with 2.20 M of NH_4Cl at

80°C for 5 hrs (1.0 g solid per 50 ml solution) without calcination between ion-exchange procedures. The samples were then subjected to typical drying treatments followed by calcination to get the H-form. It is noteworthy that the treatment conditions (duration and temperature) were first optimized to be 65°C and 2hrs, and adopted throughout for the alkaline treatment before ion-exchange experiment.

The USY zeolite samples obtained by alkaline treatment using aqueous solution of NaOH or Na_2CO_3 are hereafter designated as SDUSYx-DSy, where x and y represent the Si/Al ratio and the molarity of the solution, respectively. Those obtained using tetraalkylammonium hydroxide are noted as SDUSYx-DS-yz, where x, y, and z represent the Si/Al ratio, the tetraalkylammonium hydroxides (TM, TE, TP or TB), and the molarity of the solution, respectively. For instance, SDUSY3-DS-TE-0.10 corresponds to alkaline treated SDUSY40 zeolite (CBV901, Si/Al = 40) using 0.10 M tetraethylammonium hydroxide solution.

3.4 Characterizations

The amounts of Si and Al in the solids and filtrates were quantified by ICP-OES on a Horiba ULTIMA 2 instrument. The detail of calculation involved after the instrumental analysis can be found as part of the appendices in this report.

X-ray diffraction measurements were done on a Rigaku Miniflex II XRD powder diffraction system using CuKα radiation ($\lambda_{K\alpha1}$ = 1.54051Å, 30 Kv and 15 mA). The XRD patterns were recorded in the static scanning mode from 3.0 - 60° (2θ) at a detector angular speed of 2 °/min and step size of 0.02°. The relative crystallinity of alkaline

treated USY zeolites was estimated by comparing the peak intensity of the (533) reflection at $2\theta = 24°$ with those of NaY zeolite (assuming 100% crystallinity). The reproducibility of the crystallinity analysis was ± 8%.

Textural properties were determined by N_2 adsorption-desorption measurements at 77 K, using Micromeritics ASAP2020 adsorption analyzer. Samples were outgassed at 220°C under vacuum (10^{-5} Torr) for 3 hrs prior N_2 physisorption. The Brunauer-Emmett-Teller (BET) specific surface areas were obtained from the adsorption data in the relative pressure (P/P_0) range from 0.06-0.30, assuming 0.164 nm^2 for the cross-section of the N_2 molecule. Contributions of micropore and mesopores were calculated using the *t*-plot method described by Lippens and de Boer [142], whereas the mesopore size distribution was made using the Barret-Joyner-Halenda (BJH) pore size model applied to the isotherm adsorption branch [143].

The SEM (Scanning Electron Microscopy) images were obtained using FESEM/FIB (Tescan Lyra-3) to verify the particle size and morphology. The field Emission Dual Beam (Electron/ Focused Ion Beam) system combines high-end field-emission scanning electron microscope (FESEM) and high-performance focused ion beam (FIB) system in one chamber. Prior to the imaging, samples were prepared and gold-coated as described in part of the appendices.

HRTEM (High Resolution Transmission Electron Microscopy) images were obtained using a JEOL JEM-2000 FX microscope operating at 80 KV and equipped with a charge coupled device camera (Gatan). Samples were prepared as described for SEM experiment.

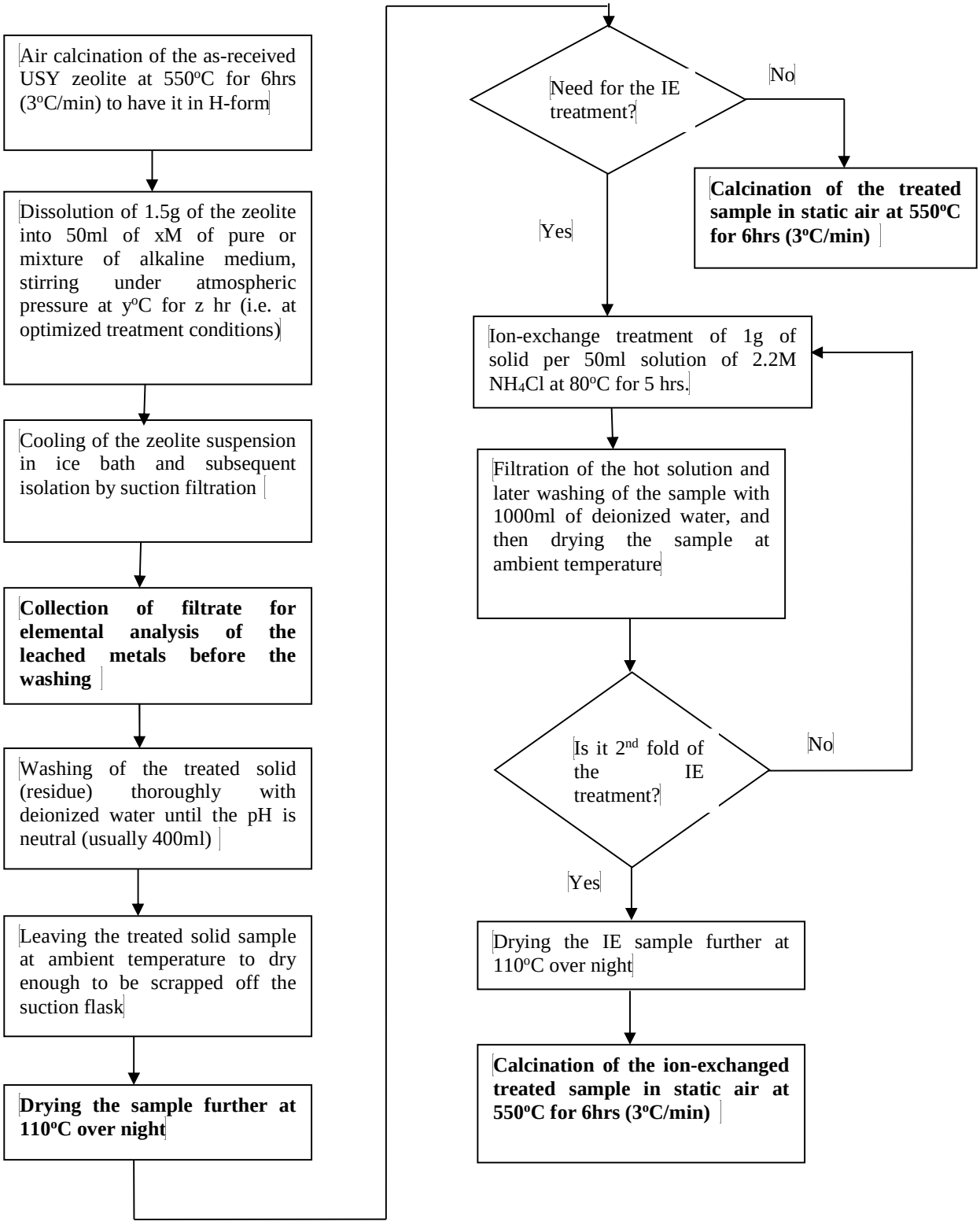

Figure 0.1 Flow chart of the post-synthetic alkaline treatment.

^{27}Al and ^{29}Si Magic Angle Spinning (MAS) NMR were measured using Bruker Avance 400 MHz wide-bore spectrometer. ^{27}Al MAS NMR spectra were obtained by a single pulse length of $\pi/4$, and relaxation delay of 0.5 s. The ^{29}Si MAS NMR spectra were obtained by 20 pulse (B1~55HZ) followed by 13 ms acquisition with ^{1}H decoupling (tppm, B1~55 HZ). Samples were spun at *ca.*4 KHz in Air using 4 mm ZrO_2 rotors. The Al and Si chemical shifts were referenced to $(NH_4)Al(SO_4)_2$ and 4,4-dimethyl-4-silapentane-1-sulfonic acid, respectively.

NH_3-TPD (Ammonia-Temperature-Programmed Desorption) was done using Micromeritics chemisorb 2750 equipped with a mass spectrometry detector (Cirrus 2, mks, spectra products). Samples (*ca.* 50 mg) were pretreated at 300 °C in helium flow (25 ml/min) for 2 hrs, followed by the adsorption of 10% NH_3/He at 100 ºC for 30 min. Thereafter, samples were purged in a helium stream for 2 hrs at 100 ºC so as to remove loosely bound ammonia (i.e. physisorbed and H-bonded ammonia). Again, the samples were heated again from 100 to 600 ºC at a heating rate of 10 ºC/min in helium flow of 25 ml/min.

3.5 Catalytic Evaluation Procedures

3.5.1 Alkylation of toluene with benzyl alcohol

The powder catalyst was sieved to a uniform particle size of 850 microns and 1g of the sieved catalyst was added to the 100ml of reactant mixture of toluene and benzyl alcohol (90:10) and the reaction was carried out in a parr pressure reactor (150 ml working volume) at 140°C and 72 psi for the studied reaction period (0-150 mins). Specifically,

the set up was initially charged with nitrogen gas and released to check for the leakage in the system. Then the heating temperature was allowed for 30 mins to equilibrate followed by pressurizing the system to 72 psi. Then, liquid samples were collected at interval within the desired reaction period (0-150 mins) and these samples were labeled and analyzed using a gas chromatograph (Agilent 7890A) equipped with an HP-5 capillary column and a flame ionization detector (FID). The limiting reagent, BzOH, was used for calibration, from which an estimate of its conversion at respective time was made from the calibration curve. The assignment of retention time for BzOH was prior confirmed by gas chromatography and mass spectroscopy (GC-MS).

3.5.2 Pyrolysis of low density polyethylene (LDPE)

The pyrolysis of LDPE (m.p≈112^0C, ρ=0.924g/ml, BDH Chemicals Limited) was performed in a Mettler Toledo TGA, SDTA851e microbalance equipped with a 34-position robot. 6mg of powdered catalysts was uniformly mixed with 18mg of LDPE in the α-Al_2O_3 crucible of the thermobalance and the degradation of the mixture (mass ratio 1:3) was done in N_2 (70cm^3 STP min^{-1}) with temperature ramping from 30 to 700^0C at 10^0C min^{-1}. The observed weight loss was interpreted as the percentage conversion of the LDPE.

3.6 RESULTS AND DISCUSSION

3.6.1 Alkaline Treatment of SDUSY40 with inorganic hydroxides and organic tetraalkyl ammonium hydroxides

3.6.1.1 Structural and Textural Properties

The XRD patterns of parent and alkaline treated SDUSY40 zeolites are shown in Fig. 3.2, while the variation in zeolite crystallinity resulting from alkaline treatments (relative crystallinity, RC) is given in Table 3.1. Parent SDUSY40 exhibits XRD reflections that are characteristic of FAU-type structure (Fig. 3.2(P)). However, upon alkaline treatment using aqueous solution of NaOH in the range of 0.01-1.0M, the long-range ordering and relative crystallinity were completely lost as evidenced by the associated amorphization (Fig. 3.2(a-e)).

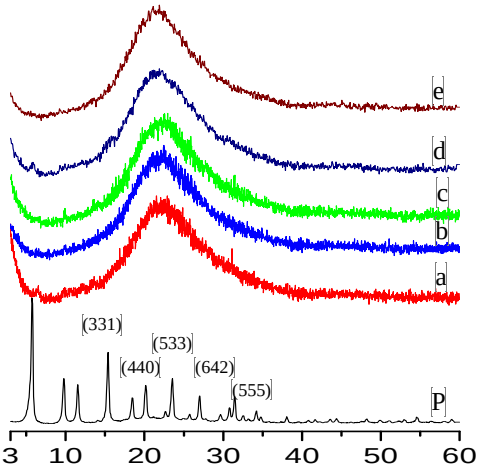

Figure 0.2 XRD patterns of parent and alkaline treated SDUSY40 with inorganic hydroxides; P: parent SDUSY40, a-e) corresponds top NaOH of 0.01, 0.10, 0.40, 0.60 and 1.0 M, respectively.

N_2-isotherms (Fig. 3.3(A)) and derived textural properties (Table 3.1) further confirm the amorphization of the SDUSY40 zeolite upon treatment with NaOH. The parent SDUSY40 exhibits type I isotherm having a plateau at relative pressure up to p/p_0 = 0.8, enhanced N_2 uptake at higher relative pressure, and hysteresis loop at p/p_0 = 0.45. This is in agreement with the microporous nature of the sample along with mesoporosity caused by the severe steaming and dealumination. Upon alkaline treatment with NaOH up to 0.30M, samples show higher N_2 uptake at $p/p_0 > 0.6$. Conversely, the uptake at $p/p_0 < 0.1$ decreased significantly as a result of severe amorphization. The Table 3.1 shows that the micropore volume of parent SDUSY40 (0.23 cm^3g^{-1}) was completely lost upon treatment with 0.01-1.0M NaOH, whereas the S_{meso} increased from 183 m^2g^{-1} (parent sample) to a maximum of 234 m^2g^{-1} (i.e. sample treated with 0.01M NaOH (SDUSY40-DS0.10)).

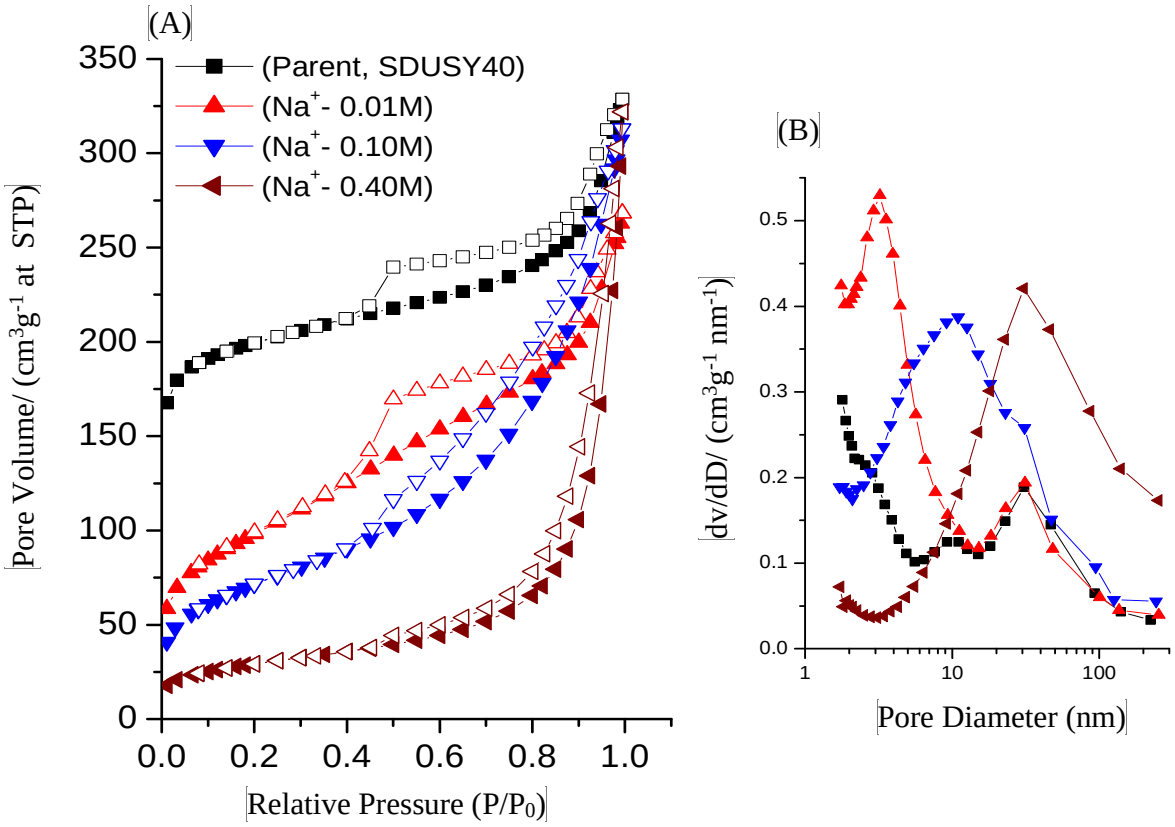

Figure 0.3 N2 adsorption isotherms (A) and corresponding BJH mesopore size distributions (B) for parent and alkaline treated SDUSY40 using NaOH. The legends in graph (A) also apply to the graph (B).

The BJH mesopore size distributions of alkaline treated SDUSY40 reveal the presence of mesopores of ~ 3.22-15.0 nm in diameter along with large mesopores that are charactertic of parent SDUSY40 (*ca.* 31 nm) (Fig.3.3(B)) upon treatment with NaOH up to 0.30M. At highly concentrated NaOH solutions, the pore system was destroyed completely resulting in large voids with diameters exceeding 40 nm. For samples treated with Na_2CO_3, the RC values from XRD data and N_2 isotherms reveal the loss of crystallinity and microposity without significant increase in the external surface area (Table 3.2 and Fig. 3.4).

Table 0.1 Treatment yields, textural and structural properties of alkaline treated SDUSY40 zeolite in 0.01-1.0 M NaOH

Sample	Yield [a] (%)	S_{BET} (m^2g^{-1})	S_{micro} [b] (m^2g^{-1})	S_{meso} [b] (m^2g^{-1})	V_t [c] (cm^3g^{-1})	V_{micro} [b] (cm^3g^{-1})	d_p [d] (nm)	RC [e] (%)
SDUSY40	-	607	424	183	0.51	0.23	11,31	51
0.05Na	88	200	10	190	0.37	0	4,9,31	0
0.10Na	78	251	17	234	0.48	0	11,31	0
0.20Na	41	289	10	279	0.69	0	12,31	0
0.35Na	23	210	10	200	0.55	0	15,31	0
0.40Na	15	101	12	89	0.50	0	31	0
0.55Na	12	63	10	53	0.35	0	46	0
0.60Na	11	65	10	55	0.40	0	47	0
0.75Na	8	57	9	48	0.35	0	46	0
1.00Na	4	13	10	3	0.04	0	87	0

[a] Yield in grams of solid after treatment per gram of starting SDUSY40; [b]: Micropore volume calculated using the *t*-plot; [c]: Total pore volume adsorbed at $p/p_0 = 0.99$; [d]: Average BJH mesopore size derived from the adsorption branch of the isotherm; [e]: Relative Crystallinity determined by XRD.

Table 3.2Treatment yields, textural and structural properties of alkaline treated SDUSY40 zeolites in 0.05-1.0 M Na_2CO_3.

Sample	Yield [a] (%)	S_{BET} (m^2g^{-1})	S_{micro} [b] (m^2g^{-1})	S_{meso} [b] (m^2g^{-1})	V_t [c] (cm^3g^{-1})	V_{micro} [b] (cm^3g^{-1})	d_p [d] (nm)	RC [e] (%)
SDUSY40	-	617	435	183	0.51	0.23	11,31	51
DS-0.05	98	204	13	191	0.36	0	6.59[f]	0
DS-0.10	94	225	20	205	0.37	0	9.26[f]	0
DS-0.20	88	235	34	201	0.37	0	9.35[f]	0
DS-0.35	87	302	31	271	0.48	0	9.28[f]	0
DS-0.45	86	286	22	264	0.48	0	9.27[f]	0
DS-0.55	82	287	28	259	0.47	0	11.1[f]	0
DS-0.60	78	287	32	255	0.47	0	15.1[f]	0
DS-0.75	75	229	21	208	0.42	0	18.3[f]	0
DS-1.00	72	133	8	125	0.22	0	22.1[f]	0

All notations are the same as in Table 3.1 and [f]: in addition to other peak at ~ 31.0 nm.

In contrast to alkaline treatment with NaOH and Na_2CO_3, the treatment of SDUSY40 in tetraalkylammonium hydroxides showed enhancement of intracrystalline mesoporosity and large preservation of the intrinsic properties of zeolite structure.

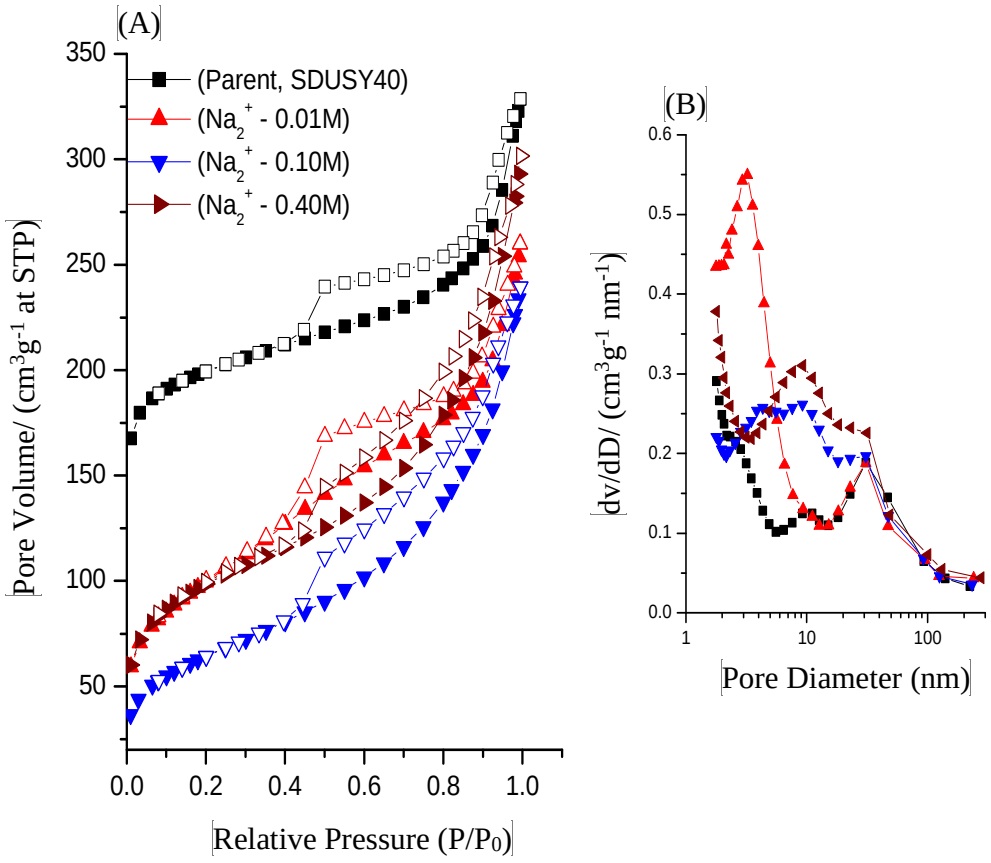

Figure 0.4 N2 adsorption isotherms (A), and (B) the corresponding pore size distributions for parent and alkaline treated SDUSY40 using Na2CO3. The legends in graph (A) also apply to the graph (B).

Specifically, the XRD patterns (Fig. 3.5) show that FAU structure and long-range crystallographic order was preserved upon treatment with tetraalkylammonium hydroxides, in contrast to studied inorganic bases. The patterns also reveal that the intensity of the main XRD reflections reduces with increasing the concentration of tetraalkylammonium hydroxides. The reduction up to 0.15M was less pronounced for TPA+ compared with TEA+ and TMA+, whereas the retention of crystallinity became significantly better for those obtained with TBA+. Table 3.3 and 3.4 show that the RC of SDUSY40 upon treatment with TBA+ up to 0.25 M was ~ 43, whereas the RC upon

treatment with TPA+ (up to 0.15 M), TEA+ (up to 0.10 M) and TMA+ (up to 0.10 M) was in the range of 43-24, 23-14, and 6-2, respectively. However, amorphization was observed for samples obtained with highly concentrated solutions; [TBA+] > 0.50 M, [TPA+] > 0.15 M, and [TMA+] > 0.10M. Surprisingly, no amorphization was observed for samples obtained with highly concentrated TEA+ solutions.

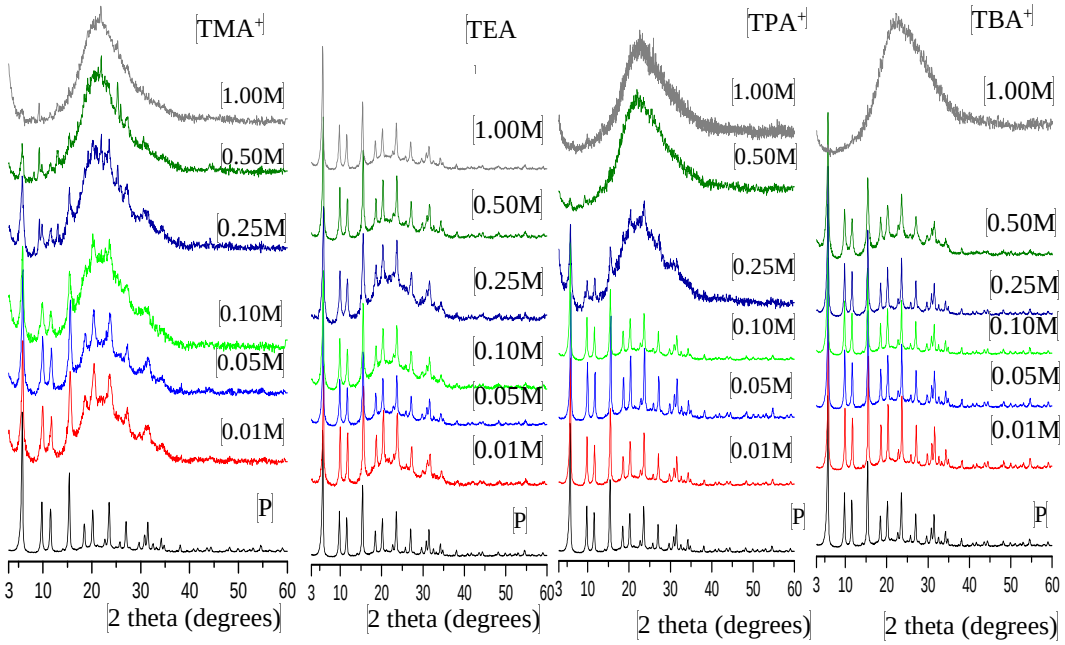

Figure 0.5 XRD patterns of alkaline treated SDUSY40 in different tetraalkylammonium hydroxide solutions in the range of 0.01-1.0 M.

N_2 adsorption-desorption analysis (Fig. 3.6, Tables 3.3-3.4) further confirmed the preservation of the zeolite microposity and the substantial increase in the external surface area in the samples. The N_2 isotherms displayed increased uptake at middle-to-high relative pressures, e.g. enhanced uptake at high pressure (p/p_0 > 0.8), compared to pristine SDUSY40 (Fig. 3.6). The enhanced uptake, which can be ascribed to the interparticle space (the so-called textural mesoporosity), was observed regardless of the nature of

included hydroxides and appears to increase with increasing the concentration. Importantly, N_2 uptake at low relative pressure (p/p_0 < 0.1) was well preserved with respect to SDUSY40, which is in contrast to NaOH based samples that showed drastic reduction in the uptake at low pressures as previously discussed.

The extent of preservation, however, depended on the structure and concentration of included organic hydroxides. Derived textural properties in Table 3.3 indicate that for samples treated with TMA+ up to 0.10M, the substantial increase in the Smeso (357 m^2g^{-1} up from 183 m^2g^{-1} (parent SDUSY40) was accompanied by drastic decrease in the Vmicro (0.06 cm^3g^{-1} down from 0.23 cm^3g^{-1} (parent SDUSY40)). TEA+-treated samples displayed better microposity preservation (0.18-0.12 cm^3g^{-1}) at comparable external surface area increase (Smeso up to 243-343 m^2g^{-1}) up to 0.10M TEA+. Whereas, TPA+-treated samples up to 0.15 M exhibited V micro (0.20-0.14 cm^3g^{-1}) and enhanced Vt (up to 0.86 cm^3g^{-1}) and Smeso (up to 456 m^2g^{-1}). When TBA+ was used, the resulting solid exhibited quite improved textural properties. Table 3.4 reveals that up to 0.25M, the Vmicro remained mostly unaffected (0.22-0.21 cm^3g^{-1}), while significantly enhanced Vt (up to 0.96 cm^3g^{-1}) and Smeso (up to 337 m^2g^{-1}) were attained. The porosity of samples obtained at [TBA+] > 0.50M proves that such high concentration is not suited to generate mesoporosity, as evidenced by the drastic decrease in Vmicro (0.01 cm^3g^{-1}) and Smeso (124 m^2g^{-1}) (Table 3.3).

Table 3.3 Treatment yields, textural and structural properties of alkaline treated SDUSY40 zeolites in 0.05-1.0 M tetraalkylammonium hydroxides (TMAOH, TEAOH, and TPAOH).

Sample	Yield [a] (%)	S_{BET} (m^2g^{-1})	S_{micro} [b] (m^2g^{-1})	S_{meso} [b] (m^2g^{-1})	V_t [c] (cm^3g^{-1})	V_{micro} [b] (cm^3g^{-1})	RC [f] (%)
SDUSY40	-	607	424	183	0.51	0.23	51 (100)
0.05TMA	87	484	155	329	0.56	0.08	4 (12)
0.10TMA	63	477	120	357	0.63	0.06	2 (6)
0.20TMA	30	428	100	328	0.57	0.05	0
0.25TMA	22	360	99	261	0.57	0.05	0
0.40TMA	18	316	96	220	0.55	0.05	0
0.75TMA	14	193	49	144	0.48	0.03	0
1.00TMA	9	173	52	121	0.52	0.03	0
0.05TEA	86	584	345	239	0.52	0.18	26 (51)
0.10TEA	74	598	255	342	0.69	0.14	15 (29)
0.15TEA	65	606	247	359	0.83	0.13	11 (20)
0.20TEA	47	556	207	349	0.91	0.11	10 (18)
0.25TEA	41	541	222	319	0.97	0.11	11 (22)

0.40TEA	41	570	285	284	0.99	0.15	18 (35)
0.50TEA	40	577	300	277	0.98	0.16	18 (35)
0.60TEA	35	542	277	265	1.00	0.15	16 (31)
0.75TEA	48	592	327	265	0.95	0.17	23 (45)
1.00TEA	41	580	322	258	0.97	0.17	22 (43)
0.05TPA	91	615	398	217	0.56	0.21	33 (63)
0.10TPA	80	709	364	345	0.71	0.19	28 (53)
0.15TPA	67	725	271	456	0.86	0.14	24 (47)
0.25TPA	35	519	112	407	0.69	0.06	5 (11)
0.40TPA	18	158	31	127	0.37	0.02	0
0.50TPA	15	131	24	107	0.53	0.01	0
0.75TPA	12	114	20	94	0.55	0.01	0
1.00TPA	10	92	17	75	0.60	0	0

All notations are the same as in Table 3.1.

The BJH-derived pore size distributions (Fig. 3.6(b)) show that in addition to the large mesopores (cavities ~ 31 nm) that are intrinsic to the pristine SDUSY40, other pores are gradually forming within the mesopore range (ca. 3-15 nm). These size distributions are not well-defined as those obtained by organosiliane-directed synthesis [144] or by surfactant-induced reassembly [145]. It was revealed that the pore diameter of these

pores, which is smaller than that of NaOH treatment, increases and broadens with increasing the concentration of tetraalkylammonium hydroxides, e.g. SDUSY40 treated in 0.05M TEA^+ exhibits smaller mesopores (~ 5.57 nm) compared to 7.62 nm and 11.1 nm for treatments in 0.10M and 0.25M, respectively (Table 3.3). It is noteworthy that the treatment of SDUSY40 with TBA^+ caused the appearance of quite broad mesopores, which were formed only at high concentration compared to other alkylammonium hydroxides (Tables 3.3-3.4). Verboekend *et al.* [83] reported the formation of mesopores in USY zeolites (covering the broad range of 2-50 nm, centered at ca. 10 nm) by treatment in (NaOH + TPAOH). Sadowska *et al.* [146] and Abello *et al.* [147] did also report the decrease in the pore diameter when the treatment involved organic hydroxides, though, their studies involved different zeolite topology, i.e. desilication of ZSM-5 in (NaOH + (TPAOH or TBAOH)).

Table 03.4 Treatment yields, textural and structural properties of alkaline treated SDUSY40 zeolites in 0.05-1.0 M tetrabutylammonium hydroxides.

Sample	Yield [a] (%)	S_{BET} (m^2g^{-1})	S_{micro} [b] (m^2g^{-1})	S_{meso} [b] (m^2g^{-1})	V_t [c] (cm^3g^{-1})	V_{micro} [b] (cm^3g^{-1})	d_p [d] (nm)	RC [f] (%)
SDUSY40	-	607	424	183	0.51	0.23	11,31	51 (100)
0.05TBA	94	604	416	188	0.53	0.22	11,31	43 (83)
0.10TBA	85	654	418	236	0.59	0.22	11,31	43 (83)
0.15TBA	73	709	420	289	0.64	0.22	6,11,31	42 (82)
0.20TBA	64	750	425	325	0.89	0.23	6,11,31	35 (67)
0.25TBA	61	757	420	337	0.96	0.22	7,11,31	34 (66)
0.40TBA	47	778	379	399	1.18	0.20	13,31	25 (49)
0.50TBA	42	746	301	445	1.30	0.16	22,45	16 (32)
0.60TBA	22	595	206	389	1.23	0.11		6 (11)
0.75TBA	13	160	36	124	0.58	0.01	-	0
1.00TBA	10	82	15	67	0.44	0	-	0

All notations are the same as in Table 3.1

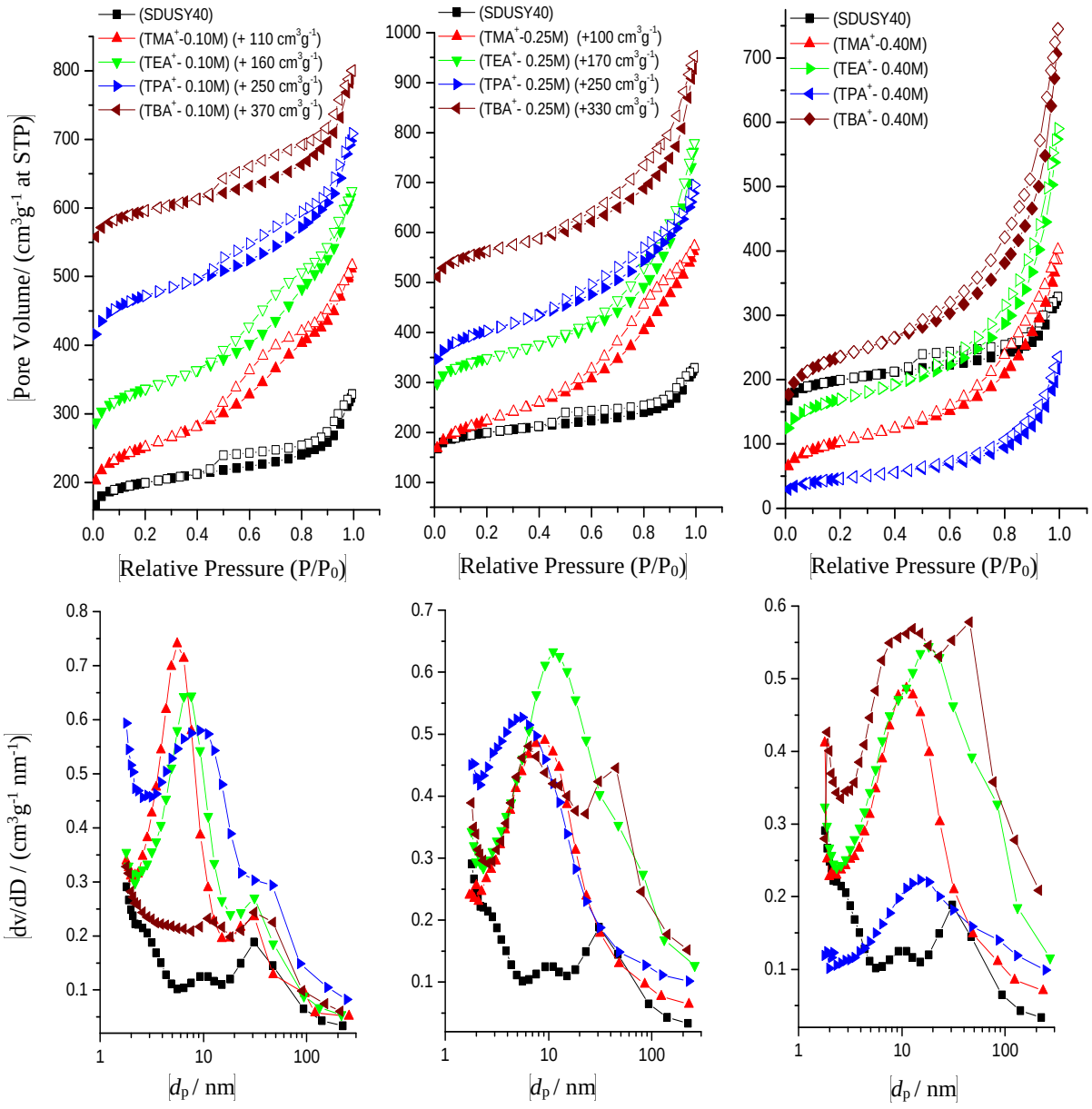

Figure 0.6 N_2 adsorption isotherms (top) and corresponding BJH mesopore size distributions (bottom) for parent and alkaline treated SDUSY40 using tetraalkylammonium hydroxides in the range of 0.10-0.40M. The legends in the top graphs also apply to the graphs shown below them.

3.6.1.2 Elemental Analysis

The ICP-OES analysis of the Si and Al content after treatment of SDUSY40 in NaOH and tetraalkylammonium hydroxides solutions are given in Tables 3.5 and 3.6, respectively. For comparative purposes, the analysis is depicted in Fig. 3.7(A-C). The Si and Al concentration in the filtrates for all samples shows the preferential selectivity of alkaline treatment for Si extraction, which increases with concentration (i.e. the amount of Al in the filtrates was much smaller than Si). This can be attributed to the fact that upon desilication of severely dealuminated USY zeolites (SDUSY40, Si/Al = 40), which is facilitated by the relative high surface area, low framework density, and tightly connected micropores [83], some Al is extracted from the framework and subsequently reinserted in the framework or extra framework (the so-called realumination process) [136].

In a striking difference, less extensive desilication of SDUSY40 zeolite upon treatment in tetraalkylammonium hydroxides was observed compared to NaOH, as suggested by the lower amount of Si in the filtrates. The desilication in tetraalkylammonium hydroxides was greatly influenced by the nature and concentration of organic cation. It was shown that the amount of Si leached to the solution in TMAOH was comparable to that in NaOH within the concentration range of 0.01-1.0 M.

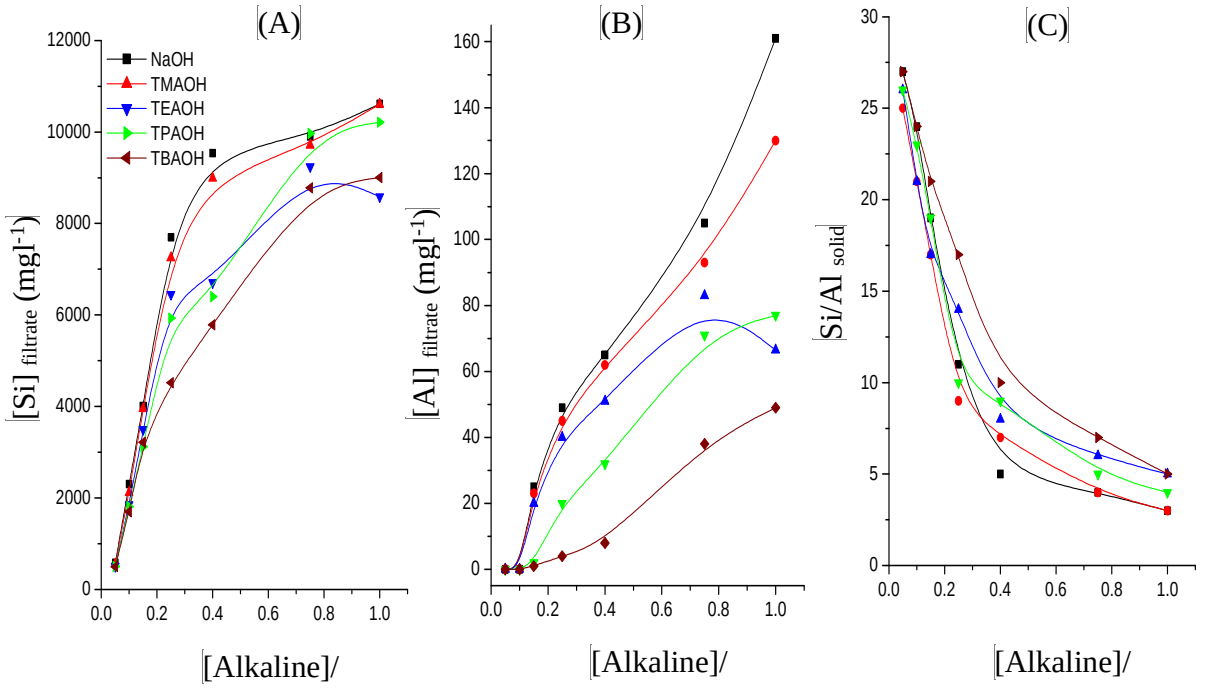

Figure 0.7 Influence of alkaline medium concentration on the amount of Si in the filtrates (A), Al in the filtrates (B), and Si/Al of the solid samples (C).

Table 03.5 Silicon and aluminum content in the solids and filtrates obtained upon alkaline treatment of SDUSY40 with inorganic hydroxides

Sample	Si/Al_{solid} [molmol^{-1}]	Filtrate		
		$(Si/Al)_{filtrate}$ [molmol^{-1}]	$[Si]_{filtrate}$ [mgL^{-1}]	$[Al]_{filtrate}$ [mgL^{-1}]
SDUSY40	32	-	-	-
0.05Na	26	-	583	0
0.10Na	24	-	2303	0
0.35Na	9	-	7697	49
0.45Na	5	-	9538	65
0.55Na	5	-	9626	74
0.75Na	4	-	9907	105
1.00Na	3	-	10613	161

Table 03.6 Silicon and aluminum content in the solids and filtrates obtained upon alkaline treatment of SDUSY40 in tetraalkylammonium hydroxides

Sample	Si/Al_{solid} [$molmol^{-1}$]	Filtrate		
		$(Si/Al)_{filtrate}$ [$molmol^{-1}$]	$[Si]_{filtrate}$ [mgL^{-1}]	$[Al]_{filtrate}$ [mgL^{-1}]
SDUSY40	32	-	-	-
0.05TMA	26	-	558	0
0.10TMA	24	-	2120	0
0.25TMA	9	161	7250	45
0.40TMA	7	145	8991	62
0.75TMA	4	104	9713	93
1.00TMA	3	82	10608	130
0.05TEA	26	-	1623	0
0.10TEA	22	1271	2542	2
0.25TEA	15	139	9472	68
0.40TEA	15	109	8425	77
0.60TEA	15	81	10005	123

0.75TEA	18	78	7000	90
1.00TEA	17	69	6750	98
0.05TPA	27	-	504	0
0.10TPA	25	-	1812	0
0.15TPA	19	1560	3120	2
0.25TPA	10	297	5931	20
0.40TPA	9	200	6401	32
0.75TPA	5	140	9968	71
1.00TPA	4	133	10214	77
0.05TBA	27	-	499	0
0.10TBA	25	-	1700	0
0.15TBA	21	3218	3218	1
0.25TBA	17	1129	4516	4
0.40TBA	14	494	6920	14
0.60TBA	9	261	9150	35
0.75TBA	7	239	9100	38
1.00TBA	5	184	9003	49

On the contrary, TBAOH exhibited the lowest reactivity towards Si extraction (with the exception of highly concentrated 1.0 M solution of TEAOH, which was less reactive than corresponding TBAOH) (Fig. 3.7a). The reactivity appears to follow; TBAOH < TPAOH < TEAOH < TMAOH ≈ NaOH. The amount of Al in the filtrates remained much smaller than that of Si, with TBAOH exhibiting the lowest amount of leached Al; i.e. $[Al]_{filtrate}$ at 0.25 M in TMA^+ (45 mgl^{-1}), TEA^+ (40 mgl^{-1}), TPA^+ (20 mgl^{-1}), and TBA^+ (4 mgl^{-1}) compared to 49 mgl^{-1} for Na^+. Accordingly, the $(Si/Al)_{filtrate}$ was around 7 times higher in TBAOH than in NaOH; i.e. at 0.25M, the $(Si/Al)_{filtrate}$ for TBAOH was 1129 compared to 297, 161, 161 and 157 for TPAOH, TEAOH, TMAOH and NaOH, respectively (Tables 3.5-3.6). Thus, it can be inferred that lower degree of aluminum leaching occurs with organic alkylammonium hydroxides, which implies that TBAOH and to a lesser extent TPAOH facilitated the re-alumination of the zeolite. The $(Si/Al)_{solid}$ of SDUSY40 dropped from 32 to 17 (TBA^+), 10 (TPA^+), 14 (TEA^+), 10 (TMA^+) and 9 (Na^+).

3.6.1.3 Morphology

The SEM images of parent and alkaline treated SDUSY40 are shown in Fig. 3.8. As it can be seen, the octahedral morphology characteristic of faujasite-type USY zeolite is clearly visible for parent SDUSY40. Upon treatment in NaOH or tetraalkylammonium hydroxides, the morphology of zeolite remained unchanged without any clear sign of globular particles, rugged surfaces or cracks. However, the average particle size of SDUSY40 dropped slightly from ~600 nm to ~550 nm upon treatment in NaOH, with the samples obtained upon treatment in tetraalkylammonium hydroxides exhibiting much

smaller particle sizes (~450-500 nm). Figures 3.9 and 3.10 show the TEM images showing the presence of homogenous distribution of mesopores.

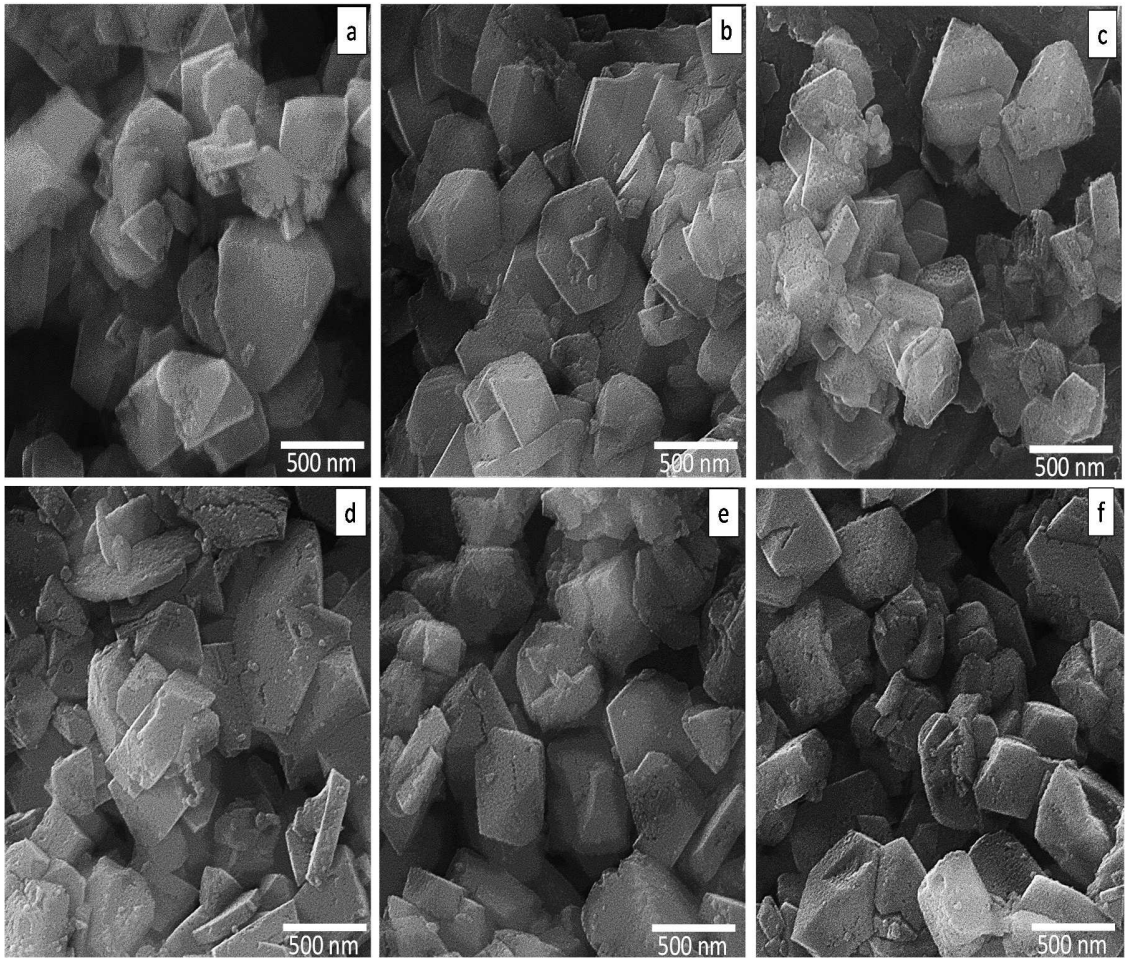

Figure 0.8 SEM images of the parent SDUSY40 (a) and treated samples; Na^+-0.10M (b), TMA^+-0.10M (c), TEA^+-0.10M (d), TPA^+-0.10M (e) and TBA^+-0.10M (f).

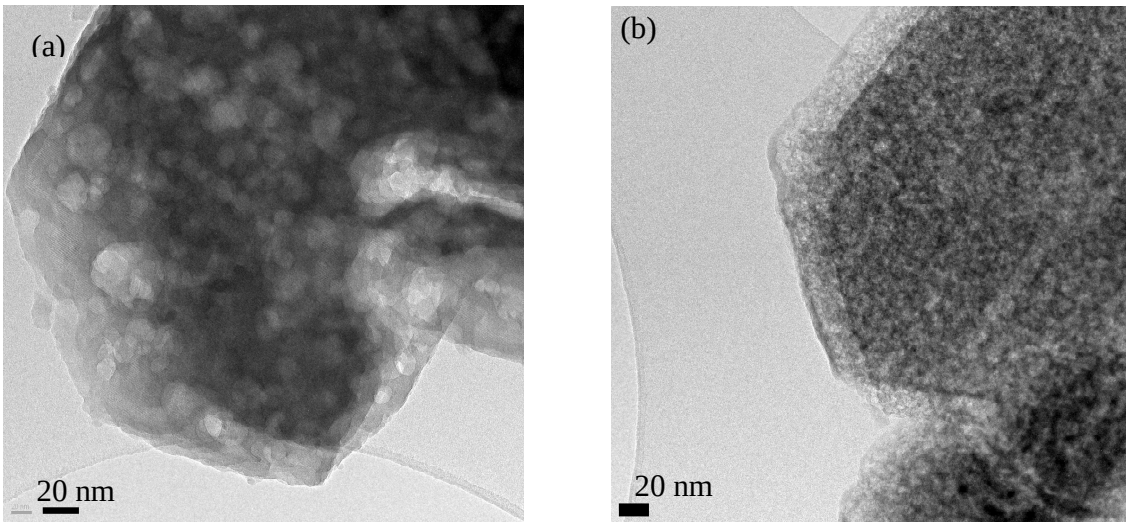

Figure 0.9 TEM images of the parent SDUSY40 (a) and NaOH (0.10M) treated SDUSY40 (b).

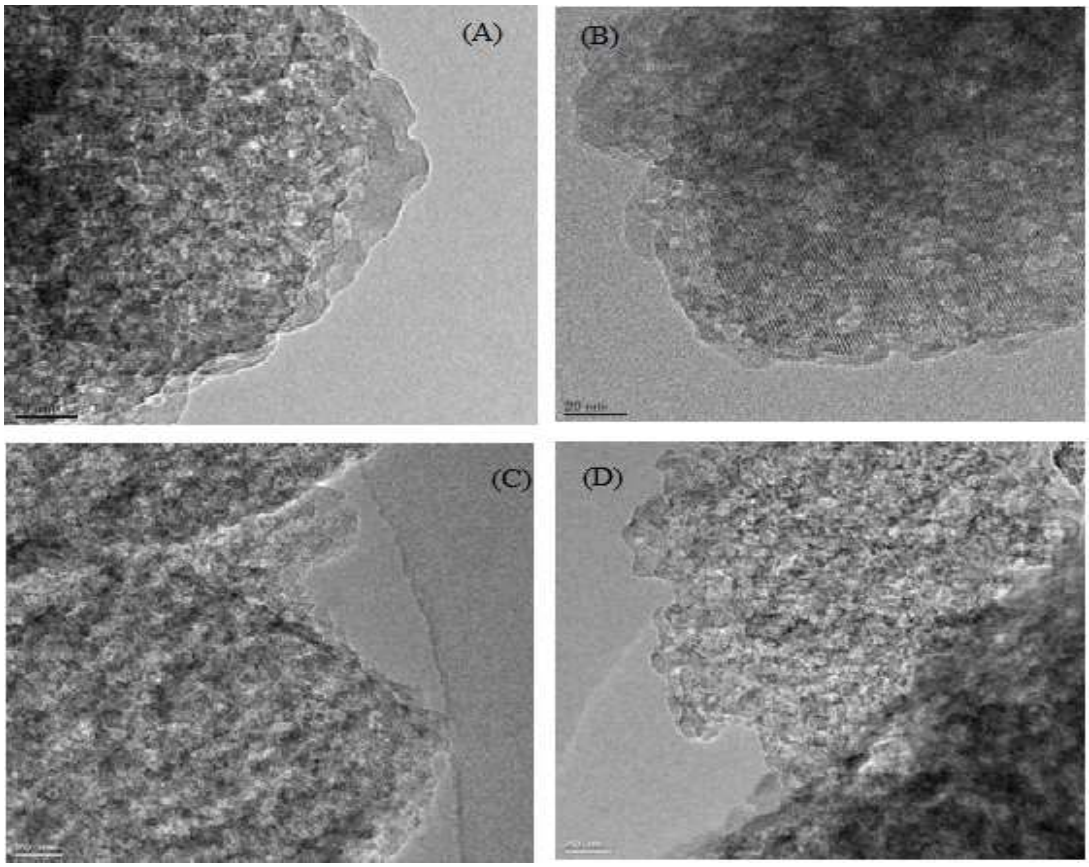

Figure 0.10 TEM images of the tetraalkylammonium hydroxides treated SDUSY40 (at 0.10M); TMA^+ (A), TEA^+ (B), TPA^+ (C) and TBA^+ (D).

3.6.2 Alkaline Treatment of SDUSY40 with Alkaline Double Mixtures

To further investigate the positive influence of tetrabutylammonium cations (TBA^+) treatment in the porosity and crystallinity of SDUSY40 zeolites, the treatment was extended to double alkaline mixture approach. In particular, two types of double mixtures were explored; i) TBA^+ + NaOH and ii) TBA^+ + organic tetraalkylammonium cations (i.e. TMA^+, TEA^+ or TPA^+).

3.6.2.1 Double Mixture of NaOH + TBAOH

Exposure of SDUSY40 zeolites to standard NaOH treatments up to 0.20 M resulted in the development of S_{meso} up to 279 m^2g^{-1} with a complete loss of microposity and crystallinity (Table 3.1, Fig. 3.2). However, when TBA^+ was included in the alkaline NaOH solution of optimum concentration, the resulting solids exhibited remarkable improvements in the microporosity and crystallinity combined with an increase in the S_{meso}.

Table 3.7 summarizes the textural, structural and yield parameters of SDUSY40 zeolites treated in 0.15M TBA^+ + NaOH in the range of 0.05-1.0 M. N_2 isotherms of samples obtained by double mixture (0.15M TBA^+ + up to 0.20M NaOH) showed increased uptakes at both low and middle-to-high relative pressures, compared to NaOH treated samples (Fig. 3.11). Accordingly, the V_{micro} was in the range of 0.22-0.19 cm^3g^{-1} accompanied with an increase in the S_{meso} up to 444 m^2g^{-1}. The corresponding NaOH treated samples exhibited complete loss of microposity and S_{meso} of 279-53 m^2g^{-1}. In contrast, treatments in solutions containing highly concentrated NaOH (0.15M TBA^+ +

[NaOH] > 0.60M) resulted in complete loss in porosity, a scenario that is similar to NaOH treatments.

The XRD patterns (Fig. 3.12) further demonstrated the positive influence of TBA^+ in the alkaline solution, as suggested by the dramatic preservation of the long-range ordering and crystallinity. The RC of SDUSY40 zeolites after treatment in 0.15TBA^+ + 0.05-0.20 M NaOH was in the range of 43-22, compared to amorphous NaOH treated samples (Table 3.7). Complete loss in crystallinity was observed for those treated in alkaline double mixtures containing highly concentrated NaOH solutions (Fig. 3.12).

Table 0.7 Treatment yields and textural-structural properties of alkaline treated SDUSY40 zeolites in 0.15M TB + 0.05-1.0 M NaOH.

Sample	Yield [a] (%)	S_{BET} (m^2g^{-1})	S_{micro} [b] (m^2g^{-1})	S_{meso} [b] (m^2g^{-1})	V_t [c] (cm^3g^{-1})	V_{micro} [b] (cm^3g^{-1})	d_p [d] (nm)	RC [e] (%)
SDUSY40	-	617	435	182	0.51	0.23	11,31	51 (100)
TBA-0.15	73	709	420	289	0.64	0.22	6,11,31	42
TBA-DS0.05	65	682	370	312	0.83	0.20	31	30
TBA-DS0.10	53	701	344	357	1.00	0.18	31	23
TBA-DS0.20	56	720	357	362	1.00	0.19	31	26
TBA-DS0.30	27	808	346	462	1.33	0.19	44	18
TBA-DS0.30-IE	-	671	277	394	1.22	0.15	-	13

TBA-DS0.40	21	793	379	414	1.62	0.19	42	18
TBA-DS0.50	16	702	421	281	1.37	0.22	45	24
TBA-DS0.55	13	690	449	241	1.12	0.24	44	25
TBA-DS0.60	10	638	447	191	1.04	0.23	45	32
TBA-DS0.65	9	604	444	160	0.86	0.23	45	35
TBA-DS0.75	6	279	189	90	0.54	0.09	46	11
TBA-DS1.00	3	12	7	5	0.05	0.00	-	0

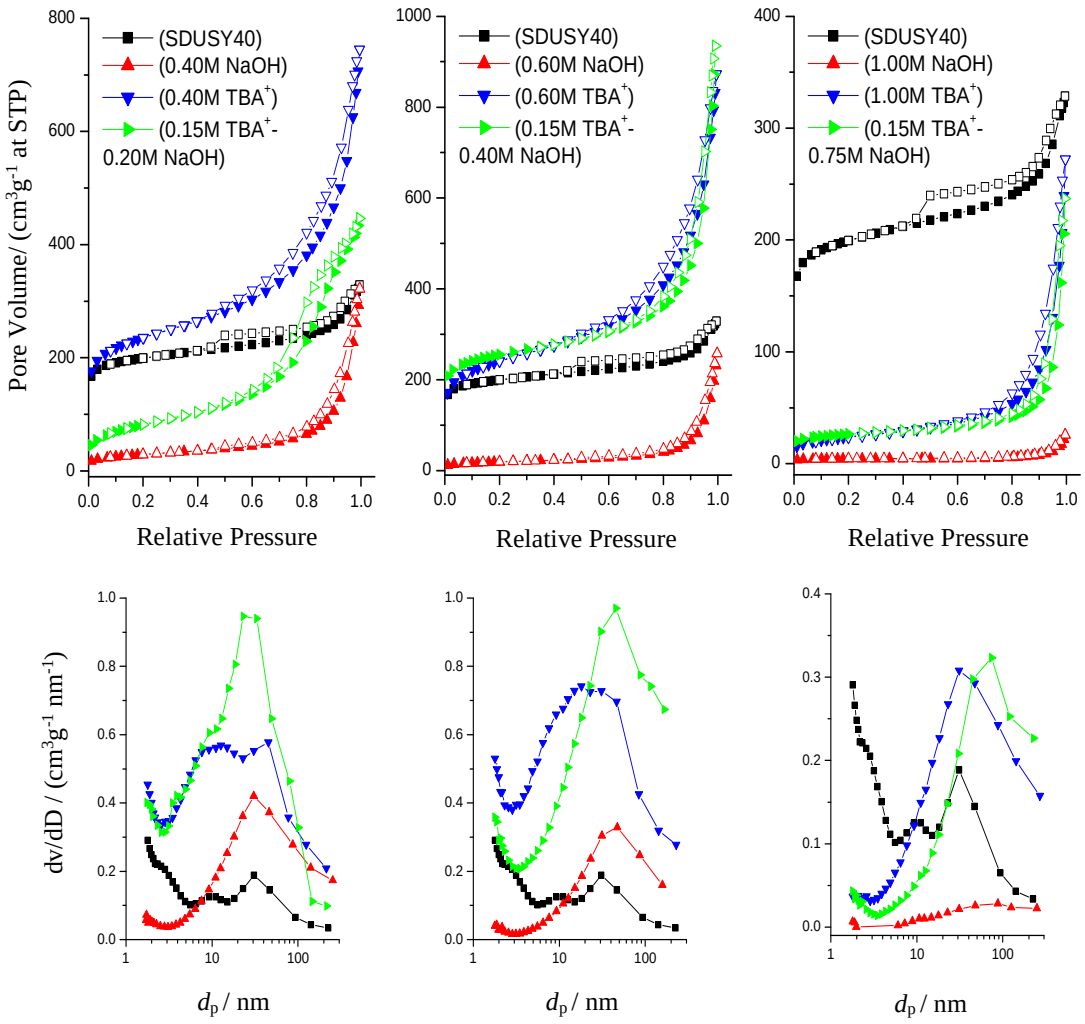

Figure 0.11 N_2 adsorption isotherms (top) and corresponding BJH mesopore size distributions (bottom) for parent and treated SDUSY40 in alkaline double mixture of 0.15M TBA^+ + 0.20-1.00M NaOH. The legends in the top graphs also apply to the graphs shown below them.

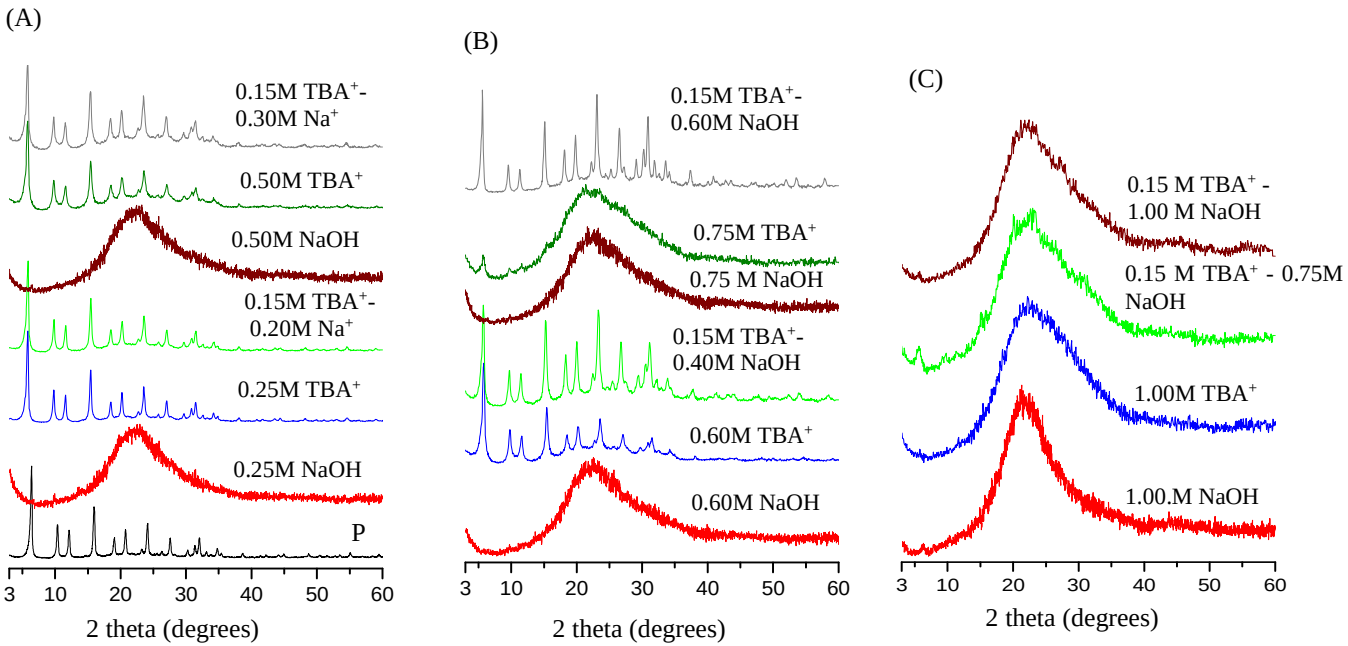

Figure 0.12 XRD patterns of treated SDUSY40 in alkaline double mixture of 0.15M TBA^+ + 0.10-1.00M NaOH; (A) 0.15M TBA^+ + up to 0.20M NaOH. (B) 0.15M TBA^+ + 0.40-0.60M NaOH, and (D) 0.15M TBA^+ + 1.00M NaOH.

3.6.2.2 Double Mixture of TBAOH + tetraalkylammonium hydroxides (TMAOH, TEAOH or TPAOH)

When treatments of SDUSY40 zeolites were done in the presence of mixture of tetraalkylammonium hydroxides at the optimum concentration, the preservation of microporosity and crystallinity, and the increase in the external surface area were even more striking than those noted for NaOH + TBA^+ mixtures. Full overview of the individual influence of each organic template on the parent SDUSY40 zeolite through the double tetraalkylammonium hydroxides mixture treatment is shown in Table 3.8.

Table 03.8 Treatment yields, textura and structural properties of alkaline treated SDUSY40 zeolites in 0.15M TBA + x organic hydroxide (TMA, TEA and TPA) (x = 0.05-0.75 M).

Sample	Yield [a] (%)	S_{BET} (m^2g^{-1})	S_{micro} [b] (m^2g^{-1})	S_{meso} [b] (m^2g^{-1})	V_t [c] (cm^3g^{-1})	V_{micro} [b] (cm^3g^{-1})	d_p [d] (nm)	RC [e] (%)
SDUSY40-TBA-0.15-TMA-0.05	74	788	400	388	0.81	0.21	6[f]	37 (72)
SDUSY40-TBA-0.15-TMA-0.10	67	775	374	401	0.97	0.19	9[f]	33 (64)
SDUSY40-TBA-0.15-TMA-0.25	47	789	325	464	1.30	0.17	16[f]	20 (39)
SDUSY40-TBA-0.15-TMA-0.50	22	634	201	433	1.21	0.11	18[f]	5 (9)
SDUSY40-TBA-0.15-TMA-0.75	17	111	42	69	0.29	0.02	31	0
SDUSY40-TBA-0.15-TEA-0.05	73	744	433	311	0.80	0.23	7[f]	37 (72)
SDUSY40-TBA-0.15-TEA-0.10	68	784	420	364	0.92	0.22	7[f]	31 (60)
SDUSY40-TBA-0.15-TEA-0.25	62	870	419	451	1.22	0.22	15[f]	31 (61)

SDUSY40-TBA-0.15-TEA-0.50	35	855	312	543	1.56	0.16	18[f]	10 (18)
SDUSY40-TBA-0.15-TEA-0.75	17	424	139	285	0.86	0.07	18[f]	7 (13)
SDUSY40-TBA-0.15-TPA-0.05	75	725	438	286	0.74	0.23	7[f]	47 (91)
SDUSY40-TBA-0.15-TPA-0.10	72	782	430	338	0.87	0.23	8[f]	41 (78)
SDUSY40-TBA-0.15-TPA-0.25	48	842	320	522	1.30	0.17	18[f]	16 (32)
SDUSY40-TBA-0.15-TPA-0.50	10	281	75	206	0.69	0.02	31	0
SDUSY40-TBA-0.15-TPA-0.75	5	143	38	105	0.31	0.01	40	0

All notations are the same as in Table 3.2.

Figure 3.13 highlights the relation between these organic cations (in terms of structure and concentration) and the yield, RC, S_{meso} and V_{micro} for SDUSY40 zeolites treated at $0.15TBA^+$ + (TMA^+, TEA^+ or TPA^+) in the range of 0.05-0.75M. It is seen there that the S_{meso} exhibited a volcano-type dependence for all double mixtures, with the maximal values exceeding 400 m^2 g^{-1} in the SDUSY40-0.15TBA-0.25TEA where the S_{meso} was enhanced with concurrent preservation of the microporosity. The RC and yield decreased with increasing the concentration, though, TEA^+ samples exhibited the lowest extent of reduction.

To illustrate more on the effects of double organic treatment, Table 3.9 presents comparative examples of selected SDUSY40 zeolites after treatment in double mixtures and corresponding single tetraalkylammonium cation. The N_2 isotherms and BJH-PSDs are shown in Fig. 3.14, whereas the XRD patterns are depicted in Fig. 3.15.

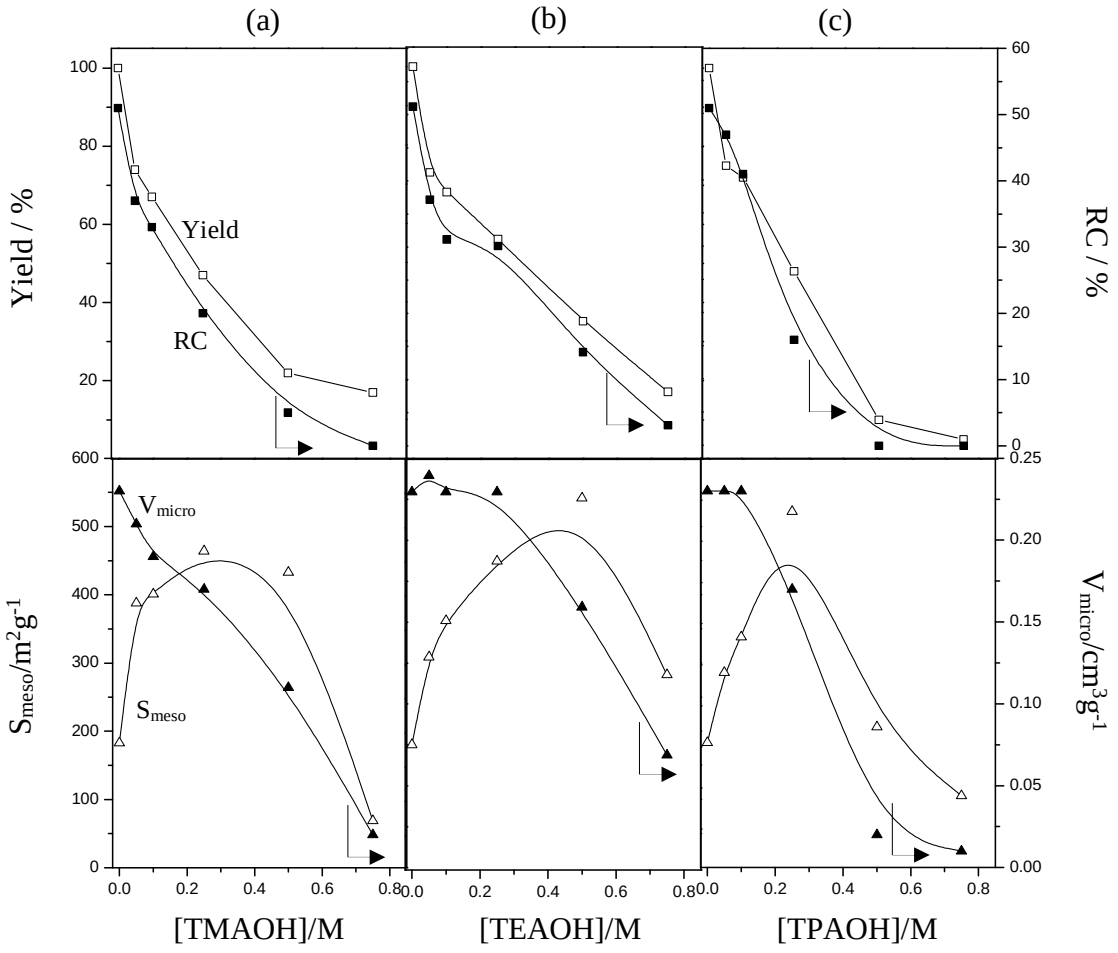

Figure 0.13 Influence of a) TMA^+, b) TEA^+, and c) TPA^+ treatments (at fixed TBA^+ of 0.15M) on yield (open squares), relative crystallinity (solid squares), mesopore surface area (open triangles), and micropore volume (closed triangles) of the SDUSY40. The pristine SDUSY40 zeolite is represented at 0 M.

Table 03.9 Treatment yields and textural-structural properties of alkaline treated SDUSY40 zeolites in 0.15M TBA + x organic hydroxide (TMA, TEA and TPA) (x = 0.05-0.25M).

Sample	Yield [a] (%)	S_{BET} (m^2g^{-1})	S_{micro} [b] (m^2g^{-1})	S_{meso} [b] (m^2g^{-1})	V_t [c] (cm^3g^{-1})	V_{micro} [b] (cm^3g^{-1})	RC [e] (%)
SDUSY40	-	607	424	183	0.51	0.23	51 (100)
SDUSY40-TBA0.20	64	750	425	325	0.89	0.23	35 (67)
SDUSY40-TBA0.25	61	742	405	337	0.96	0.21	39
SDUSY40-TBA0.40	48	759	361	398	1.15	0.19	30
SDUSY40-TBA0.45	42	789	351	437	1.21	0.18	17 (34)
SDUSY40-0.15TBA-0.05TMA	74	788	400	388	0.81	0.21	37 (72)
SDUSY40-0.15TBA-0.10TMA	64	775	374	401	0.97	0.19	33 (64)
SDUSY40-0.15TBA-0.25TMA	47	789	325	464	1.30	0.17	20 (39)

SDUSY40-TMA0.10	63	477	120	357	0.63	0.06	2
SDUSY40-TMA0.25	30	428	100	328	0.57	0.05	0
SDUSY40-TMA0.40	22	360	99	261	0.57	0.05	0
SDUSY40-TBA0.15-TEA0.05	73	744	433	311	0.80	0.23	37 (72)
SDUSY40-TBA0.15-TEA0.10	68	784	420	364	0.92	0.22	31 (60)
SDUSY40-TBA0.15-TEA0.25	62	870	419	451	1.22	0.22	31 (60)
SDUSY40-TBA0.15-TEA0.25	54	883	402	481	1.24	0.21	32
SDUSY40-TEA0.20	47	556	207	349	0.91	0.11	10 (18)
SDUSY40-TEA0.25	41	541	222	319	0.97	0.11	11 (22)
SDUSY40-TEA0.40	41	570	285	284	0.99	0.15	18 (35)
SDUSY40-TEA0.45	34	520	251	268	0.97	0.13	14 (27)

SDUSY40-TBA0.15-TPA0.05	75	725	438	286	0.74	0.23	47 (91)
SDUSY40-TBA0.15-TPA0.10	72	768	430	338	0.87	0.23	41 (78)
SDUSY40-TBA0.15-TPA0.25	48	842	320	522	1.30	0.17	16 (32)
SDUSY40-TPA0.15	67	725	271	456	0.86	0.14	24
SDUSY40-TPA0.25	35	519	112	407	0.69	0.06	5
SDUSY40-TPA0.40	18	158	31	127	0.37	0.02	0

All notations are the same as in Table 3.1

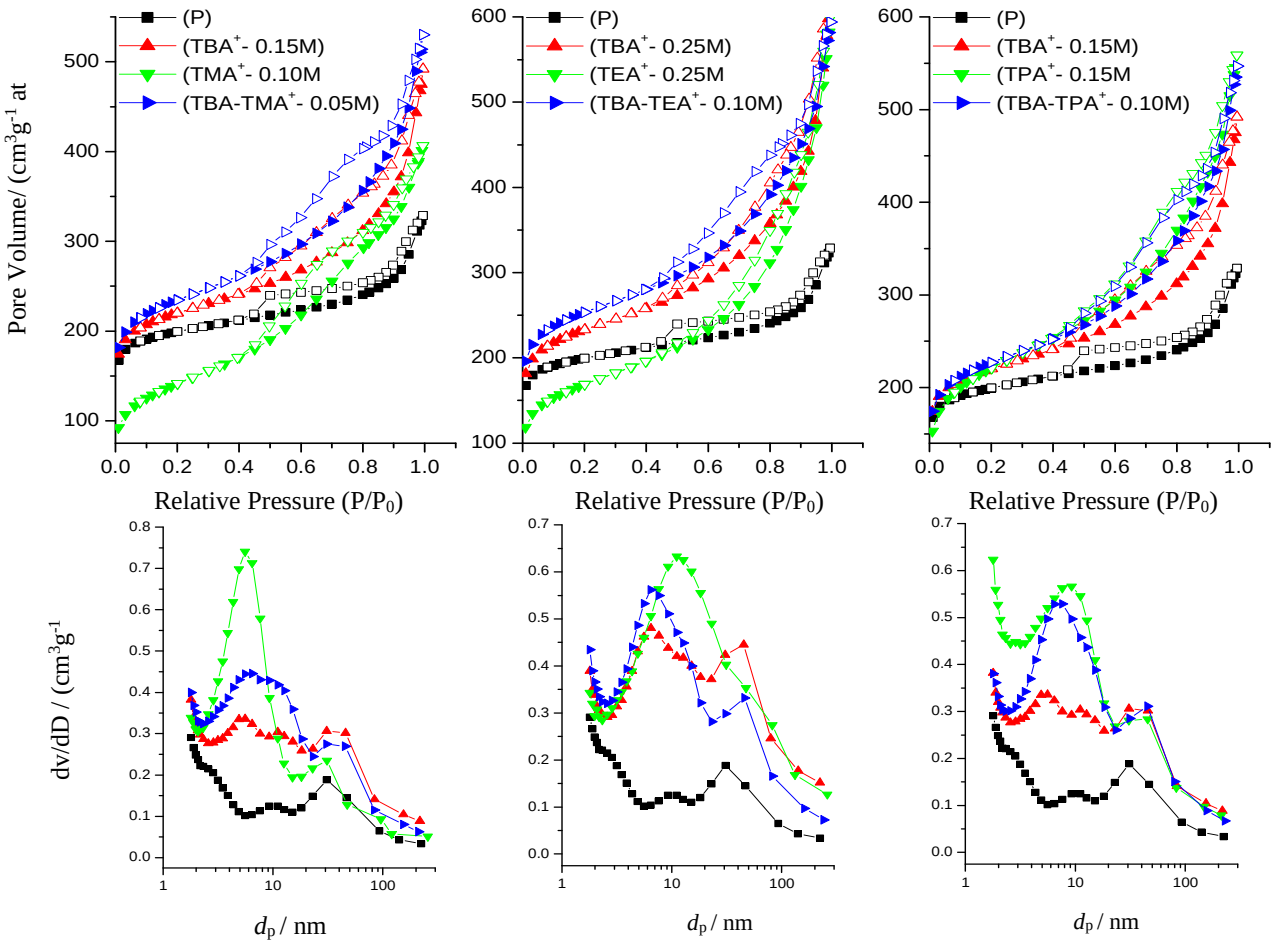

Figure 0.14 N_2 adsorption isotherms (top) and corresponding BJH mesopore size distributions (bottom) for SDUSY40 treated with mixture of tetraalkylammonium hydroxides in the range of 0.05-0.25M. The legends in the top graphs also apply to the graphs shown below them.

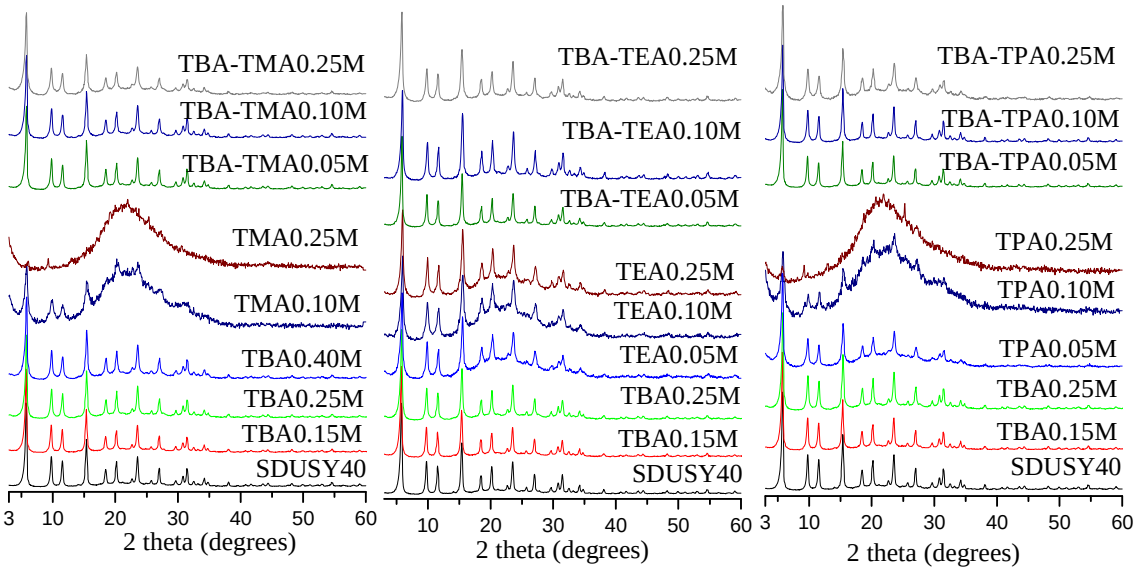

Figure 0.15 XRD patterns of SDUSY40 treated with mixture of tetraalkylammonium hydroxide solutions in the range of 0.05-0.25 M.

SDUSY40 treated in mixture of ($0.15TBA^+ + 0.25TEA^+$) displayed a similar N_2 uptake at $p/p_0 > 0.1$ compared to SDUSY40-TEA-0.40, but the uptake at low relative pressures ($p/p_0 < 0.1$) was fully preserved with respect to parent SDUSY40 (Fig. 3.14b). The corresponding BJH PSDs of SDUSY40-0.15TBA-0.25TEA (bottom part of Fig. 3.14b) reveal that in addition to the large cavities (~ 31 nm), there were mesopores of ca. 15 nm, which are slightly smaller than those observed for 0.40 TEA samples (*ca.* 18 nm).

Accordingly, the derived textural properties showed that SDUSY40-0.15TBA-0.25TEA displayed a V_{micro} of 0.22 cm^3g^{-1} and a S_{meso} of 451 m^2g^{-1}, compared to V_{micro} of 0.13 cm^3g^{-1} and S_{meso} of 301 m^2g^{-1} (SDUSY40-0.40TEA). The crystallinity loss determined by X-ray diffraction patterns (Fig. 3.15, Table 3.9) was limited to 40%, compared to 70% for SDUSY40-0.40TEA. Moreover, the yield of solid after treatment was about 57%, compared with 41% for 0.40M TEA^+ (Table 3.9), suggesting a lower extent of solid leaching. It can be also seen that double mixtures based samples exhibited higher Si/Al ratios compared to the ones obtained after treatments with single hydroxides, i.e. the Si/Al decreased from 32 (parent SDUSY40) to 16 (0.15TBA-0.25TEA), compared to 8 (0.40TEA). The analysis of filtrate solutions (Table 3.10) revealed that 0.15TBA-0.25TEA samples exhibited lower amount of leached aluminum (21 mgL^{-1}) compared to 51 mgL^{-1} for 0.40TEA.

Treatments involving other double organic mixtures; namely ($TBA^+ + TMA^+$) and ($TBA^+ + TPA^+$), also resulted in improved textural and structural properties compared to those performed in corresponding single template. However, they appear to be less effective than ($TBA^+ + TEA^+$) mixture. Table 3.9 shows that 0.15TBA-0.10TMA sample displayed a V_{micro} of 0.19 cm^3/g and a S_{meso} of 401 m^2/g, compared to V_{micro} of 0.05 cm^3/g

and S_{meso} of 328 m^2g^{-1} (SDUSY40-0.25TMA). SDUSY40-0.15TBA-0.25TPA sample exhibited substantial increase in S_{meso} (522 m^2g^{-1}) at the expense of microposity (0.17 cm^3g^{-1}), compared to V_{micro} of 0.02 cm^3g^{-1} and S_{meso} of 127 m^2g^{-1} (SDUSY40-0.40TPA).

Table 3.10 Silicon and aluminum content in the solids and filtrates obtained upon alkaline treatment of SDUSY40 in double tetraalkylammonium hydroxides mixture and corresponding single hydroxides.

Sample	Si/Al_{solid} [$molmol^{-1}$]	Filtrate		
		$(Si/Al)_{filtrate}$ [$molmol^{-1}$]	$[Si]_{filtrate}$ [mgL^{-1}]	$[Al]_{filtrate}$ [mgL^{-1}]
SDUSY40	32	-	-	-
0.15M TBA + x M TMA, TEA, TPA (x = 0.05-1.0 M)				
SDUSY40-0.15TBA0.05TMA	22	956	2868	3
SDUSY40-0.15TBA0.10TMA	19	717	3587	5
SDUSY40-0.15TBA0.25TMA	14	337	5727	17
SDUSY40-0.15TBA-0.50TMA	8	109	9627	88
SDUSY40-0.15TBA-0.75TMA	9	47	10475	225
SDUSY40-0.15TBA-1.00TMA	7	45	10502	234
SDUSY40-0.15TBA-0.05TEA	22	744	2974	4
SDUSY40-0.15TBA-0.10TEA	19	681	4085	6

SDUSY40-0.15TBA-0.25TEA	16	247	5177	21
SDUSY40-0.15TBA-0.25TEA	16	318	6670	21
SDUSY40-0.15TBA-0.25TEA-IE	16	-	-	-
SDUSY40-0.15TBA-0.50TEA	12	109	9460	87
SDUSY40-0.15TBA-0.75TEA	6	42	9850	236
SDUSY40-0.15TBA-1.00TEA	6	33	10050	304
SDUSY40-0.15TBA-0.05TPA	22	1261	2522	2
SDUSY40-0.15TBA-0.10TPA	20	828	3313	4
SDUSY40-0.15TBA-0.25TPA	13	717	5735	8
SDUSY40-0.15TBA-0.50TPA	5	346	9350	27
Corresponding monocomponent Mixture				
SDUSY40-0.20TMA	14	350	6300	18
SDUSY40-0.25TMA	9	161	7250	45
SDUSY40-0.40TMA	7	145	8991	62
SDUSY40-0.20TEA	15	224	8062	36
SDUSY40-0.25TEA	15	139	9472	68
SDUSY40-0.40TEA	15	109	8425	77

SDUSY40-0.25TPA	10	297	5931	20
SDUSY40-0.40TPA	9	200	6401	32
SDUSY40-0.20TBA	20	1606	4817	3
SDUSY40-0.25TBA	17	1129	4516	4
SDUSY40-0.40TBA	14	494	6920	14

3.6.3 Acidic Properties

The ^{27}Al MAS NMR spectra of parent and treated SDUSY40 are shown in figure 3.16(f). Parent SDUSY40 exhibits two broad resonance lines at ~57 and 0 ppm, which are feature of tetrahedral framework Al (T_d) and octahedral extra framework Al (O_h) (generated by severe dealumination), respectively. The spectra of NaOH treated samples (Fig. 3.17(a)) reveal the presence of only tetrahedral Al sites, suggesting the realumination of the extra-framework Al upon desilication [83]. However, treatment in tetraalkylammonium hydroxides appears to prevent the realumination of extra-framework species as suggested by the appearance of octahedral sites (Fig. 3.17(b-c)). Careful examination of these spectra reveals that increasing the concentration of TPA^+ (> 0.25M) and TBA^+ (> 0.15M) appears to favor the realumination (Fig. 3.16). It is worth noting that these findings are in agreement with ICP-OES measurements, which show low amount of Al in the filtrates.

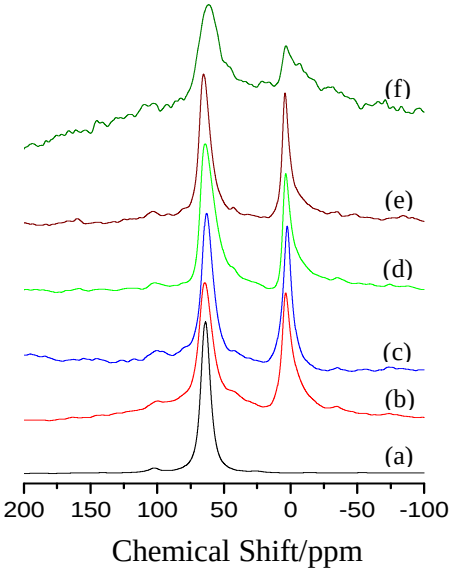

Figure 0.16 ^{27}Al MAS NMR spectra for parent HY and dealuminated USY zeolites; a) HY (Si/Al = 2.3), b) USY (Si/Al = 2.6), c) VSUSY (Si/Al = 6), d-f) SDUSY of Si/Al = 15, 30 and 40, respectively.

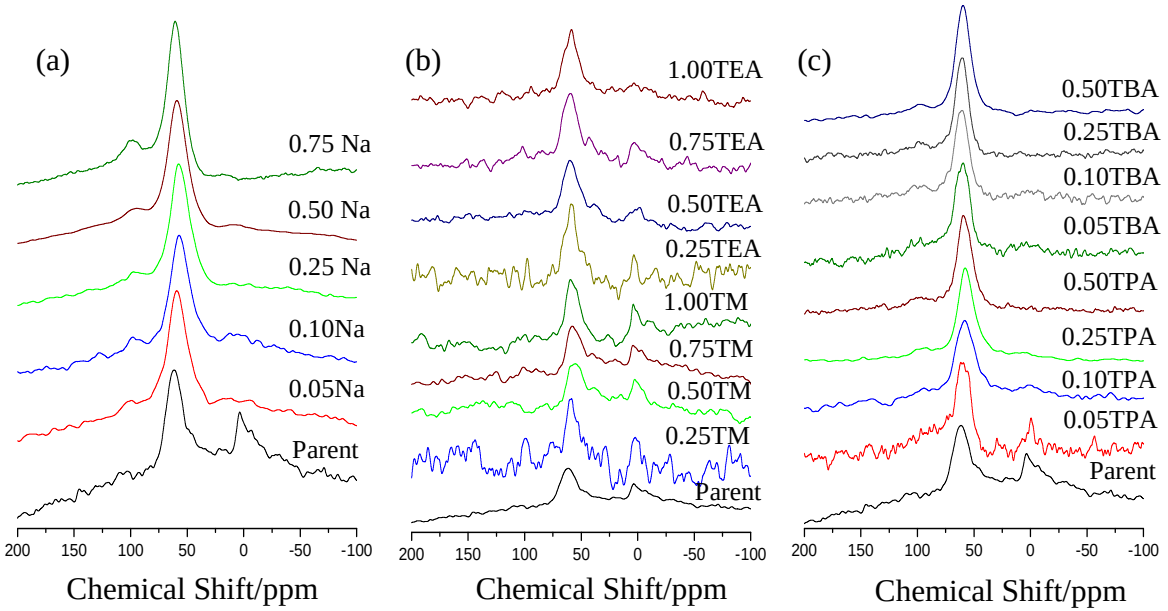

Figure 0.17 ^{27}Al MAS NMR spectra for parent and treated SDUSY40 in NaOH and organic tetraalkyl ammonium hydroxides in the range of 0.05-1.0 M; (a) NaOH, (b) TMA^+ and TEA^+, and (c) TPA^+ and TBA^+.

3.6.4 Alkaline Treatments of dealuminated Y zeolites of lower Si/Al (Si/Al = 30-15)

The lower Si/Al dealuminated Y-zeolites (SDUSY30 and SDUSY15) have more aluminum species in the framework to imply more acid centers than in SDUSY40. Figure 3.16(d-e) show that these Al species are largely present in the octahedral position and these offer internal PDA role in reducing the extent of silicon dissolution and thus reduce the extent of mesopore generation as compared to in SDUSY40. Tables 3.11-3.14 summarize the yield, structural and textural properties of some treated SDUSY15 with mono and binary mixture of alkaline solution(s).

Table 03.11 Treatment yields, textural and structural properties of alkaline treated SDUSY15.

Sample	Yield [a] (%)	S_{BET} (m^2g^{-1})	S_{micro} [b] (m^2g^{-1})	S_{meso} [b] (m^2g^{-1})	V_t [c] (cm^3g^{-1})	V_{micro} [b] (cm^3g^{-1})	d_p [d] (nm)	RC [e] (%)
SDUSY15	-	765	519	246	0.56	0.27	8,23	67 (100)
SDUSY15-0.05Na	98	441	34	410	0.42	0.02	3,8,23	0
SDUSY15-0.10Na	86	383	39	344	0.44	0.02	3,8,23	0
SDUSY15-0.20Na	56	365	44	321	0.66	0.02	8,25	0
SDUSY15-0.35Na	32	269	13	256	0.80	0	15	0
SDUSY15-0.40Na	30	191	15	176	0.72	0	18	0
SDUSY15-0.55Na	21	132	15	117	0.56	0	22	0
SDUSY15-0.05Na_2	100	464	47	417	0.45	0.02	2,8,23	0

SDUSY15-0.10Na_2	94	333	39	294	0.33	0.02	3,8,23	0
SDUSY15-0.20Na_2	95	206	23	182	0.31	0.01	3,8,23	0
SDUSY15-0.10TMA	83	770	414	356	0.65	0.22	3,9,31	44 (66)
SDUSY15-0.20TMA	66	851	409	442	0.92	0.21	5,11,31	37 (55)
SDUSY15-0.45TMA	51	890	390	500	1.17	0.21	7,13,44	29 (43)
SDUSY15-0.10TEA	83	817	500	317	0.68	0.26	3,11,31	60 (89)
SDUSY15-0.25TEA	78	824	501	323	0.72	0.26	4,11,30	55 (83)
SDUSY15-0.30TEA	71	814	497	317	0.85	0.26	6,13,46	54 (80)
SDUSY15-0.35TEA	68	815	500	315	0.86	0.26	5,13,40	54 (80)
SDUSY15-0.45TEA	66	820	501	320	0.88	0.26	4,13,40	53 (79)
SDUSY15-0.10TPA	91	783	502	281	0.64	0.26	9,31	55 (83)

SDUSY15-0.20TPA	75	883	495	388	0.81	0.26	9,30	48 (72)
SDUSY15-0.35TPA	65	981	475	506	0.91	0.25	4,11,45	45 (67)
SDUSY15-0.35TPA-T	-	903	373	530	0.97	0.20	5,11,46	27 (40)
SDUSY15-0.45TPA	60	972	420	552	0.99	0.22	4,11,44	34 (51)
SDUSY15-0.10TBA	89	777	534	243	0.63	0.28	9,31	67 (100)
SDUSY15-0.15TBA	84	770	528	242	0.68	0.28	9,31	64 (95)
SDUSY15-0.20TBA	82	771	525	246	0.72	0.28	11,30	64 (95)
SDUSY15-0.25TBA	79	770	520	250	0.77	0.27	4,11,31	52 (78)
SDUSY15-0.30TBA	75	772	522	250	0.76	0.27	4,11,30	59 (88)
SDUSY15-0.30TBA-T	-	771	500	271	0.82	0.26	5,11,31	57 (86)
SDUSY15-0.35TBA	63	785	516	269	0.81	0.27	4,11,30	53 (79)

SDUSY15-0.45TBA	61	787	501	286	0.86	0.26	5,11,31	51 (76)

All notations are the same as in Table 3.1

Table 3.12 Treatment yields, textural and structural properties of alkaline treated SDUSY15 zeolite in mixture of x M (tetraalkylammonium hydroxides; TMA, TEA, TPA or TBA; x = 0.05-0.35M) + *x* M NaOH (*x* = 0.05-0.30M).

Sample	Yield [a] (%)	S_{BET} (m^2g^{-1})	S_{micro} [b] (m^2g^{-1})	S_{meso} [b] (m^2g^{-1})	V_t [c] (cm^3g^{-1})	V_{micro} [b] (cm^3g^{-1})	d_p [d] (nm)	RC [e] (%)
SDUSY15	-	756	514	242	0.55	0.27	8,23	67 (100)
0.10TEA-0.15Na	54	988	422	566	0.22	1.07	5,11,45	32 (47)
0.25TEA-0.05Na	66	870	478	392	0.25	0.85	4,11,46	50 (75)
0.25TEA-0.15Na	41	908	336	572	0.18	1.31	15	20 (30)
0.05TPA-0.05Na	87	774	503	271	0.65	0.20	9,30	59 (89)
0.05TPA-0.15Na	72	926	491	435	0.85	0.26	3,9,45	52 (78)

0.05TPA-0.30Na	45	927	447	480	1.26	0.24	15,46	35 (52)
0.10TPA-0.05Na	76	855	520	335	0.75	0.27	13,46	62 (92)
0.10TPA-0.15Na	69	927	503	429	0.85	0.27	4,9,45	53 (79)
0.10TPA-0.30Na	47	903	403	547	1.25	0.21	15,46	32 (48)
0.25TPA-0.05Na	61	984	437	547	1.00	0.23	5,11,45	37 (55)
0.25TPA-0.15Na	56	922	421	500	0.94	0.22	4,11,46	39 (59)
0.05TBA-0.05Na	83	799	527	272	0.68	0.28	11,30	61(91)
0.05TBA-0.15Na	73	810	512	299	0.81	0.27	8,13,30	51 (76)
0.05TBA-0.30Na	53	850	519	331	1.23	0.27	23	40 (60)
0.10TBA-0.05Na	81	793	520	273	0.73	0.27	13,30	61 (92)
0.10TBA-0.15Na	74	795	522	282	0.78	0.27	15,31	55 (83)

0.05TBA-0.30Na	53	801	493	308	1.18	0.26	30	42 (65)

All notations are the same as in Table 3.1

Table 3.13 Treatment yields, textural and structural properties of alkaline treated SDUSY15 zeolites in *x* M TPA + *y* M TEA (*x* = 0.05-0.25M, *y* = 0.05-1.0M).

Sample	Yield [a] (%)	S_{BET} (m^2g^{-1})	S_{micro} [b] (m^2g^{-1})	S_{meso} [b] (m^2g^{-1})	V_t [c] (cm^3g^{-1})	V_{micro} [b] (cm^3g^{-1})	d_p [d] (nm)	RC [e] (%)
SDUSY15	-	756	514	242	0.55	0.27	8,23	67 (100)
x M TPA + y M TEA (x = 0.05-0.15 M, y = 0.10-0.50 M)								
SDUSY15-0.05TPA-0.05TEA	88	797	510	287	0.64	0.27	9,30	64 (95)
SDUSY15-0.05TPA-0.10TEA	85	818	510	308	0.71	0.27	3,9,45	63 (94)
SDUSY15-0.05TPA-0.25TEA	74	835	505	330	0.83	0.27	4,11,44	54 (81)
SDUSY15-0.05TPA-0.50TEA	62	825	495	330	0.91	0.26	5,13,45	49 (74)

SDUSY15-0.05TPA-0.75TEA	54	842	492	350	1.05	0.26	8,15,46	47 (70)
SDUSY15-0.05TPA-1.00 TEA	52	859	486	373	1.14	0.25	18	38 (57)
SDUSY15-0.10TPA-0.25TEA	71	870	520	350	0.84	0.27	4,11,45	51 (76)
SDUSY15-0.10TPA-0.25TEA	71	830	510	320	0.77	0.27	4,11,45	55 (82)
SDUSY15-0.10TPA-0.25TEA-T	-	822	498	324	0.84	0.26	5,11,45	54 (80)
SDUSY15-0.10TPA-0.50TEA	63	875	505	370	1.00	0.26	5,11,45	49 (74)
SDUSY15-0.10TPA-0.75TEA	53	869	474	395	1.15	0.25	9,18	36 (55)
SDUSY15-0.10TPA-1.00TEA	41	860	441	419	1.42	0.23	23	32 (48)
SDUSY15-0.15TPA-0.05TEA	77	858	514	344	0.76	0.27	4,9,30	60 (89)
SDUSY15-0.15TPA-0.10TEA	75	883	518	365	0.81	0.27	4,9,45	57 (85)
SDUSY15-0.15TPA-0.25TEA	67	887	517	370	0.87	0.27	4,10,45	47 (71)

SDUSY15-0.15TPA-0.50TEA	59	885	505	380	1.01	0.26	4,11,44	48 (72)
SDUSY15-0.15TPA-0.75TEA	48	881	464	417	1.22	0.24	15,32	34 (51)
SDUSY15-0.25TPA-0.03TEA	70	829	525	309	0.77	0.27	4,11,45	48 (72)
SDUSY15-0.25TPA-0.05TEA	68	920	475	443	0.87	0.25	4,11,45	47 (71)
SDUSY15-0.25TPA-0.10TEA	64	987	456	531	0.95	0.24	4,11,44	39 (58)
SDUSY15-0.25TPA-0.10TEA-T	-	864	434	430	0.87	0.23		35 (52)
SDUSY15-0.25TPA-0.25TEA	59	935	458	477	0.98	0.24	5,11,45	41 (62)
SDUSY15-0.25TPA-0.50TEA	52	860	418	442	1.12	0.21	8,11,45	31 (46)
SDUSY15-0.25TPA-0.75TEA	36	891	397	494	1.54	0.21	18	32 (48)

All notations are the same as in Table 3.1

Table 3.14 Treatment yields, textural and structural properties of alkaline treated SDUSY15 zeolites in *x* M TBA + *y* M TEA (*x* = 0.05-0.35M, *y* = 0.05-1.0M).

Sample	Yield [a] (%)	S_{BET} (m^2g^{-1})	S_{micro} [b] (m^2g^{-1})	S_{meso} [b] (m^2g^{-1})	V_t [c] (cm^3g^{-1})	V_{micro} [b] (cm^3g^{-1})	d_p [d] (nm)	RC [e] (%)
SDUSY15	-	756	514	242	0.55	0.27	8,23	67 (100)
x M TBA + y M TEA (x = 0.05-0.25 M, y = 0.05-1.0 M)								
SDUSY15-0.05TBA-0.05TEA	91	765	522	243	0.57	0.27	9,35	67 (100)
SDUSY15-0.05TBA-0.10TEA	85	776	524	252	0.67	0.27	9,45	66 (98)
SDUSY15-0.05TBA-0.25TEA	77	823	520	303	0.75	0.27	4,9,45	62 (94)
SDUSY15-0.05TBA-0.50TEA	67	813	499	314	0.84	0.26	6,13,45	60 (90)
SDUSY15-0.05TBA-0.75TEA	68	800	470	330	0.90	0.25	5,13,45	54 (80)
SDUSY15-0.10TBA-0.05TEA	83	750	510	240	0.63	0.27	9,46	56 (84)

SDUSY15-0.10TBA-0.10TEA	73	757	520	237	0.66	0.28	4,9,45	58 (87)
SDUSY15-0.10TBA-0.25TEA	68	804	514	290	0.88	0.27	5,11,44	57 (85)
SDUSY15-0.10TBA-0.50TEA	62	875	510	366	0.91	0.27	5,11,45	51 (76)
SDUSY15-0.10TBA-0.50TEA-T	-	860	480	380	1.01	0.25	6,13,44	46 (69)
SDUSY15-0.10TBA-0.50TEA-30	76	808	521	286	0.72	0.27	9,45	63 (94)
SDUSY15-0.10TBA-0.50TEA	66	850	510	340	0.80	0.27	5,11,44	55 (82)
SDUSY15-0.10TBA-0.50TEA-T	-	855	505	350	0.90	0.27		44 (66)
SDUSY15-0.10TBA-0.75TEA	55	873	480	400	1.07	0.25	7,15,45	41 (61)
SDUSY15-0.10TBA-1.00TEA	43	910	447	463	1.36	0.23	18,45	36 (55)
SDUSY15-0.35TBA-0.05TEA	75	812	522	289	0.77	0.27	4,11,30	60 (90)
SDUSY15-0.35TBA-0.10TEA	73	826	520	306	0.81	0.27	4,11,46	56 (85)

SDUSY15-0.35TBA-0.25TEA	65	823	480	343	0.83	0.25	5,11,44	51 (76)
SDUSY15-0.35TBA-0.50TEA	57	932	461	471	1.13	0.24	4,11,45	36 (53)
SDUSY15-0.35TBA-0.75TEA	44	919	391	528	1.32	0.21	15	22 (33)

All notations are the same as in Table 3.1

Table 03.15 Comparative textural properties of selected alkaline treated SDUSY40, SDUSY30, and SDUSY15 with binary mixture based strategy.

	Sample	S_{BET} (m^2g^{-1})	S_{meso} [b)] (m^2g^{-1})	V_{micro} [b)] (cm^3g^{-1})
SDUSY40	SDUSY40	607	183	0.23
	0.10TBA	654	236 (+29%)	0.22 (-4%)
	0.10TBA-0.10TEA	784	364 (+99%)	0.22 (-4%)
	0.10TBA-0.25TEA	870	451 (+146%)	0.22 (-4%)
	0.10TBA-0.50TEA	855	543 (+197%)	0.16 (-30%)
SDUSY30	SDUSY30	764	258	0.27
	0.10TBA	810	298 (+16%)	0.27
	0.10TBA-0.10TEA	880	357 (+39%)	0.27
	0.10TBA-0.25TEA	913	393 (+52%)	0.27
	0.10TBA-0.50TEA	924	450 (+74%)	0.24 (-11%)
SDUSY15	SDUSY15	756	242	0.27
	0.10TBA	762	247 (+2%)	0.27
	0.10TBA-0.10TEA	757	237 (-2%)	0.27
	0.10TBA-0.25TEA	804	290 (+20%)	0.27

	0.10TBA-0.50TEA	875	366 (+51%)	0.27

For the sake of clarity and easy comparison, Table 3.15 shows the comparative textural properties of selected alkaline treated SDUSY40, SDUSY30, and SDUSY15 with binary mixture based strategy. The increase in S_{meso} and preservation of V_{micro} in a given Si/Al ratio depends on type and concentration of the desilicating and/or PDA. The observed decrease in amount of S_{meso} at a reasonable preservation of $V_{micro,}$ with decrease in Si/Al of the studied dealuminated Y-zeolites can be ascribed to the fact that AlO_4^- plays shielding role against the OH^- attack in lower Si/Al dealuminated Y-zeolites.

And since the major interest of this work is to prove the success of novel method of generating secondary pore networks in addressing the accessibility and diffusivity challenges while preserving the intrinsic properties, the synthesized hierarchical forms of the SDUSY15 (where less mesopore creation was obtained by this approach due to higher Al content (Table 3.15)) were tentatively employed in some catalytic activity evaluations to make convincing claim that binary mixture of organic alkaline media is superior in creating substantial mesopore networks.

3.6.5 Catalytic activity evaluations

To ensure the functionality of the generated secondary pore network, the catalytic performances of the modified SDUSY15 zeolite samples were evaluated in the pyrolysis of low density polyethylene (LDPE) and in the Friedel Craft alkylation of toluene with

benzyl alcohol. These tests gave insight to the role of hierarchical structures in the enhanced activity performance of the samples.

3.6.5.1 Degradation of LDPE

LDPE is a polymer that consists of long branched hydrocarbon chains, and its degradation is useful application in the chemical method of recycling plastic waste to produce fine chemicals [148]. Acid sites in zeolite catalyst enable the degradation of LDPE at lower temperatures and also give selectivity towards desired products. The initiation step of the degradation requires both weak (to abstract hydride from the polymer) and strong acid sites (to protonate the C-C bond), and the polyethylene molecule passes through successive β-scissions to give lower molecular weight fragments [149-152]. The catalytic activity was measured by evaluating the weight loss of the mixture of polymer and catalyst (3:1) [153]. Figures 3.18 and 3.19 show the LDPE conversion profiles in terms of weight loss against temperature. As it can be seen, different degrees of secondary pore networks influence the pyrolysis temperature compare to the parent zeolite. There exists a progressive decrease in the degradation temperature over the hierarchical zeolite. For instance, a reduction of 29^0C (at T_{50}) was observed for material modified by binary mixture, TB-0.10M-TE-0.50M (S_{meso} = 366m^2g^{-1}), while the corresponding mono components (TBA-0.60 (S_{meso} = 300m^2g^{-1}) and TEA-0.60 (S_{meso} = 312m^2g^{-1})) show poor performance with respect to SDUSY15 (Fig. 3.18). The easy accessibility and better transport through mesopore creation has been pointed to be the dominating factor behind the activity differences [153].

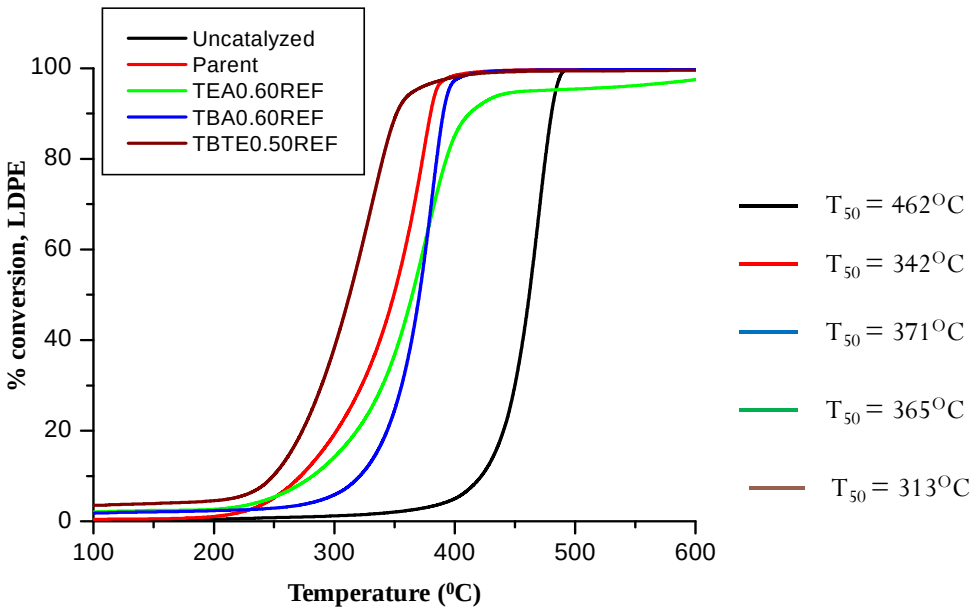

Figure 0.18 LDPE conversion using binary and mono component organic hydroxide modified SDUSY15**.**

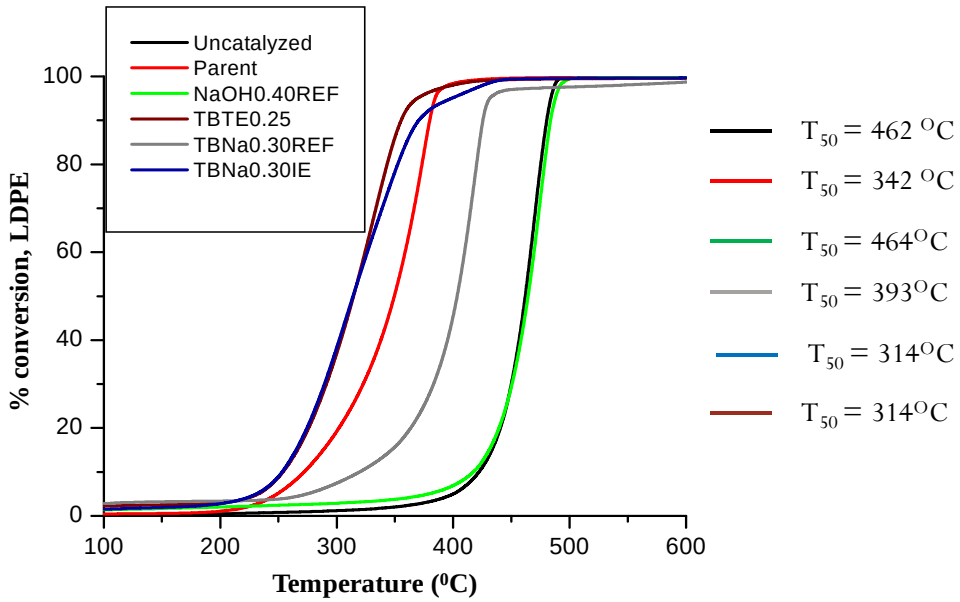

Figure 0.19 Comparative LDPE pyrolysis by double organic and ion-exchanged TB-Na treated SDUSY15.

Furthermore, the binary mixture of double organic type shows similar activity with ion-exchanged TB-NaOH mixture as shown in Fig. 3.19. This thus saves the extra effort and time required to carry-out ion-exchanged procedure in the case of TB-Na, which showed poor performance without ion-exchanged. This points out the fact that the new approach of binary mixture enables the bypass of the crucial, but energy and time-consuming, ion-exchange steps in the desilication procedure.

3.6.5.2 Friedel-Craft Alkylation of Toluene

To further establish the enhanced activity of the newly designed hierarchical dealuminated Y-zeolites, the catalysts were tested in the alkylation of toluene with benzyl alcohol. The GC-MS analysis of the reactants and obtained products resulted to the chemical reaction equation represented in the Fig. 3.20. The alkylation requires relatively strong acid sites that must be accessible by these bulky reagents. The obtained trend was a similitude of that of LDPE pyrolysis. TPTE-0.25M treated sample displayed similar percentage conversion to the ion-exchanged TBNa-0.30M treated sample, both above the parent sample (SDUSY15).

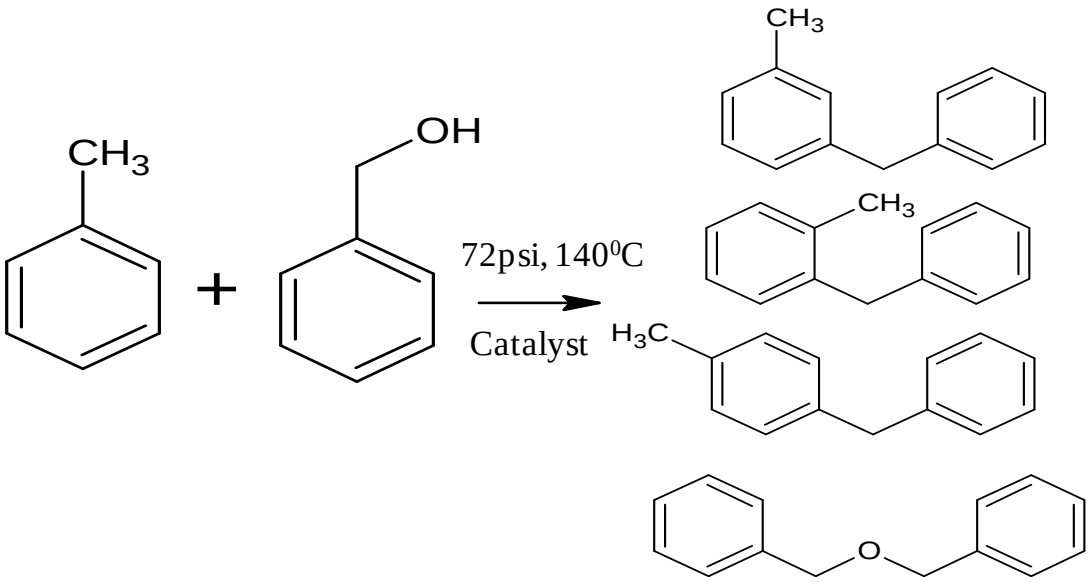

Figure 0.20 Chemical equation of Friedel-Craft alkylation of toluene with benzyl alcohol.

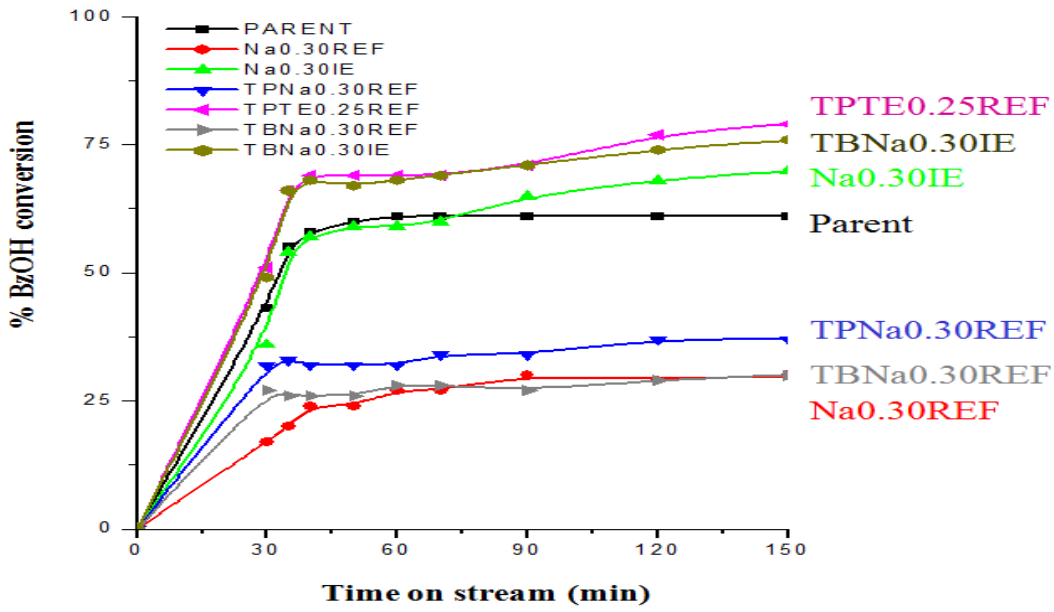

Figure 0.21 Percentage conversion of benzyl alcohol against time-on-stream.

3.7 Summary

A number of tentative conclusions can be drawn from the above results. First, the negative impacts of single NaOH, TMAOH, and TEAOH treatments on the porosity and the crystallinity of SDUSY40 zeolites were clearly minimized upon following the double mixture approach. Second, treatments in aqueous double organic mixtures (in particular, $TBA^+ + TEA^+$) appear to be more effective than those of (TBA^+ + NaOH) treatments. For example, it was possible to develop substantial external surfaces up to 451 m^2g^{-1} (about 2.5 times larger than that of the parent zeolite), while strongly enhanced V_t (up to 1.22 cm^3g^{-1}) and almost unaffected microposity (V_{micro} of 0.22 cm^3g^{-1}) were attained. The loss in crystallinity was limited to 40% at a solid yield of 60%. Treatments in TBA^+ + NaOH mixture resulted in comparable mesoposity (S_{meso} = 444 m^2g^{-1}), however, 21% reduction in micropore (from 0.23 cm^3g^{-1} down to 0.19 cm^3g^{-1}), low solid yield of 42%, and crystallinity loss of 55% were obtained. Third, the efficiency of double tetraalkylammonium mixtures showed a clear dependence on the concentration and the nature of included tetraalkylammonium cations, whereas that of TBA^+ + NaOH mixtures on the concentration of NaOH. Fourth, the superior activity of material modified by double tetraalkylammonium mixtures can be evaluated by the degradation of low density polyethylene, as well as the alkylation of toluene with benzyl alcohol.

CHAPTER 4

ALKALINE TREATED DEALUMINATED Y-ZEOLITE AS AN EXCELLENT ADSORBENT FOR HEAVY METAL IONS REMOVAL IN WATER TREATMENT

4.1 Background Information

Heavy metals are major crucial environmental contaminant from both natural and man-made sources. For instance, lead gets into water bodies from acid mine drainage release and into the atmosphere through fuel combustion [1-4], and the acceptable limit of this contaminant in for drinking water is 15 ppb and 50 ppb by USEPA and WHO respectively [6,7]. Consequently, the chemical analysis of metal ions requires sample pretreatment to separate the target analytes from the interfering matrix and preconcentrate to the analytical measurable amounts [154]. Aside the influence of significant matrices and complex formation on normal instrumental analysis, most heavy metals present in concentration near the detection limit of the instrument [155-157]. So preconcentration is a necessity prior to their determination as it offers reasonable sensitivity and selectivity, promotes detection limit and thus enables better accuracy [158].

The known preconcentration procedures are not limited to coprecipitation, liquid-liquid extraction (LLE), microextraction and solid phase extraction (SPE) [159-162] but the SPE has striking benefits such as low cost due to low or no consumption of organic solvents, rapid phase separation, ease to be used with online or off-line mode of different

detection techniques, high recovery as well as high enrichment factor [159-163]. The extraction of metal-ions by SPE is more exhaustive than LLE due to multiple equilibrium based extraction in the SPE [154]. Good chemical and thermal stability, high recovery percentage, surface contact with sample solution, pure and low leachability of impurities, and reversible adsorption, as well as porous and large surface area are reported features of good SPE materials [164-169].

To this end, the choice of appropriate adsorbent is a key for SPE, and many materials are being proposed and investigated [170]. Metal-ions preconcentration has been done with sorbents like ion exchange resins [171], microcrystalline naphthalene [172], XAD resins [173], cellulose [174], Lewatit S 100 [175], polyurethane foam [176], nanometer titanium dioxide [177], modified silica gel [178,179], and recently, LTA and Y-type zeolites [180]. Meanwhile, porous structure, large surface area, selective adsorption, high adsorption capacity, and high purity standards are features that give activated carbon top ranking among the sorbents for environmental pollution control [181,182]. It is noteworthy that high cost of production and regeneration of spent activated carbon makes it less economical (in spite of its widely use) than zeolite as adsorbent medium for the heavy metals removal from water [183]. Large scale refinery waste products, spent zeolites match activated carbon but surpass clay as sorbent for extraction and concentration of toxic metals (As, Pb, Hg) from waste water. The developed surface area, pore structure and polarity due to hydroxyl groups located on the zeolite surface have contributive effect [184]. Modified zeolites are well useful in the catalyst application, separation processes and pollution control of the heavy metal ions and organic pollutant, among others [185-188].

As part of modern developments in the analytical science within the last decade, a miniaturized form of SPE called µ-SPE was reported by Basheer *et al.,* 2006. The µ-SPE is a simple, accurate and effective pretreatment technique with a drawback of typically more than 30 mins extraction time requirement [189]. To surpass this time issue, which is also common to other methods when adopted alone, the idea of combining different microscale sample preparation methods became a common and acceptable practice. An example reported by Ge and Lee (2012) was AA-µ-SPE where the µ-SPE was inserted in a sample and agitated by magnetic stirring for certain time [190]. While the polypropylene membrane sieve the particulates from the sample matrices on the sorbent surface, the selectivity of the µ-SPE device yet lies on the good choice of sorbent materials [188-190]. So, the combination of excellent sorbent material and efficient extraction method is paramount among other considerable factors.

Although the hierarchical ultrastable Y (USY) zeolites are widely used in various catalytic applications (see previous chapter), yet their use as efficient sorbents when modified appropriately is yet to be fully explored. The choice of this type of zeolite is due to the characteristic large surface area with cavities (due to superdealumination) that can harbor heavy metal ions and the modification by alkaline treatment proved to enhance the adsorption capacity of this typical zeolite material. This work investigated the enhanced heavy metal ions sorption potential of the modified superdealuminated ultrastable Y (SDUSY) zeolite by quaternary ammonium cations based alkaline treatment using agitation-assisted µ-solid-phase extraction technique.

4.2 Experimentals

4.2.1 Reagents, Instruments and Materials

Reagents: All reagents used were of analytical grade; sodium hydroxide, NaOH (97+%, Aldrich), tetrabutyl ammonium hydroxide (40 wt.% in H_2O, Sigma-Aldrich), and nitric acid, HNO_3 were obtained from J.T. Baker (Philips Burg, NJ). The ultra-pure water (pH=5.6) was prepared using Milli-Q (Milford, MA) system. The lead (Pb), cadmium (Cd), nickel (Ni), cobalt (Co), copper (Cu) and arsenic (As) standard solution for ICP-OES instrument were used to prepare all the working solutions needed.

Instruments: Double Leopard 16 inch Hand Sealer (Impulse) machine, Bransonic 32 Ultrasonic bath (Dimension bath DxHxW = 15x14x30cm), Magnetic stirrer, Metrohm 691 pH/ion meter using a glass-calomel electrode was used to amend the pH of working solution. Other instruments such as FTIR, SEM, BET surface analyzer, XRD, ICP-OES were detailed in section 3.4.

Materials: Prior to use, all glassware and plastic bottles were thoroughly cleaned by soaking in 10% dilute HNO_3 for 12 hours and later rinsed with ultrapure water. The polypropylene membrane sheet (157µm thickness and 0.2µm pore size) was bought from Membrana (Wuppertal, German). The SDUSY zeolite used in this study was supplied by Zeolyst International. Severe steaming and dealumination of the pristine NaY zeolite (CBV100) resulted to CBV720, CBV760 and CBV901 of Si/Al ratio of 15, 30 and 40, respectively. These samples were coded SDUSY15, SDUSY30 and SDUSY40 respectively but the SDUSY40 was the main concern of this adsorption study. Prior to

post-synthetic treatments, the as-received SDUSY40 was air-calcined at 550°C for 6 hrs (5°C/min), so as to ascertain its H-form.

4.2.2 Preparation of working samples

A wide range of working solution was made by spiking aliquots of typically 20 ml ultra-pure water with different known concentration of target analytes and subsequently adjusted to different pH using 0.1M NaOH and 0.1M HNO_3. Thereafter, extraction was conducted on these samples using µ-SPE device parked with zeolite materials as novel sorbents.

4.2.3 Methods of post-synthesis modification and characterization of the zeolite materials

4.2.3.1 Post-synthesis Alkaline Treatments

The modification of the commercial H-form of SDUSY40 zeolites was performed as reported in the previous chapter. Summarily, a mixture of 0.15M TBAOH and 0.20M NaOH was made up of a 50ml alkaline solution heated up to optimized temperature (65°C) in a flask connected to a reflux in oil bath. Then, 1.5 g of SDUSY40 zeolite was added to the heated solution and kept at that temperature while stirring at 800 rpm for 2 hrs, under atmospheric pressure. Afterwards, the zeolite suspension was cooled down immediately using an ice bath, and then isolated by suction filtration. The solid product (residual) was washed adequately with 400 ml deionized water to have neutral pH, and then dried at ambient temperature for 30 minutes, followed by drying at 110°C for

minimum of 10 hrs. Thereafter, the alkaline treated sample was calcined in static air at 550°C (holding time 6 hrs, 3°C/min). It is noteworthy that modified SDUSY zeolite sample for adsorption study was excluded from undergoing ion-exchange procedures of the alkaline treatment. This was because ion-exchange formed the rationale of the application of the modified material in heavy metal ions removal from water. So, after calcination, the modified zeolite sample was characterized and evaluated for comparative adsorption studies with the unmodified one (as reference).

4.2.3.2 Characterization of the zeolite materials

Both the SDUSY40 (reference) and AT-SDUSY (modified) zeolite materials were characterized using state-of-the-art spectroscopic and imaging techniques with respective objectives. The FTIR (Nicolet 6700 spectrometer-Thermo electron, USA), provided by OMNIC with a deuterated triglycine sulfate (DTGS) detector, was used to ascertain the functional groups present in the zeolite samples. The samples were made into pellets with addition of KBr and the spectra were obtained by using transmittance mode within 4000-400cm^{-1} wave number range. The background correction of the spectra was performed by 16 scans with resolution 2cm^{-1} for the background noise correction. Other characterization techniques employed are as reported in section 3.4, with the same ICP-OES on a Horiba ULTIMA 2 instrument used to determine the concentration of elements in the study.

4.2.4 Extraction, desorption and regeneration procedures

4.2.4.1 Fabrication of micro-SPE device

The µ-SPE device was prepared as described by Basheer *et al.*, 2009 [191]. The polypropylene membrane sheet was carefully cut and heat-sealed to make a tea-bag-like envelope with an open end through which the sorbent was packed and then heat-sealed. A typical packaging has the dimension of 150mm x 50mm and contains 25±0.02 mg of the sorbent material. To ensure consistency in the weight measurement, each µ-SPE device was re-weighed and trimmed at edges carefully.

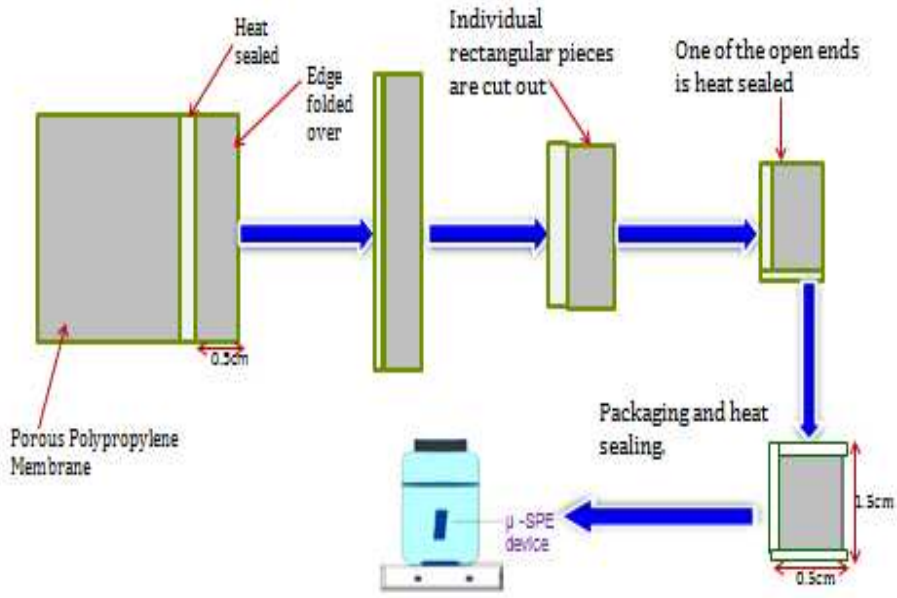

Figure 4.1 Schematic diagrams of steps in the fabrication of µ-SPE device.

4.2.4.2 Agitation Assisted µ-SPE (AA-µ-SPE)

The extraction procedure began with conditioning of the µ-SPE device in acetone for 10 minutes to open the pores of the membrane, followed by drying with lint-free tissue and then placed in 10ml of ultra-pure water in a glass vial. Henceforth, a pair of tweezers was used to handle the cleaned µ-SPE device in the remaining extraction and desorption steps. The AA-µ-SPE was achieved by placing a prepared µ-SPE device into 20ml of water sample spiked with a known concentration of analyte(s) (heavy metal ions e.g. 10mg/L of Pb^{2+}) with stirring bar rotating at 1200 rpm for extraction period (5-30 minutes). The sample vial containing the extraction device, magnetic stirrer and sample volume was sealed with cap and positioned inside water bath system to maintain a certain temperature for isotherm adsorption evaluation.

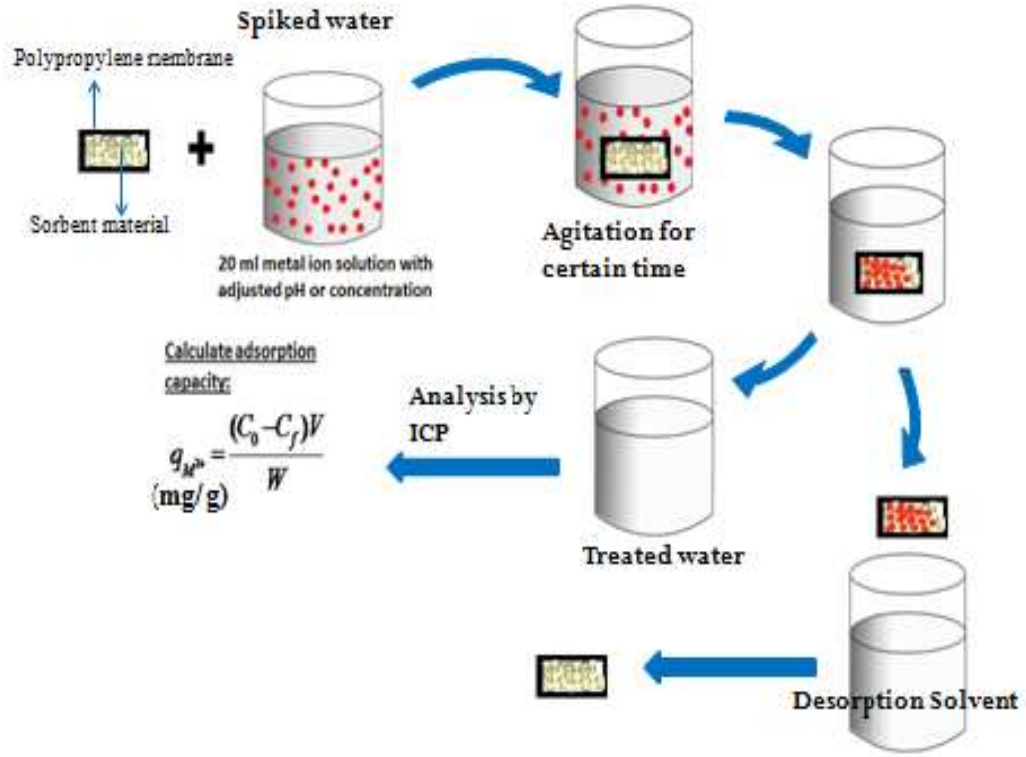

Figure 4.2 Scheme of AA-µ-SPE procedure.

4.2.4.3 Recovery and sorbent regeneration

The recovery of adsorbed metal ion analytes was achieved by placing the extraction devices in small vials containing x ml of yM HNO_3 for certain time t minute under ultra-sonication to give complete desorption. This choice of desorbing solvent was made to conform to the matrix standard for elemental analysis using ICP-OES. Subsequently, the reusability of the extraction device was investigated. For certain time interval, three cycles of recovery experiments as well as carry-over tests were performed to assess the reusability of the µ-SPE device. The solutions from these were separately analyzed for heavy metal ions content, measured in triplicates by ICP-OES.

4.2.5 Instrumental and data analysis

The solutions from the desorption step were individually analyzed for heavy metal ions content, measured in triplicates by ICP-OES. The obtained data from the instrumental analyses were used to compute the sorption capacity of the target analytes by both SDUSY40 and AT-SDUSY zeolites using the following expressions:

$$\text{Removal efficiency } (\%) = \frac{(C_o - C_e) \times 100}{C_o} \quad (4.1)$$

$$q_e = \frac{(C_o - C_e) \times V}{m} \quad (4.2)$$

where q_e is the amount of sorbed analyte ions (mg/g), C_o and C_e are the initial and equilibrium concentration of the analyte ions in the sample solution (mg/l) respectively, m is the adsorbent mass (mg) and V is the sample volume (ml).

The obtained results from the calculations were further used in kinetic and isotherm studies and the outcomes were subsequently presented for discussions.

4.3 Results and discussion

4.3.1 Characterization of the SDUSY40 and AT-SDUSY zeolite sorbents

Various combinations of spectroscopic techniques reveal the textural, structural and morphological properties of the studied sorbent materials. Inspection of the FTIR spectra (Fig. 4.3) shows the presence of the following peaks at wave number *ca*. 3400 cm^{-1} representing the isolated (terminal) silanol (Si–OH) group and *ca.* 2900 cm^{-1}

representing C-H saturated aliphatic hydrocarbon of chain mode, amongst other. Importantly, the spectra clearly indicate the enhancement of silanol group in the AT-SDUSY.

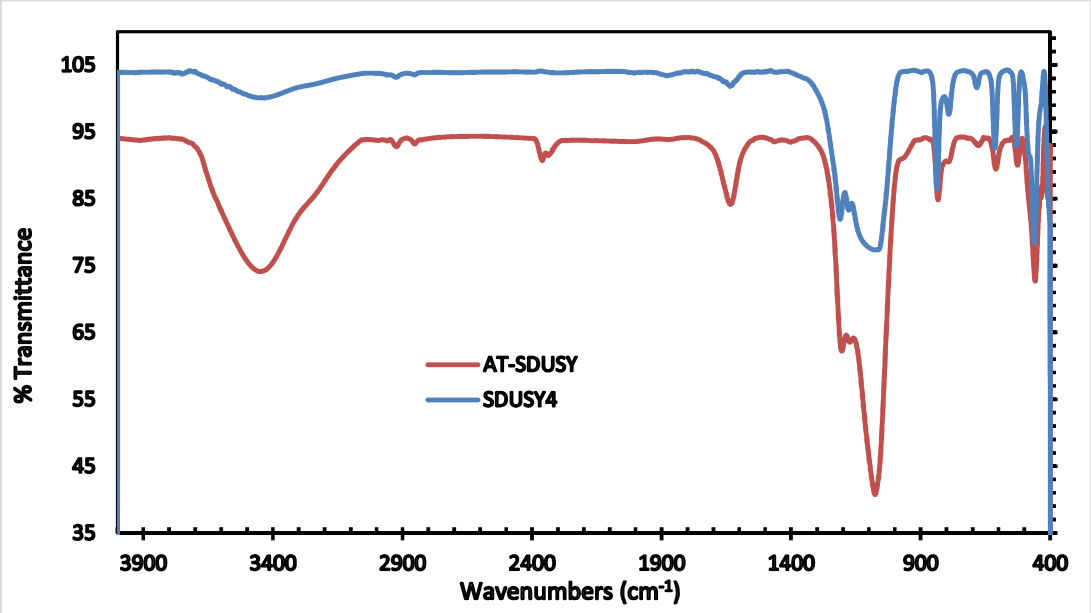

Figure 4.3 Comparative FTIR spectra of SDUSY40 and AT-SDUSY.

The XRD patterns in Fig. 4.4 show the comparative structural stability of the AT-SDUSY zeolite and the SDUSY in displaying highly pure crystalline faujasite (FAU) structure XRD pattern [192]. The scanning electron microscopy (SEM) images (Fig. 4.5) show the presence of octahedral morphology characteristic of Faujasite crystals containing large mesopores in AT-SDUSY [193] and no significant changes like any clear sign of globular particles, rugged surfaces or cracks, except for crystal size reduction, was noticed upon modification.

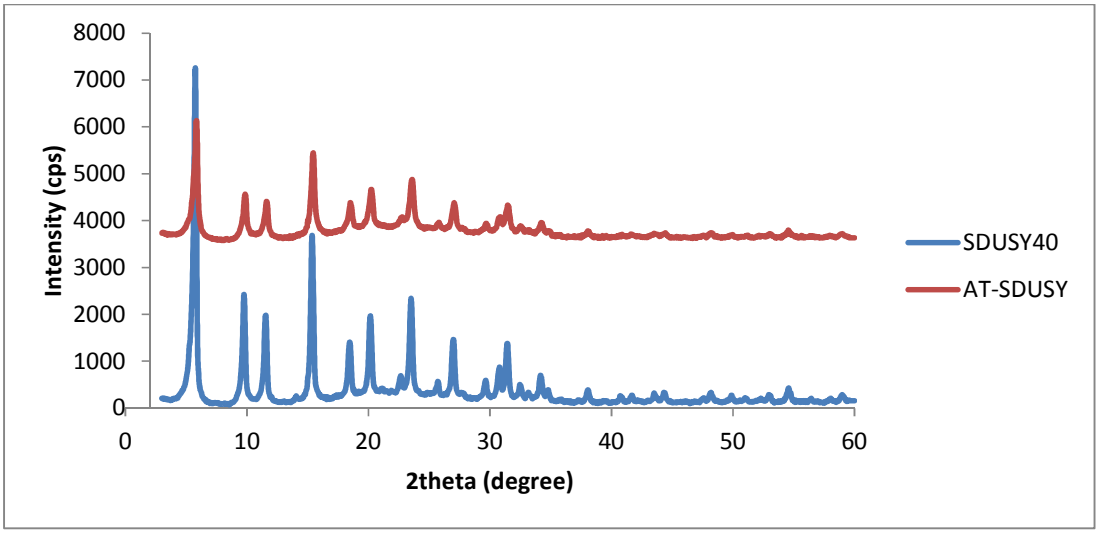

Figure 4.4 Comparative XRD patterns of SDUSY40 and AT-SDUSY

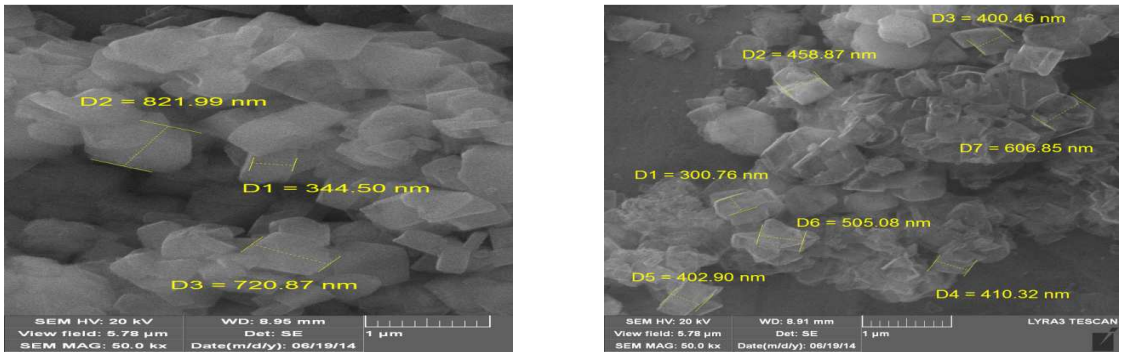

Figure 4.5 SEM images of SDUSY40 (left) and AT-SDUSY (right).

The Table 4.1 gives the comparative structural and textural data of the zeolite sorbent materials at a glance. Using TBAOH as pore growth moderator in the modification approach minimizes the negative impacts of single NaOH treatments on the porosity and the crystallinity of SDUSY40 zeolites (see previous chapter). Obviously, the AT-SDUSY has improved external surface area and large pore sizes that enhanced its adsorption properties over SDUSY40. The Si/Al ratio reduction showed the preferential leaching of

silicon from the solid that gave rise to the mesopores in the zeolite crystal upon the alkaline treatment [136].

Table 4.1 Textural and structural properties of the SDUSY40 and AT-SDUSY zeolites.

Material	Si/Al	RC (%)	S_{BET} (m^2g^{-1})	S_{micro} (m^2g^{-1})	S_{meso} (m^2g^{-1})	V_{micro} (cm^3g^{-1})	APD (nm)
SDUSY40	32	51	607	424	183	0.23	11,31
AT-SDUSY	17	26	720	357	362	0.19	15,31

4.3.2 Optimization of adsorption processes

4.3.2.1 Suitability of zeolite as excellent sorbent material

The cations, present within the zeolite framework to balance the net charges of Al^{3+} and Si^{4+}, are facile and can easily be exchanged with other cations like Pb^{2+}, Cd^{2+}, Cu^{2+}, Cr^{3+}, etc [194]. Several parameters are capable of influencing the exchanged process of ion sorption/removal from water. Examples of such parameters that were investigated for optimum heavy metal ions removal in this study include temperature and pH of the spiked water, initial concentration of cations in solution, zeolite mass, zeolite Si/Al ratio as well as modification of zeolite.

4.3.2.2 Effect of Si/Al Ratio on heavy metal ion removal

As shown in Fig. 4.6, the sorption efficiency which is a reflection of the cation exchange capacity (CEC) of the zeolite, increases with the decrease in Si/Al ratio, at the same mass. This is because an increase in Si/Al ratio of zeolite gives a decrease in the framework charge and then decrease in the numbers of cations that can be exchanged, meaning a drop in the CEC. The SDUSY40 (Si/Al=32) has the higher Si/Al ratio and lower sorption of metal ions in cation exchange than AT-SDUSY (Si/Al=17). This thus justifies the effect of modification in improving the sorption capacity of such silica-rich zeolite.

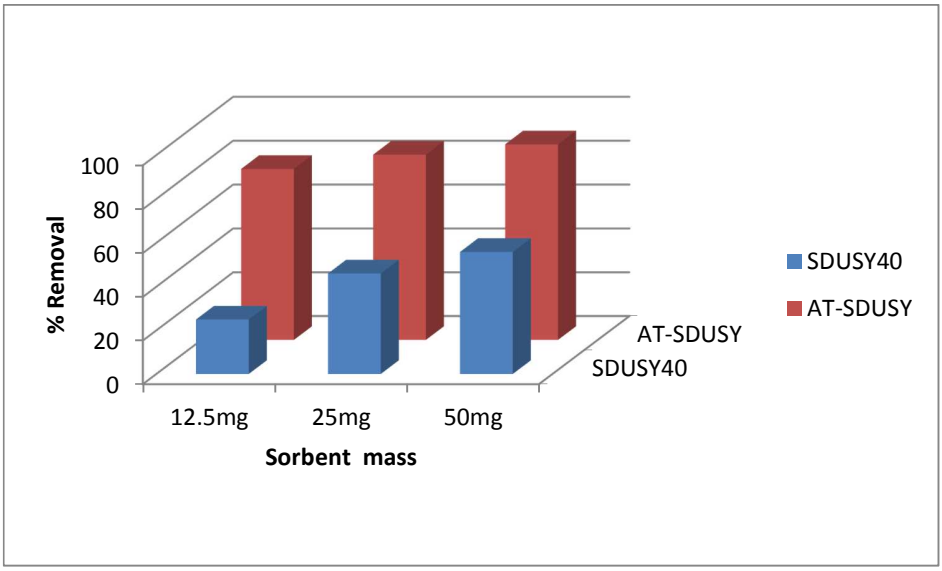

Figure 4.6 Sorbent mass and modification effect on the sorption of Pb^{2+} ion from water by SDUSY40 and AT-SDUSY (pH=6, C_0=10mg/L, t=20mins, V=25ml, T=298K).

4.3.2.3 Sorbent mass and modification effect on sorption performance

The sorbent mass (dosage) has significant effect on the adsorption efficiency, depending on the initial adsorbate concentration. At initial concentration of 10 mg/L Pb^{2+}, 20 mins

contact time, 20 ml of the spiked water at pH of 6, an increase in the removal percentages was obtained with increase in sorbent mass for all the Si/Al ratios studied (Fig. 4.6). This can be attributed to the increase in surface area with the increase in the mass of the porous sorbent materials. For example, SDUSY40 has its removal percentage increase from 24.98% to 55.84% for mass increase from 12.5 to 50 mg.

Upon modification, we obtained AT-SDUSY that showed significant improvement in the percentage removal of the Pb^{2+} analyte at a comparable sorbent mass over the SDUSY40. At a mass of 12.5 mg, about 212% increase in lead metal ion removal was obtained by AT-SDUSY (78.06%) as compared to SDUSY40 (24.98%). In addition, it is noteworthy that increase in percentage removal with increase in sorbent mass is relatively smaller in the AT-SDUSY. This is possibly because the available surface area for adsorption gets saturated largely with small mass and this means that a reasonable percentage removal can be achieved with small dosage of modified zeolite. This observation reveals the potential of the AT-SDUSY40 for excellent adsorption and enrichment of the trace amount of the studied metal ions.

4.3.2.4 Effect of sample pH on extraction

The affinity of sorbent for selective sorption of certain metal ions relates to the functional group present in the sorbent [195,196]. As shown in the FTIR result, both SDUSY40 and AT-SDUSY have the same isolated silanol functional group that can be ascribed to the sorption of heavy metal ions. So, it is expected to observe the same pattern of adsorption, except in the quantity. The pH of the solution influences significantly the adsorption of the metal ion on the surface of the adsorption material as there exists competition

between the hydrogen ion and target metal ions to adsorb on the material surface at low pH and also likely formation of sparingly soluble hydroxide precipitate of metal ions at high pH [195]. So, the sorption capacity of studied metal ions was measured in the sample pH range of 2-8 (triplicate) for both SDUSY40 and AT-SDUSY zeolite materials. Although at different quantitative level, both zeolite materials adsorbed studied lead metal ions at optimum pH = 6. At pH > 7, the obtained decrease in metal ions removal can be attributed to the precipitation of M(OH)n that is capable of contaminating the sorbent surface. Also, the low sorption capacities at low pH support the use of acidic medium in recovering the adsorbed metal ions.

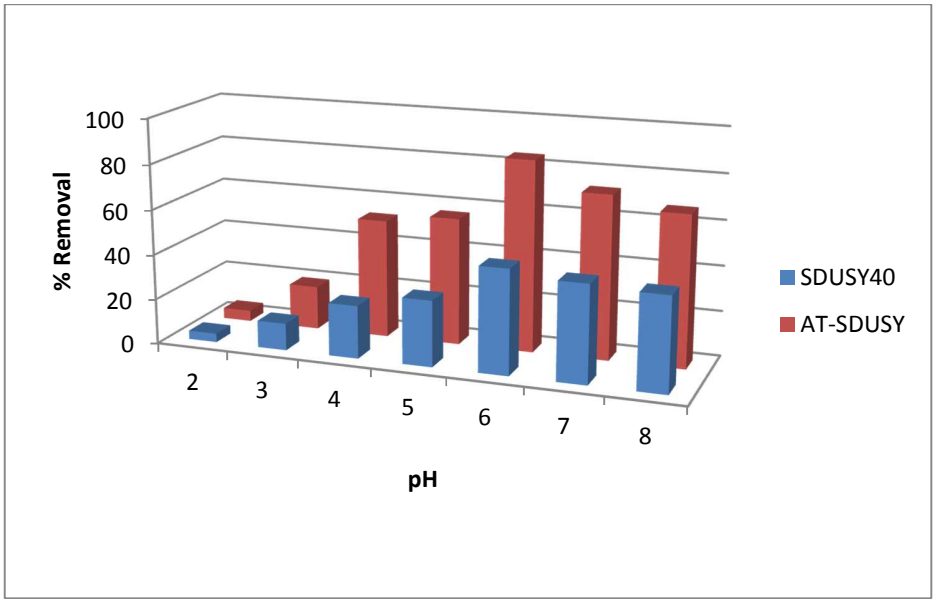

Figure 4.7 Effect of pH on the sorption of Pb^{2+} ion from water by SDUSY40 and AT-SDUSY (m=25mg, C_0=10mg/L, t=20mins, V=25ml, T=298K).

4.3.2.5 Matrix effect and selectivity

In the real situation, other notable heavy metal ions often co-exist in water to be treated. So, it is necessary to investigate the matrix effect, vis-a-viz the selectivity of the sorbent materials to particular metal ion(s). Remarkably, the same optimum pH of 6 was obtained for sorption capacity in the presence of other studied heavy metal ions by both SDUSY40 and AT-SDUSY, with the exceptional preference/selectivity for Pb^{2+} which has highest ionic radius over other metal ions with smaller ionic radii (Co^{2+}, Ni^{2+} and Cd^{2+}) (Fig. 4.8).

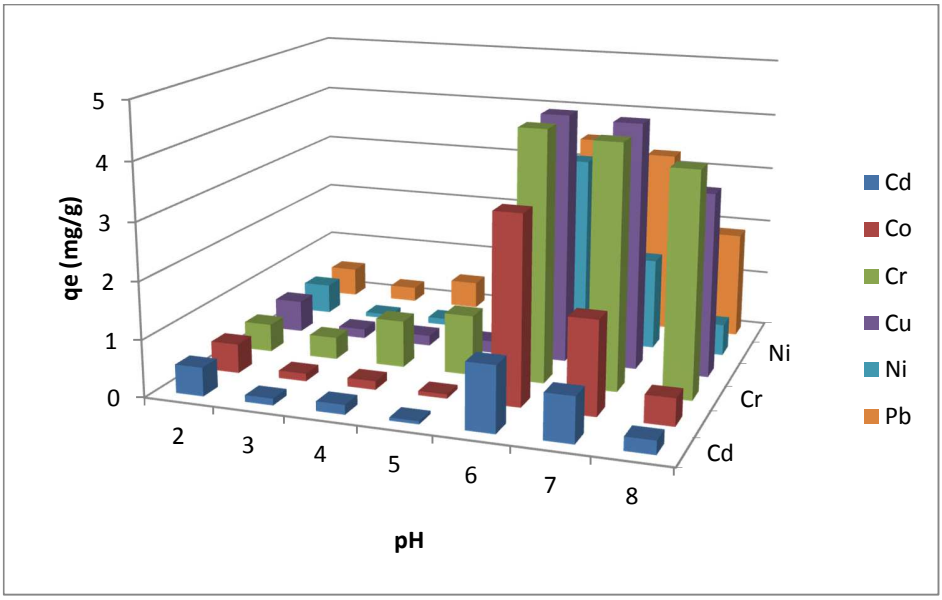

Figure 4.8 Matrix effect and selective sorption of metal ions by AT-SDUSY at different pH (m=25mg, C_0=10mg/L, t=20mins, V=25ml, T=298K).

Zeolites selectivity in relation to cations and anions is a vital property in water treatment procedure. The preference for certain ions depends on field strength in zeolite pore. Usually the more charged cations (generally heavy metals such as Cr^{3+}) have higher ability to be attracted toward a site of opposite charge than others cations with less charge

such as Pb^{2+},Co^{2+}, etc. For solution containing different ions of the same charge, the preference increases with increasing atomic number [197,198]. Low field strength zeolites (i.e those with higher Si content than Al), such as SDUSY40 and AT-SDUSY, have more preference for cations with lower charge density (Cr^{3+}, Cu^{2+}, Pb^{2+}) than those cations with high charge density. The selectivity of AT-SDUSY towards the studied heavy metal ions exist in the series: Cr^{3+}>Cu^{2+}> Pb^{2+}> Co^{2+} ≈ Ni^{2+}> Cd^{2+}. The APD in Table 4.1 shows the presence of large cavities in the studied sorbent materials.

4.3.2.6 Contact time effect

The Fig. 4.9 gives the sorption capacities as a function of time (for some selected metal ions; Cr^{3+}, Pb^{2+}, and Cd^{2+}), showing the quite rapid adsorption with the first few minute of contact time up to a saturation time. Further increase in contact time showed insignificantly increased removal after 20 mins because the surface area of the sorbent become saturated and thus reduces the adsorption process and then resulted in a low adsorption capacity. Thus, equilibrium contact time of 20 mins was adopted, and these three metal ions were rather given more attention in the rest of this study.

4.3.2.7 Effect of initial concentration

The obtained results as indicated in the plots (Fig. 4.10) showed that in both zeolites, the adsorption increases with increase in initial concentration resulting to increase in the quantity of metal ion adsorbed onto zeolite surface, and the concentration gradient can be attributed as the driving force.

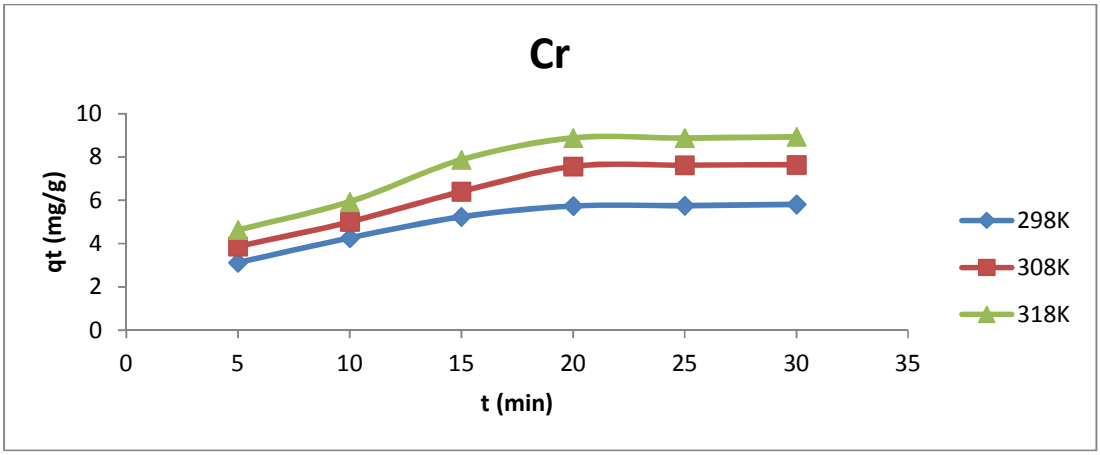

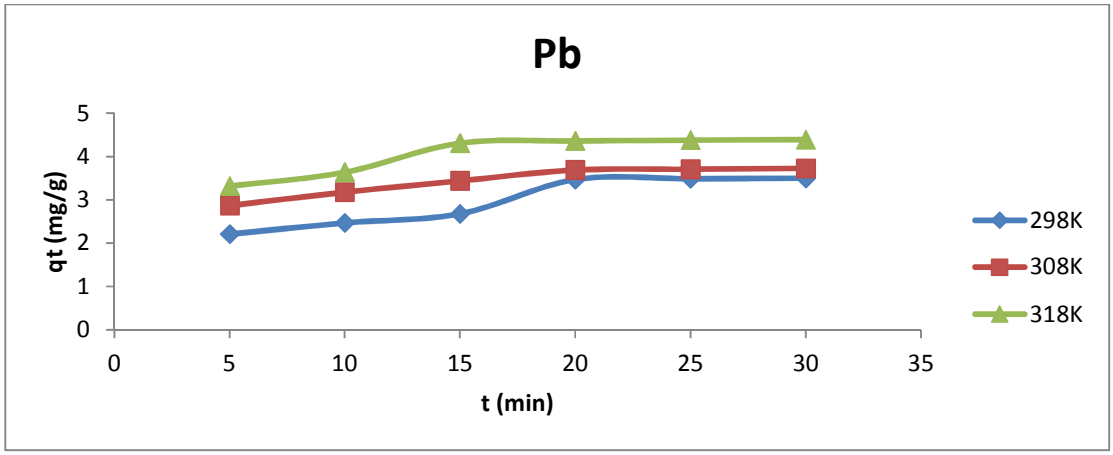

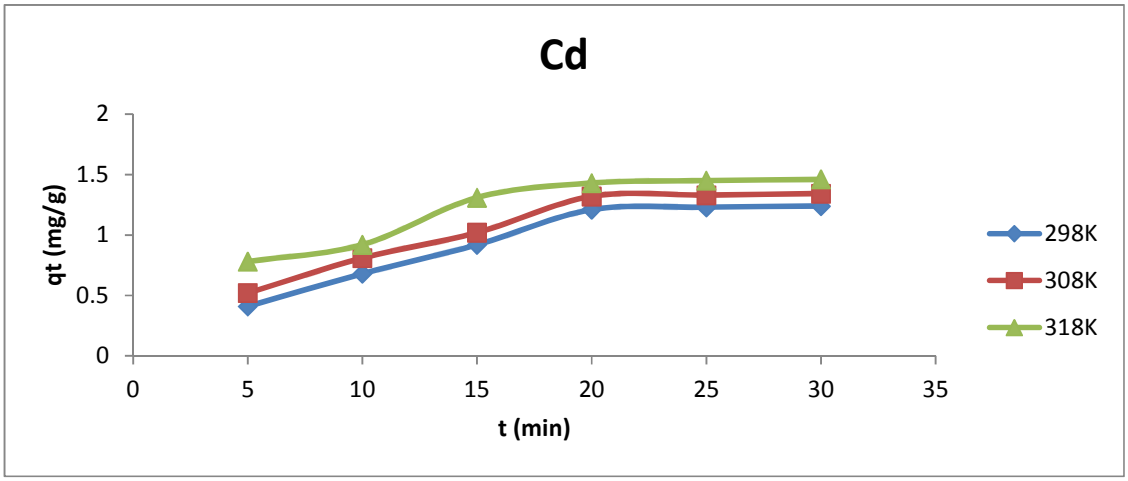

Figure 4.9 Contact time effect obtained for Cr^{3+}, Pb^{2+} and Cd^{2+} ions adsorption on AT-SDUSY at 298K, 308K and 318K (m=25mg, C_0=10mg/L, pH=6, V=25ml).

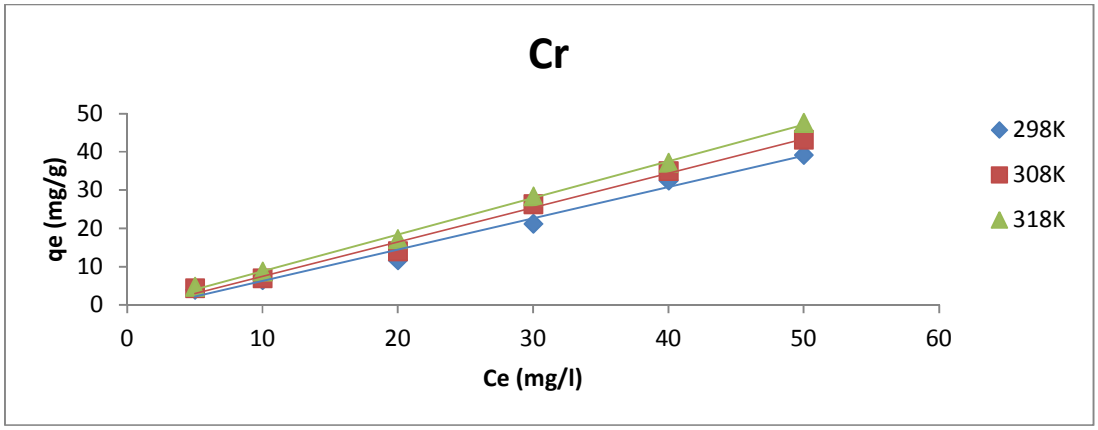

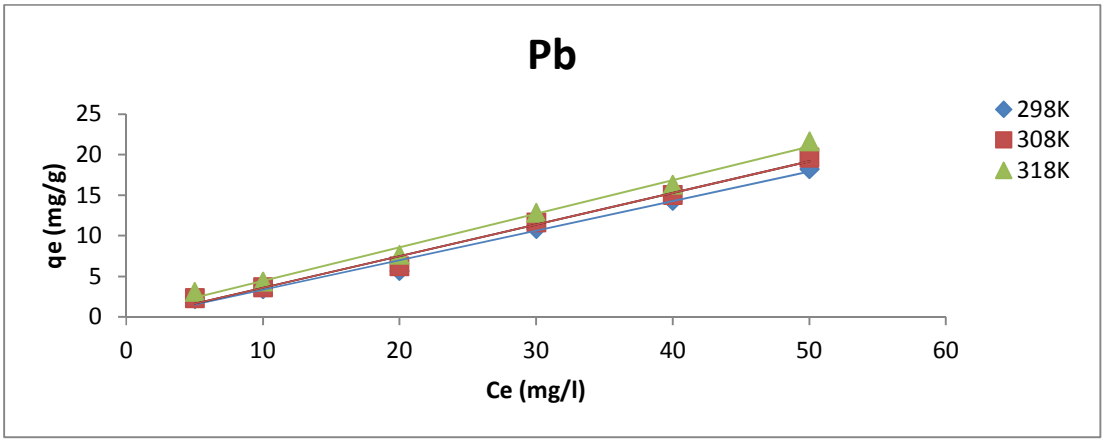

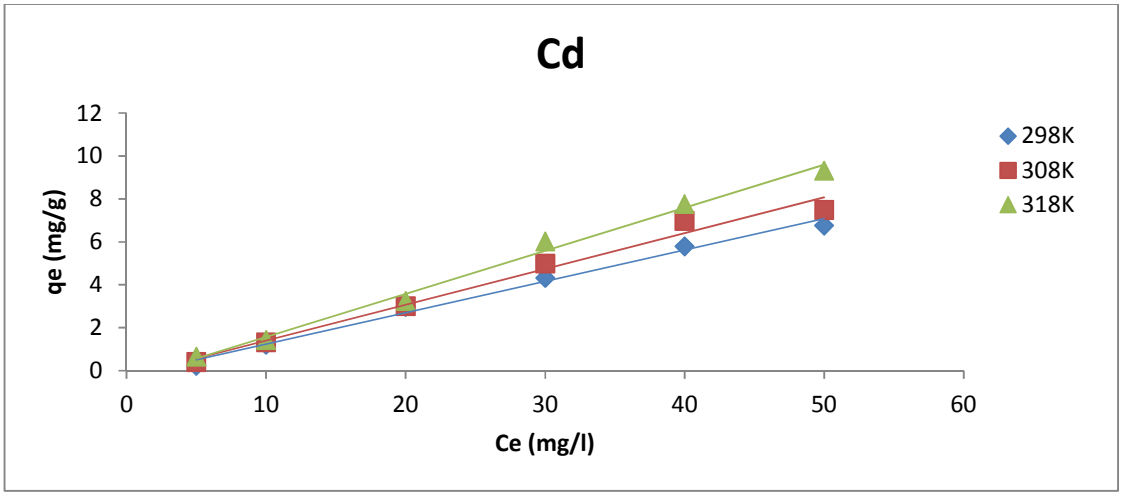

Figure 4.10 Initial concentration effect obtained for Cr^{3+}, Pb^{2+} and Cd^{2+} ions adsorption on AT-SDUSY at 298K, 308K and 318K (m=25mg, t=20mins, pH=6, V=25ml).

4.3.2.8 Temperature Effect

Of all the considerable parameters, the temperature plays a major role in the adsorption of the heavy metal ions onto the surface of the adsorbent. The observed enhancement in the sorption with increase in temperature suggested the endothermic nature of the adsorption process.

4.3.2.9 µ-SPE device regeneration

The applicability of modified zeolite for metal ion recovery in water treatment requires the efficient regeneration so that the adsorbed metal ions can be recovered in concentrated form and the zeolite reused. The reversibility of electrostatic field-, polarizability- and molecular sieve- based adsorption studies enables the reusability of zeolite and remarks zeolites as cost-effective adsorption media [183]. The choice of the instrumental analysis of the metal ions prevented the use of organic solvent for desorption, and also, the obtained result in the pH effect on the adsorption suggested better recovery of the sorbed metal ions in acidic medium. This can be because the hydroxyl groups in the zeolite become protonated in acidic medium, and do not attract the positively charged metal ions and therefore release the metal ions into recovery solution. Consequently, 5ml (adequately soaked the device) of 1M HNO_3, under 5 mins ultra-sonication gave almost complete recoveries and availed the sorbent device for re-use. This was established by the insignificant changes in the metal ions removal performance of the sorbent device after three cycles of re-use (Fig. 4.11).

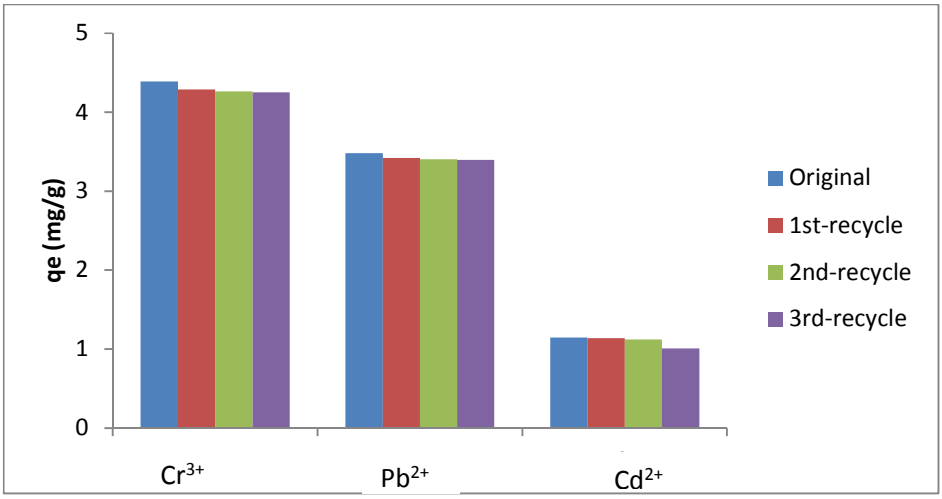

Figure 4.11 The adsorption capacities of selected metal ions by original and regenerated sorbent.

4.3.3 Adsorption kinetic studies

In order to ascertain the mechanism of the adsorption, three models (see section 2.5.4 for details) were explored in this study and in each case the degree of goodness of the linear plot of the kinetic models was judged from the value of the coefficient of determination of the plot, a considerable criterion for the determination of adequacy of a kinetic model [107,199].

4.3.3.1 Lagergren pseudo first-order kinetics

The Lagergren pseudo first order expression is given as:

$$\log(q_e - q_t) = \log q_e - \left(\frac{K_1}{2.303}\right) t \qquad (4.3)$$

where K_1 is the rate constant (min^{-1}), q_e is the amount of adsorbed at equilibrium (mg/g), and q_t is the amount adsorbed at time t (mg/g).

The parameters obtained from the plot of equation 4.3 are summarily presented in the section of Table 4.2. The discrepancies between the experimental and calculated q_e are large with low R^2 values (≤ 0.96) for different metal ions at different temperature. Thus, it shows that the data did not fit to this kinetic model (Fig. 4.12).

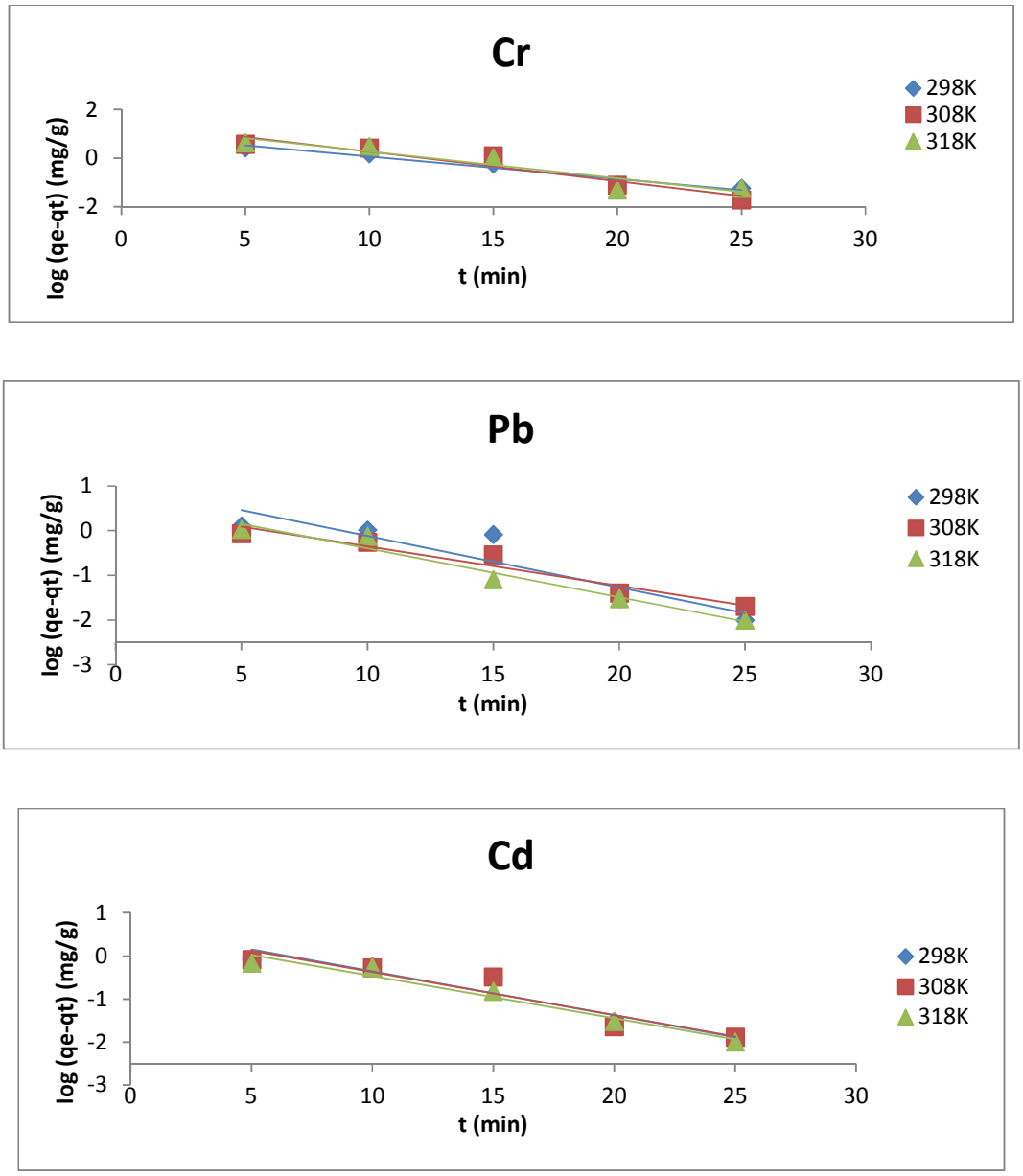

Figure 4.12 Pseudo-first order kinetic plots obtained for Cr^{3+}, Pb^{2+} and Cd^{2+} ions adsorption on AT-SDUSY at 298K, 308K and 318K.

4.3.3.2 Pseudo second-order kinetics

Unlike pseudo first-order, the pseudo second-order kinetics was found to show a better fit towards the sorption of studied heavy metals for the entire sorption period. Its mathematical expression can be written as:

$$\frac{t}{q_t} = \frac{1}{h} + \frac{t}{q_e} \quad (4.4)$$

$$h = K_2 q_e^2 \quad (4.5)$$

where K_2 is the rate constant (g/mg.min) and h is the initial sorption rate (mg/g.min).

The slight differences between the experimental and calculated q_e can be ascribed to experimental error. The mostly high R^2 values were obtained for different metal ions at different temperature. It can also be said that the pseudo second-order sorption mechanism predominated and that the overall sorption rate seems to be controlled by a physisorption of adsorbate on adsorbent surface [200,201].

Although the dependence of the rate constant on the temperature could not be ascertained, yet the **h** (initial sorption rate) values were found to increase with temperature for the three studied metal ions (Fig. 4.13 and Table 4.2). It is also noteworthy that the sorption of Pb^{2+} was strangely enhanced more than Cr^{3+} at higher temperatures (308K and 318K) and this is perhaps due to more accommodation of the largely sized Pb^{2+} (120 pm) into the cavities of AT-SDUSY with more grip than smaller size but highly charged Cr^{3+}. However, the expected trend was observed in terms of **h**-values at the room temperature (Cr^{3+}>Pb^{2+}>Cd^{2+}).

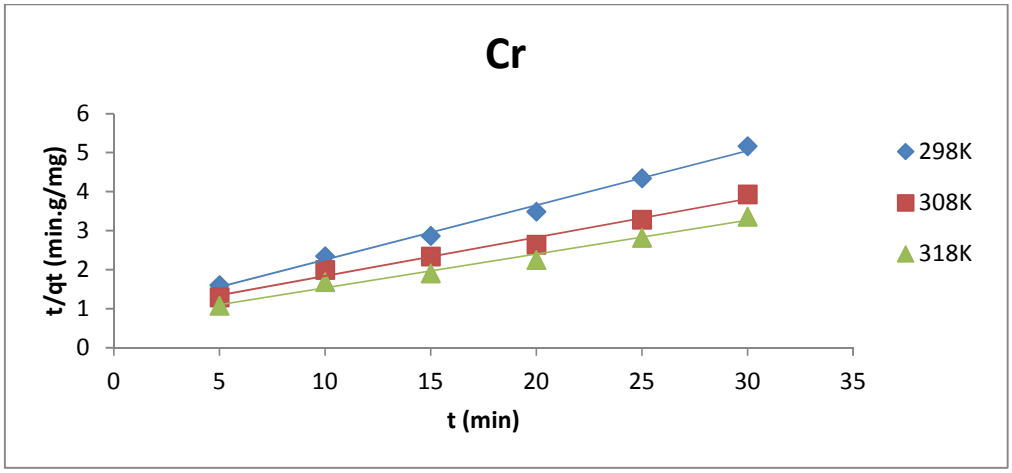

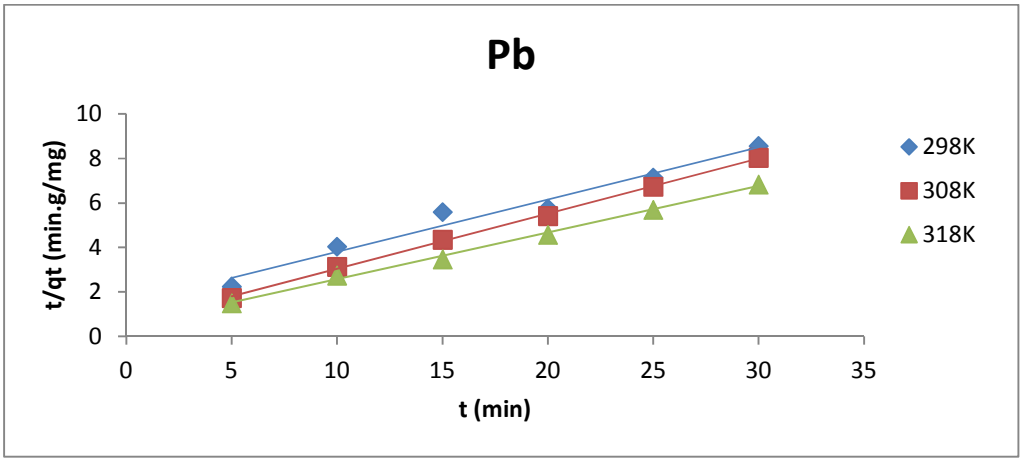

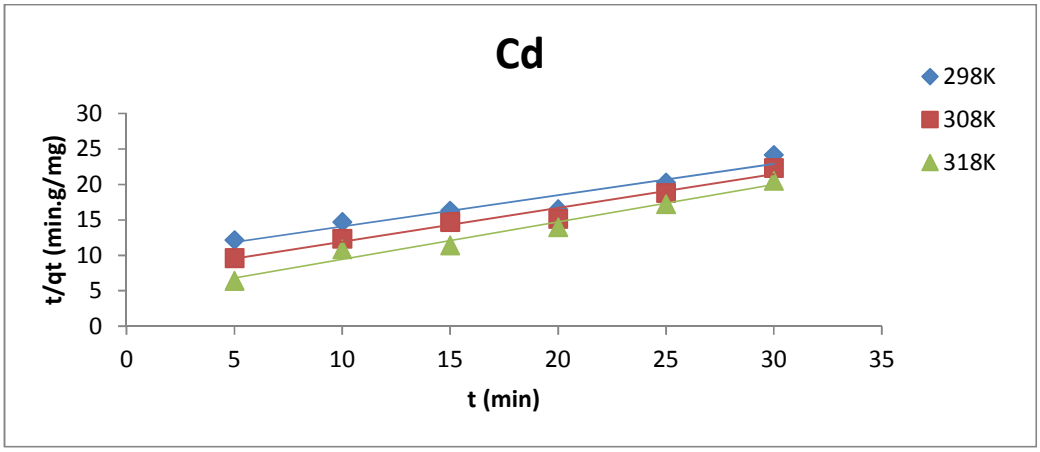

Figure 4.13 Pseudo-Second order kinetic plots obtained for Cr^{3+}, Pb^{2+} and Cd^{2+} ions adsorption on AT-SDUSY at 298K, 308K and 318K.

Table 4.2 Kinetic parameters obtained for Cr^{3+}, Pb^{2+} and Cd^{2+} ions adsorption on AT-SDUSY at 298K, 308K and 318K.

Ions		Pseudo-first order kinetics				Pseudo-second order kinetics				Interparticle diffusion Model		
	T (K)	q_e,exp (mg/g)	$K_1(10^1)$ (min^{-1})	$q_{e,}$cal (mg/g)	R^2	K_2 (10^2) (g/mg.min)	q_e, cal (mg/g)	h (mg/g.min)	R^2	K_{id} (mg/g.$min^{1/2}$)	C (mg/g)	R^2
Cr^{3+}	289	5.81	2.11	9.77	0.95	2.26	7.16	1.16	0.99	0.86	1.52	0.90
	308	7.64	2.80	30.19	0.91	1.15	10.10	1.17	0.98	1.28	1.18	0.93
	318	8.93	2.53	23.40	0.88	1.11	11.56	1.49	0.98	1.45	1.67	0.91
Pb^{2+}	289	3.5	2.65	10.71	0.85	3.76	4.26	0.68	0.97	0.46	1.11	0.90
	308	3.73	2.03	3.39	0.94	10.70	4.03	1.74	1.00	0.28	2.30	0.94
	318	4.39	2.51	4.94	0.96	9.11	4.78	2.08	1.00	0.36	2.63	0.84
Cd^{2+}	289	1.24	2.35	4.60	0.92	2.01	2.27	0.10	0.93	0.24	0.00	0.92
	308	1.34	2.29	4.13	0.90	3.18	2.10	0.14	0.97	0.26	0.00	0.94
	318	1.46	2.27	3.31	0.96	6.66	1.90	0.24	0.97	0.30	0.00	0.82

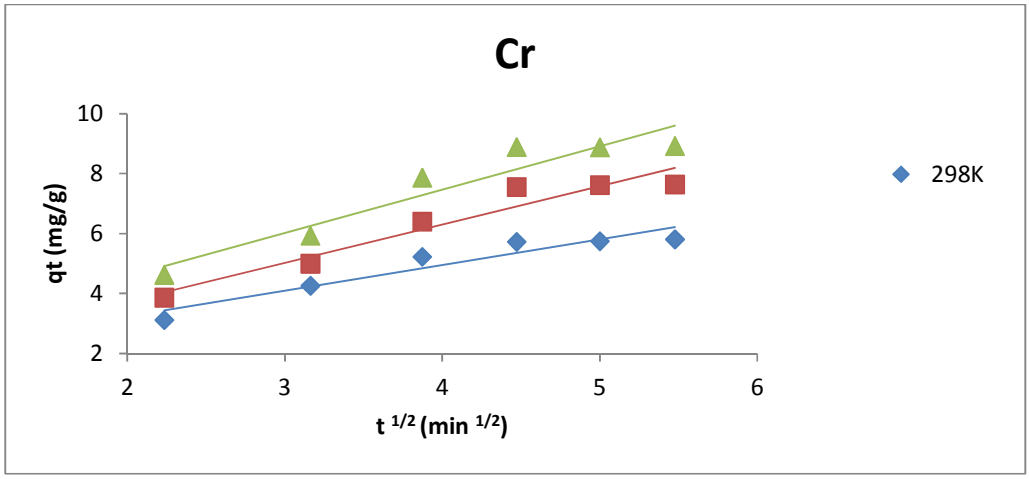

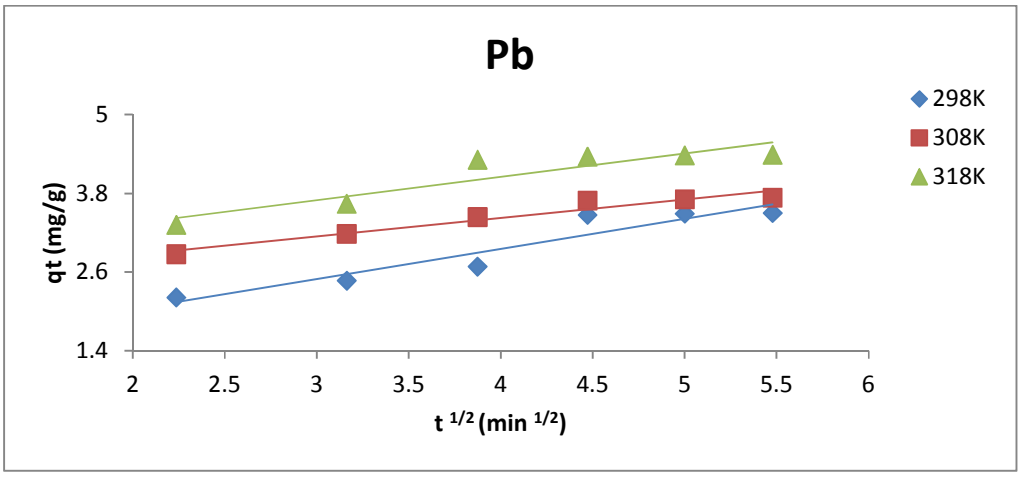

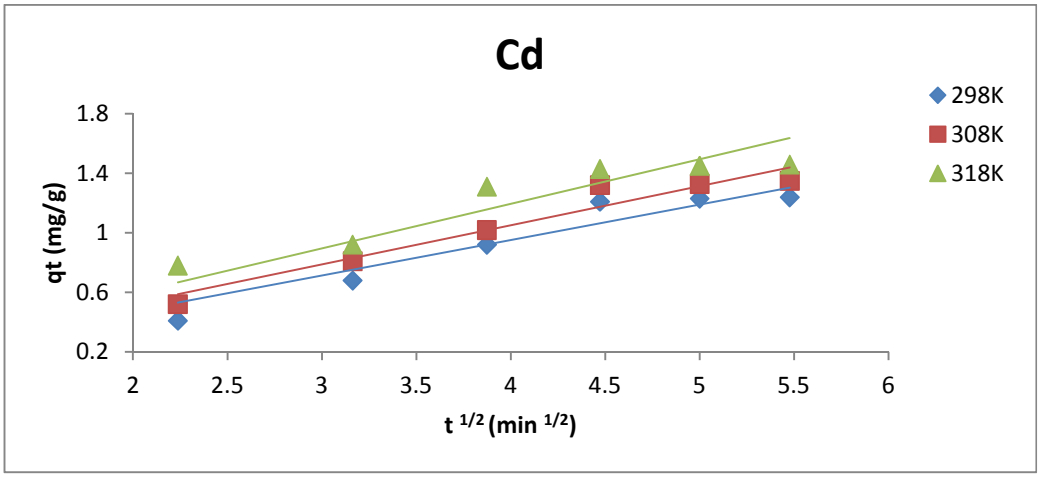

Figure 4.14 Intraparticle diffusion model (Morris-Weber) plots obtained for Cr^{3+}, Pb^{2+} and Cd^{2+} ions adsorption on AT-SDUSY at 298K, 308K and 318K.

4.3.3.3 Intra-particle diffusion kinetic model

The Morris-Weber equation plots did not pass through the origin, except for Cd^{2+} (Fig. 4.14), yet all have low R^2 values (Table 4.2). Thus, the mechanism involved could not be a diffusion based and so there exists a complicated mechanism [202].

$$q_t = K_{id} t^{\frac{1}{2}} + c \quad \textbf{(}4.6)$$

where K_{id} is the rate constant of the intraparticle transport (mg/g.$min^{1/2}$), q_t is the amount adsorbed at time t (mg/g).

4.3.4 Adsorption isotherm studies

The isotherms suggest the pattern of adsorption of the adsorbate on the adsorbent surface. For instance, while Langmuir predicts the monolayer adsorption pattern, Freundlich adsorption isotherm gives information about the surface heterogeneity as well as the exponential distribution of active sites and their energies (Baker *et al*., 2009) [203].

4.3.4.1 Langmuir model

The linearized form of Langmuir model equation (4.7) was used to make a plot in Fig. 4.13.

$$\frac{1}{q_e} = \frac{1}{C_e} \cdot \frac{1}{b\, Q_o} + \frac{1}{Q_o} \quad (4.7)$$

where q_e is the equilibrium ion uptake ($mg.g^{-1}$), *Ce* represents the equilibrium concentration ($mg.L^{-1}$), *b* is the sorption equilibrium constant ($L.mg^{-1}$) and Q_o *is* the maximum adsorption capacity ($mg.g^{-1}$).

$$R_L = \frac{1}{1 + b C_o} \quad (4.8)$$

The isotherms are regular positive and reflect the efficiency of the AT-SDUSY for heavy metal ions removal from water over a wide range of concentration. As shown in Fig. 4.15, the amount of metal ions sorbed increased with temperature, further indicating the endothermic nature of the adsorption process. The $0<R_L<1$ was obtained for the studied metal ions (Table 4.3), indicating the favorable type of the isotherms [101-102,204].

4.3.4.2 Freundlich model

The Freundlich isotherm expression in logarithmic form is as written in equation 4.9,

$$\log q_e = \log K_F + \left(\frac{1}{n}\right) \log C_e \quad (4.9)$$

where n and K_F are Freundlich isotherm constants related to adsorption intensity and adsorption capacity respectively.

It is fondly used for non-ideal multilayer sorption on heterogeneous surfaces [205]. The Fig. 4.16 shows that the sorption of the studied metal ions fit well into the Freundlich isotherm model, with good linearity. As shown in the Table 4.3, both sorption intensity (n) and sorption capacity (K_F) increased with temperature, with K_F following the trend $Cr^{3+}>Pb^{2+}>Cd^{2+}$at all temperatures while the sorption intensity is differently higher for Pb^{2+}. The enhanced sorption at higher temperatures can be due to the increase in active

site available for sorption and/or change in pore size which perhaps enhanced the rate of sorption of the metal ions [206].

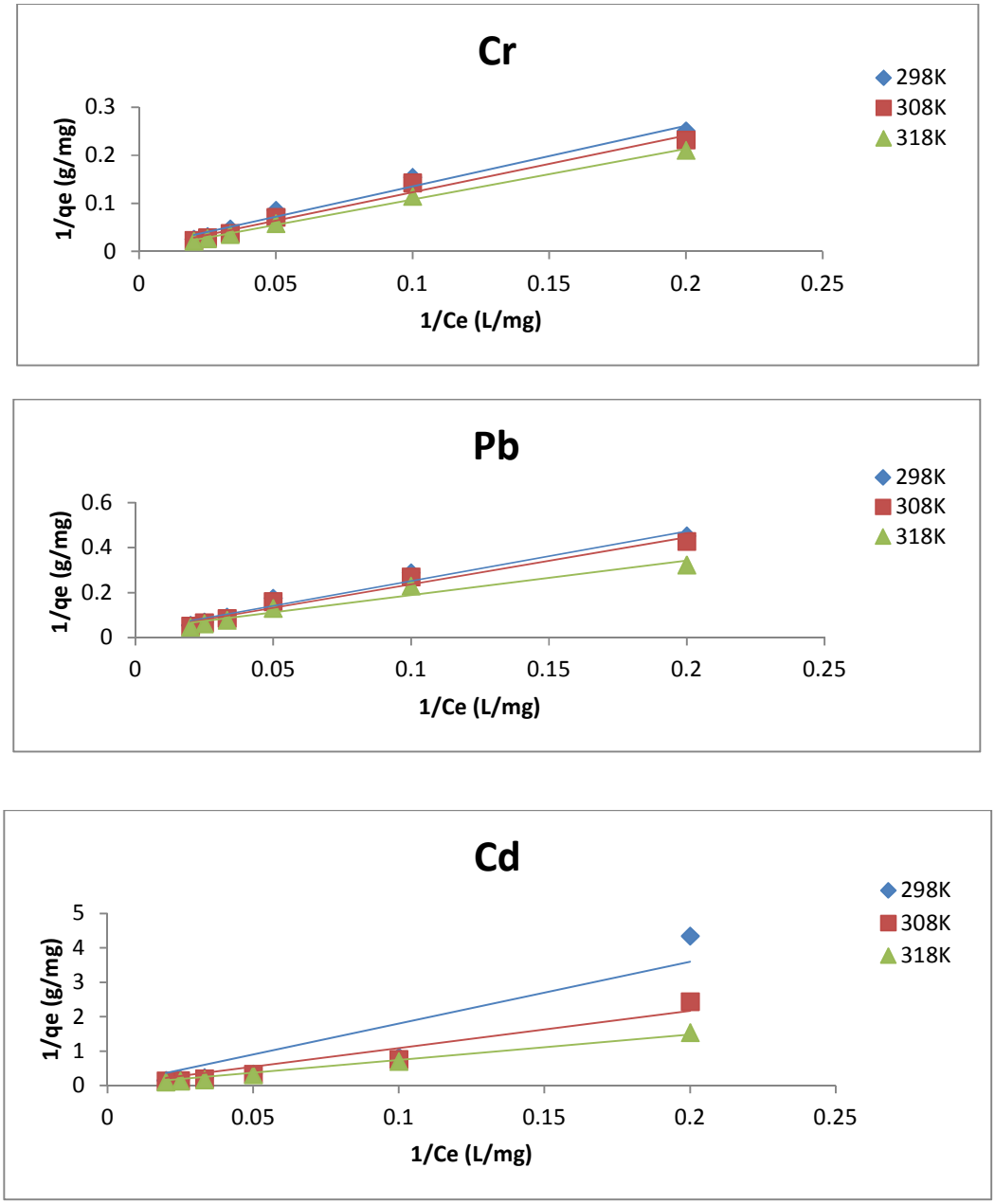

Figure 4.15 Langmuir Isotherm plots obtained for Cr^{3+}, Pb^{2+} and Cd^{2+} ions adsorption on AT-SDUSY at 298K, 308K and 318K.

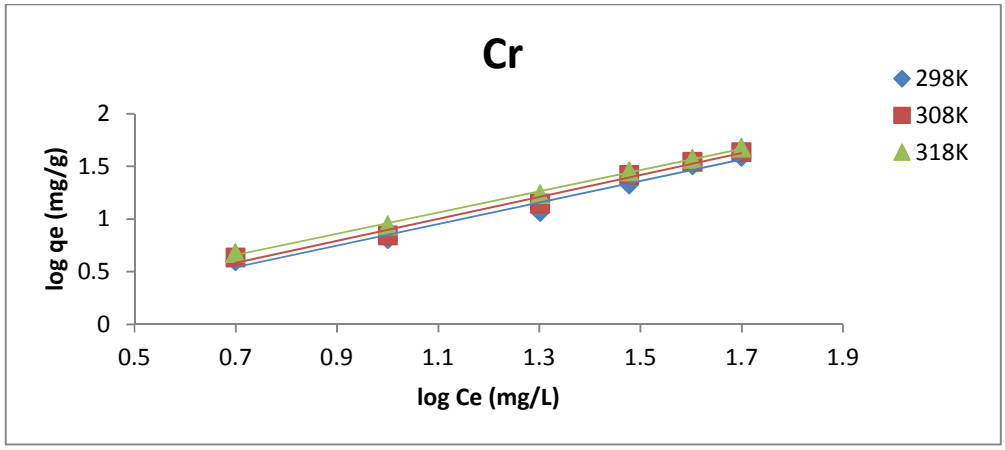

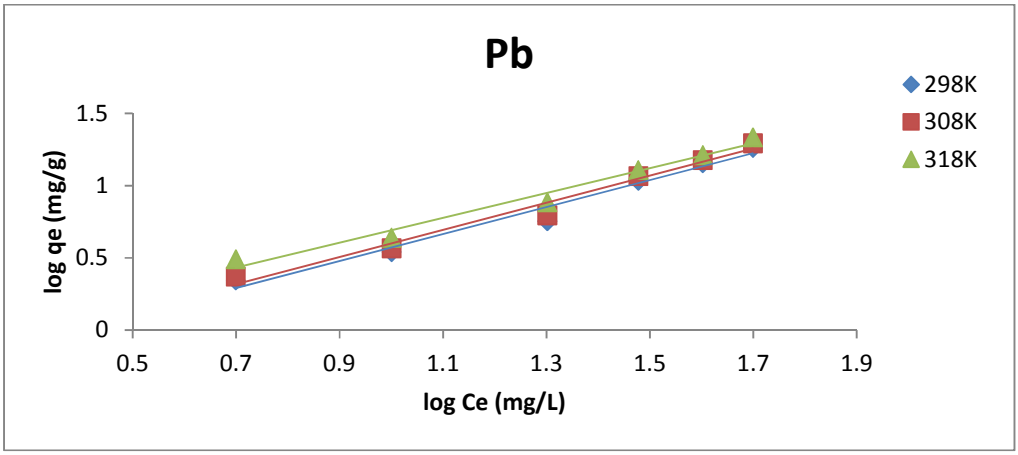

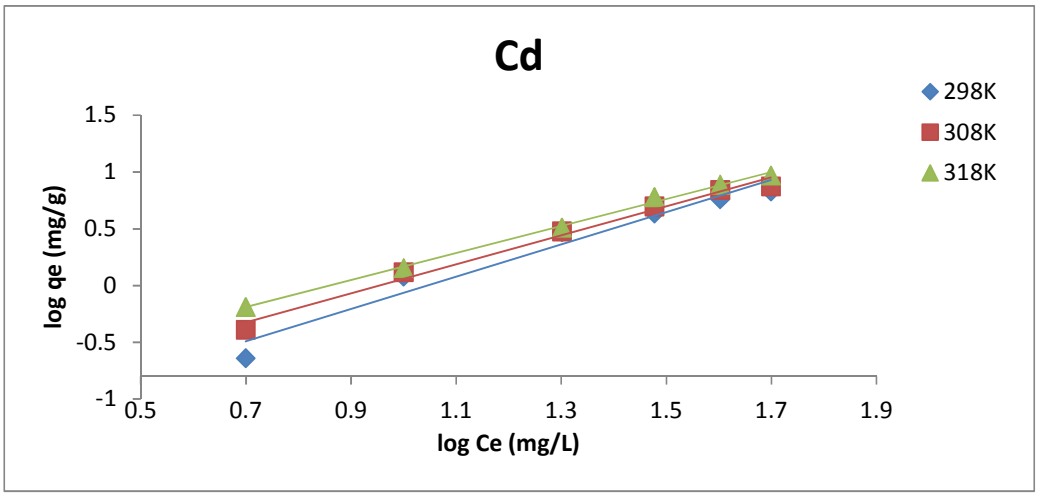

Figure 4.16 Freundlich Isotherm plots obtained for Cr^{3+}, Pb^{2+} and Cd^{2+} ions adsorption on AT-SDUSY at 298K, 308K and 318K.

Table 4.3 Isotherm parameters obtained for Cr^{3+}, Pb^{2+} and Cd^{2+} ions adsorption on AT-SDUSY at 298K, 308K and 318K.

Metal		Langmuir isotherm parameters				Freundlich isotherm parameters				Temkin isotherm parameters		
	T (K)	Q_o, (mg/g)	b (10^2) (L/mg)	R^2	R_L	K_F (10^2) (mg/g)	1/n, (mg/g)	n	R^2	K_T (10^2) (L/mg)	b_T (KJ/mol)	R^2
Cr^{3+}	289	109.9	7.22	0.98	0.73	67.07	1.02	0.98	0.98	67.66	2.42	0.98
	308	200.0	4.24	0.98	0.83	71.86	1.04	0.97	0.99	72.78	2.46	0.99
	318	434.8	2.18	0.99	0.90	89.19	1.01	0.99	1.00	89.28	2.62	1.00
Pb^{2+}	289	70.53	1.42	0.97	0.58	43.21	0.94	1.07	0.98	40.79	2.65	0.98
	308	75.79	1.32	0.97	0.60	45.76	0.94	1.06	0.98	43.50	2.73	0.98
	318	84.68	2.24	0.95	0.47	67.83	0.86	1.16	0.98	63.66	3.08	0.98
Cd^{2+}	289	200	0.03	0.85	0.98	3.28	1.42	0.70	0.96	9.03	1.74	0.96
	308	333	0.03	0.93	0.99	6.11	1.27	0.78	0.98	11.15	2.01	0.99
	318	500	0.03	0.99	0.98	9.51	1.19	0.84	1.00	13.83	2.22	1.00

4.3.4.3 Temkin isotherm model

From the Temkin adsorption isotherm expression in equation (4.10), the amount of energy required for the absorption by one layer on the adsorbent's surface can be obtained.

$$\ln q_e = \left(\frac{RT}{b_T}\right) \ln K_T + \left(\frac{RT}{b_T}\right) \ln C_e \quad (4.10)$$

where b_T is the Temkin constant related to the sorption heat in kJ/mol, K_T is the binding energy constant at equilibrium; an equivalence of maximum binding energy (L/g), R is the universal gas constant (0.008314J/mol-K) and T is the absolute temperature in Kelvin (K). The Fig.4.17 shows the good linearity of the plots and as shown in the Table 4.3, the sorption heat at a particular temperature was comparatively higher for Pb^{2+}, perhaps due to its largest size among the ions studied.

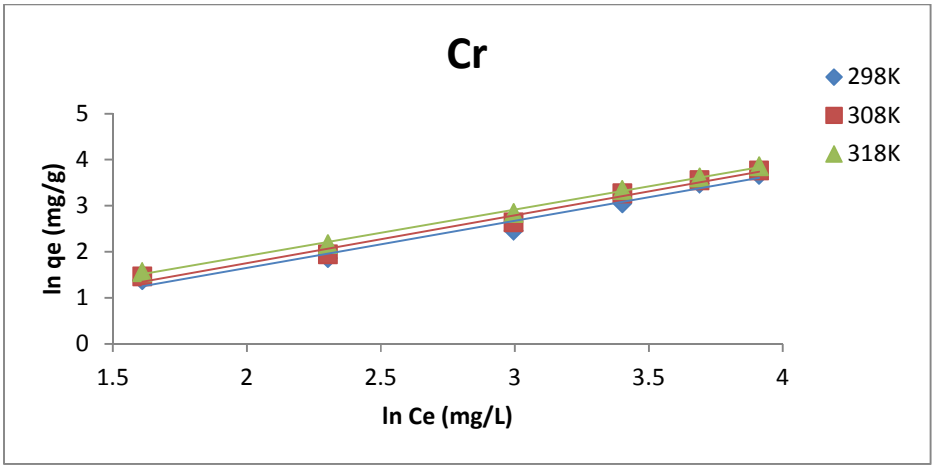

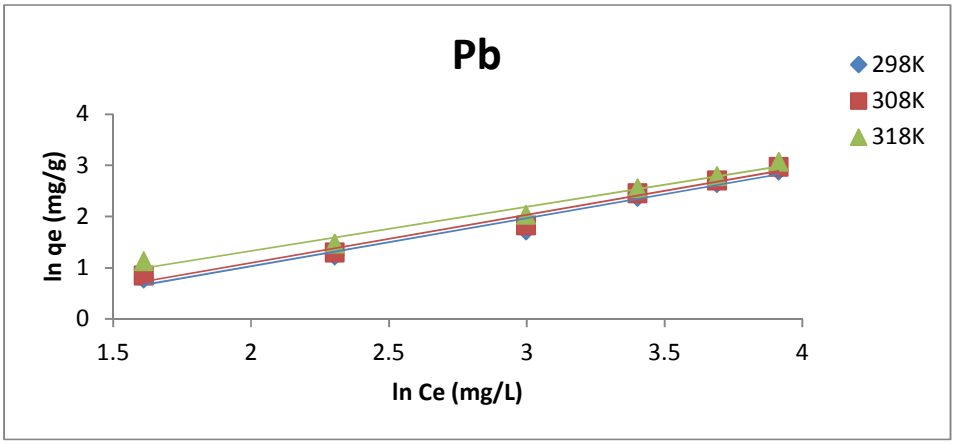

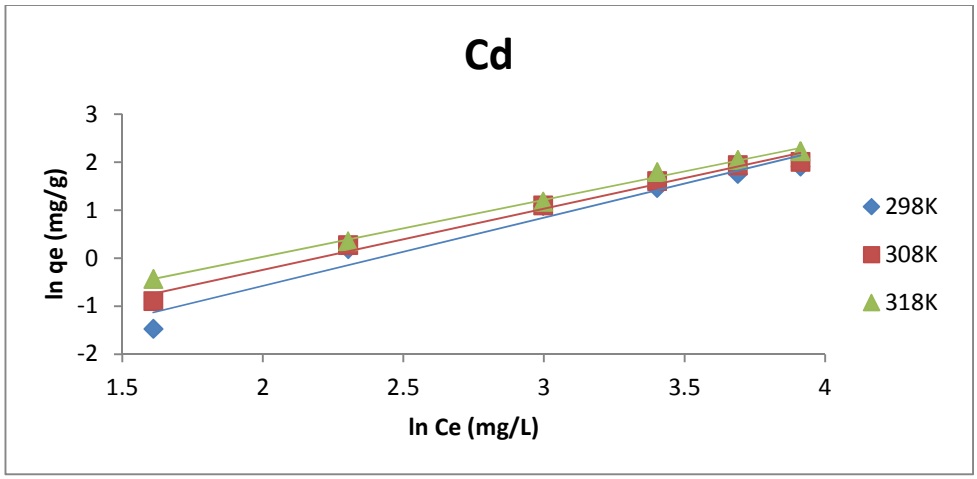

Figure 4.17 Temkin Isotherm plots obtained for Cr^{3+}, Pb^{2+} and Cd^{2+} ions adsorption on AT-SDUSY at 298K, 308K and 318K.

4.4 Summary

The superdealuminated faujasite (FAU) Y-type zeolite was modified via alkaline treatment to achieve increment in the surface area and enhancement of the isolated silanol functional group that assisted in sorption process of heavy metal ions from water. The modified zeolite, AT-SDUSY, showed better adsorption properties than the parent zeolite, SDUSY40. The kinetic data agreed more to the pseudo second order kinetics and the isotherm showed a favorable type with more conformity to Freundlich isotherm. The obtained results obviously showed that the heavy metal ions sorption process was endothermic and the sorbent materials showed more selectivity to lead ion in the solution. The trimodal mesoporous zeolite packed µ-SPE device coupled with ICP-OES provided excellent alternative for routine analysis of lead (II) ion in the matrix of heavy metal ions like cadmium(II), nickel(II), cobalt(II), chromium(III) and copper (II) ions in water system. The other heavy metal ions removal and softening of hardwater can be well achieved with this economical AT-SDUSY zeolite as a novel sorbent material.

CHAPTER 5

CONCLUSION AND RECOMMENDATIONS

5.1 Conclusion

The results gave insight about the nature of modification obtained during various alkaline treatments, and improved the knowledge about the physico-chemical implications as related to the expected catalytic performance as well as enhanced adsorption properties. Quaternary ammonium cation based alkaline treatment showed elegant approach to obtain hierarchical dealuminated Y-zeolites with different degree of mesoporosity. The organic tetraalkylammonium hydroxides as desilicating agents moderately controlled the kinetic of the silicon dissolution depending on their level of hydrophobicity, effective cationic diameters and thus steric hinderance in the trend $TBA^+ \approx TPA^+ > TEA^+ > TMA^+ >> Na^+$ at the same concentration. The inclusion of bulky organic templates, such as TBA^+ and TPA^+, as external pore directing agents convincingly redeemed the negative impact of sole inorganic hydroxide on the zeolite structure as desilicating agent but the time-consuming ion-exchange step is still required.

Remarkably, our new approach of double organic mixtures (in particular, $TBA^+ + TEA^+$ and $TPA^+ + TEA^+$) showed more effectiveness than those of (TBA^+ + NaOH) treatments, and thus gave a chance to bypass the crucial ion-exchange step in the alkaline treatment procedures, thereby saving time and energy. It is noteworthy that the said efficiency of

double tetraalkylammonium mixtures yet depends on the concentration and the nature of included tetraalkylammonium cations, as well as the Si/Al ratio of the dealuminated Y zeolites. The degradation of low density polyethylene at lower temperature, as well as higher conversion of alkylating agent (benzylalcohol) within shorter period in the studied Friedel-Craft alkylation of toluene, convincingly proved this supremacy, at a comparable concentration.

This study further showed the efficiency of modified dealuminated FAU-type Y-zeolite as adsorbent in heavy metal ions removal, alongside the catalytic activity evaluations. Aside the large surface area, the nature of pores present in an adsorbent played a significant role in its adsorption performance. The choice of this type of zeolite was due to the characteristic large surface area with cavities (due to dealumination) that could harbor heavy metal ions and the modification by alkaline treatment proved to enhance the adsorption capacity of the zeolite material as revealed in this study. The modified zeolite showed better adsorption properties than the untreated zeolite. The kinetic data obtained agreed more to the pseudo second order kinetics while the isotherm showed a favorable type with more agreement to Freundlich isotherm pattern. The obtained results obviously showed that the heavy metal ions sorption process was endothermic and the sorbent materials showed more selectivity to lead ion in the solution. The AT-SDUSY could be an excellent alternative solid phase extraction (SPE) sorbent for routine analysis of trace lead ion in water samples. Interestingly, removal of many heavy metal ions and softening of hard water could be well achieved using the economical modified zeolite material parked micro-SPE device.

5.2 Recommendations

This approach of modification can be extended to other zeolites for various applications in catalysis and separation science. Kinetic studies of this new desilication approach may unveil interesting knowledge behind the pore directing role of one quaternary ammonium cation in the presence of other at the same and/or varying concentration. Also, a more insightful research effort should be directed towards the scalable application of the materials made by this new approach. In addition, the AT-SDUSY can be investigated for the removal of all kinds of heavy metal ions in the real waste water treatment and pollution control.

Appendices

Detailed Procedures in Sample Preparation and Data Processing.

Appendix A: Sample Preparation Procedure for ICP Analysis of Zeolites

(A1.) <u>Sample Digestion Procedure</u>

- ✓ Weigh 50 mg of powdered zeolite samples into platinum crucible.
- ✓ Add 300 mg of powdered lithium metaborate to the sample and mix thoroughly. Avoid spill of the contents from crucible while mixing.
- ✓ Put inside the furnace (pre-heated at 300 ^{0}C) and let the sample be heated for 5 mins then adjust the furnace temperature to 1000 ^{0}C set point. Upon reaching 1000 ^{0}C, let the sample be heated for 15 minutes more, then remove from the furnace and let it cool down for few minutes.
- ✓ Wash the outside of platinum crucible with distilled water, and then put inside the 50-ml clean beaker.
- ✓ Add 10 ml of 10% HNO_3 inside the platinum crucible, then add distilled water up to 25-30 ml mark (depends on the shape and size of the crucible) or until just a little above the lid of the crucible. Pour distilled water using wash bottle aiming at the sides of the beaker and not inside the crucible.
- ✓ Put the beaker with crucible on a hot plate at 100 ^{0}C with moderate stirring by putting small stirring bar inside the crucible. Leave the solution on the hot plate for 1 to 2 hrs depending on the content of the beaker or wait till the water level reach the lid of the crucible.

- ✓ Transfer the digested solution to a clean 50 ml volumetric flask. Rinse the beaker and crucible analytically and add the rinse to the solution in the flask. Repeat 2-3 times each using very little amount of water enough to rinse the beaker and the crucible completely. Dilute the solution to the mark of 50 ml volumetric flask.

NOTE: The procedure does not require filtration of the digested solution, because clear solution should be achieved after these steps. Otherwise, digestion should be repeated.

(A2.) Calculation of ICP Result (Silica – Alumina)

The result obtainable during measurement is in mg of element (analyte) per liter of the solution examined. Without any previous preparation and/or dilution, the result obtained is the final one (mg/L = ppm), but when there is sample dilution prior to analysis, some additional calculation is needed. For example, assume that one digests 50 mg of the zeolites in acid, and the final volume of the sample is 50 ml, after which the solution is measured on ICP-OES to detect 38.15 mg/L of Si and 2.64 mg/L of Al. As the need arises, the digested solution is further digested using 5 mL of it to 50 mL final dilution. Then the actual amount of Si and Al, SiO_2 and Al_2O_3 in w/w% and mole ratio can be calculated as follows:

Available Data:

Weight of sample = 0.050 g, Volume of solution = 50 mL

$$Dilution\ factor\ (\boldsymbol{DF}) = \frac{Volume\ of\ solution}{weight\ of\ sample} = \frac{50ml}{0.05g} = 1000mL/g$$

2nd Dilution Factor = **10**

Actual Reading: **Si** = 38.15 mg/L , **Al** = 2.64 mg/L

Sample Calculation**:**

$$\boldsymbol{Total\ Si} = (38.15\ mg/L) * (1000mL/g) * 10 = 381{,}500\ mg/kg\ \ of\ zeolites$$

$$\%\ \boldsymbol{Si} = \mathbf{38.15}\%$$

$$\boldsymbol{Total\ Al} = (2.64\ mg/L) * (1000mL/g) * 10 = 26{,}400\ mg/kg\ \ of\ zeolites$$

$$\%\ \boldsymbol{Al} = \mathbf{2.64}\%$$

$$\%\ \boldsymbol{SiO_2} = \%\ Si * \frac{MW\ of\ SiO_2}{MW\ of\ Si} = 38.15\% * \left(\frac{60.08}{28.09}\right) = \mathbf{81.64}\%$$

$$\%\ \boldsymbol{Al_2O_3} = \%\ Al * \frac{MW\ of\ Al_2O_3}{(2 * MW\ of\ Al)} = 2.64\% * \left(\frac{101.96}{53.96}\right) = \mathbf{4.99}\%$$

$$\%\ \boldsymbol{mol\ SiO_2} = \frac{\%\ SiO_2}{MW\ of\ SiO_2} = \frac{81.64}{60.08} = \mathbf{1.35887}$$

$$\%\ \boldsymbol{mol\ Al_2O_3} = \frac{\%\ Al_2O_3}{MW\ of\ Al_2O_3} = \frac{4.99}{101.96} = \mathbf{0.04894}$$

$$\boldsymbol{Mol\ ratio}\ \left({}^{SiO_2}/_{Al_2O_3}\right) = \frac{1.35887}{0.04894} = \mathbf{27.77}$$

Appendix B: Sample Preparation Procedure for SEM Imaging Experiment

- ✓ Dispersion of few amount of zeolite sample in about 10ml of ethanol
- ✓ Follow by sonication of the mixture for 10 minutes.
- ✓ Then, addition of three (3) droplets of ethanol containing the still floating material parts (without disturbing the sediment) onto the clean SEM stub and wait for the

ethanol to evaporate. The addition of 3 droplets of supernatant is repeated once again.

- ✓ After the evaporation of ethanol, the SEM stub is labeled according to the sample code.
- ✓ Thereafter, the sample is given gold-coating (40 sec duration of coating after 10 minutes vacuum saturation).
- ✓ Finally, the sample successfully coated with gold is imaged under SEM.

Appendix C: Detailed Procedure for Pyrolysis of LDPE Tests

(C1.) Weighing, Mixing and Experiment

- ✓ Weigh 60 mg of catalyst and add to 180 mg of LDPE and mix thoroughly to have well blended mixture (mass ratio 1:3);
- ✓ Take about 8-10mg and put into the α-Al_2O_3 pan of the thermobalance and carry out the degradation of the mixture under N_2 (70 cm^3 STP min^{-1}) with temperature ramping from 30 to 700^0C at 10^0C min^{-1}.
- ✓ Check and ensure that the final weight percent is *ca.* 25%, representing the %wt of the catalyst only
- ✓ Process the data to calculate percentage conversion of the LDPE at different temperature from weight loss data.

(C2.) Data Processing and Calculation

- ✓ Copy and paste the data to new excel worksheet;
- ✓ Delete the columns for time and % weight to remain only that of **temperature (T) and actual weight (X_i);**
- ✓ Record the actual weight at final temperature as the weight of the catalyst in the initial mixture, $\mathbf{X_f}$;
- ✓ Subtract this weight of the catalyst from each of the actual weight entries in all the rows, to give a column labeled as actual weight of the LDPE at respective temperature, **(X_i-X_f);**
- ✓ Compute the % weight loss of LDPE as below where XX is the value of **(X_i-X_f)** at first temperature entry (i). By this, the first entry in this column must be 100%.
    - $\%\ wt\ present = \frac{(X_i - X_f) * 100}{XX}$
- ✓ Calculate for each entry the % conversion as:
    - $\%\ conversion, LDPE = (100 - \%\ wt\ present, LDPE)$
- ✓ Make a plot of **% conversion** (y-axis) against **Temperature** (x-axis)

Appendix D: Activity Testing Procedure for Toluene Alkylation with Benzyl alcohol Using Parr 4848 Reactor Controller

(D1.) Catalyst Sieving

Make the powder catalyst into pellet by pressing it with mechanical pressure of *ca.* 1000 pounds for 30 secs using Carver Laboratory Press (Perkin-Elmer, Model C, SN: 31006-

682). Then sieve the catalyst pellet(s) to have a uniform particle size of 850 microns. Thereafter, weigh 1 gm of the sieved catalyst to be added to the feed for the reaction.

(D2.) Feed Loading

Only two-third of the volume capacity of the reaction vessel can be used for the complete feed. So, put 100 ml of the reaction mixture of toluene and benzyl alcohol (90:10) inside the vessel and add the 1 gm of sieved catalyst and assemble the set-up of the Parr 4848 Reactor Controller (150 ml working volume) whose temperature ramping condition set to reach 140°C within 30 mins and 72 psi for the studied reaction period (0-180 mins).

(D3.) Assembling and Charging of the set-up for Leakage Check

Ensure the head sits levelly on the cylinder vessel and tighten all bolts first with hand and then lock with 25 ft lb torque to ensure uniform loading on all the bolts. Then, complete the assembly of the set-up by making all the necessary connections and subsequently check for the leakage in the assembly by smartly charging the set-up up to 10 psi (see the reactor indicator) with little amount of nitrogen gas and observe for possible drop in the system pressure (due to leakage) for 10 sec. The leakage can be due to the rupture of the flexible graphite gasket, improper lock of the vessel, opening of any of valves. These likely causes of leakage should be addressed timely to minimize the contact time of catalyst with the feed prior to attaining the reaction condition. In the case of rupture, the gasket should be replaced.

(D4.) Heating, Pressurizing and Sampling

Having ensured that there is no leakage in the system, the pressure is released to zero psi and the set-up is heated to 140^0C (typically within 30mins. Obviously, the pressure will be rising as temperature increases but it will not reach the desired 72 psi for the reaction. When the temperature is reached, the set-up is the pressurized up to 72 psi, the rotor is set for 800 rpm and the sample (at t = 30 mins) is taken. Sampling continues at different time-on-stream and only about 0.5ml is taken at each sampling. It is likely that pressure drops after each sampling, and then the drop is made up for by gently pressurized the set up back to 72 psi.

(D5.) GC Analysis

Label the liquid samples collected at different time accordingly and analyze them using a gas chromatograph (Agilent 7890A) equipped with an HP-5 capillary column and a flame ionization detector (FID).

(D6.) Calibration curve and Conversion calculation

Prepare different standard concentrations (0.05 - 2 M) of the limiting reagent, BzOH, and carry out GC analysis to obtain their respective area under curve from the chromatogram. Then, the area under curve is plotted against the concentration to obtain a calibration curve, from which an estimate of BzOH conversion at respective time can be made. Note that the assignment of retention time for BzOH should be done earlier with gas chromatography and mass spectroscopy (GC-MS).

$$Conc_{stock}(moldm^{-3}) = \frac{(density(gcm^{-3}) * \%\, purity * 1000)}{mw(gmol^{-1})}$$

$$Conc_{BzOH,stock}(moldm^{-3}) = \frac{\left((1.045\ gcm^{-3}) * 0.98 * 1000\right)}{(108.14\ gmol^{-1})} = 9.47M$$

$$Conc_{std-1}(M) = \frac{Conc_{stock}(M) * V_{stock}(ml)}{V_{std-1}(ml)}$$

$$Conc_{std-1}(M) = \frac{(9.47\ M) * (53\mu L)}{(10\ mL)} = 0.05\ M$$

Table 6.1 Area under curve from chromatogram for BzOH calibration curve**.**

Standard codes	Retention Time (min)	Concentration (M)	Area under curve
Std-1	8.68	0.05	872.016
Std-2	8.7	0.1	1727.157
Std-3	8.73	0.2	3397.249
Std-4	8.8	0.5	8643.344
Std-5	8.91	1	20300.15
Std-6	9.04	2	42670.6

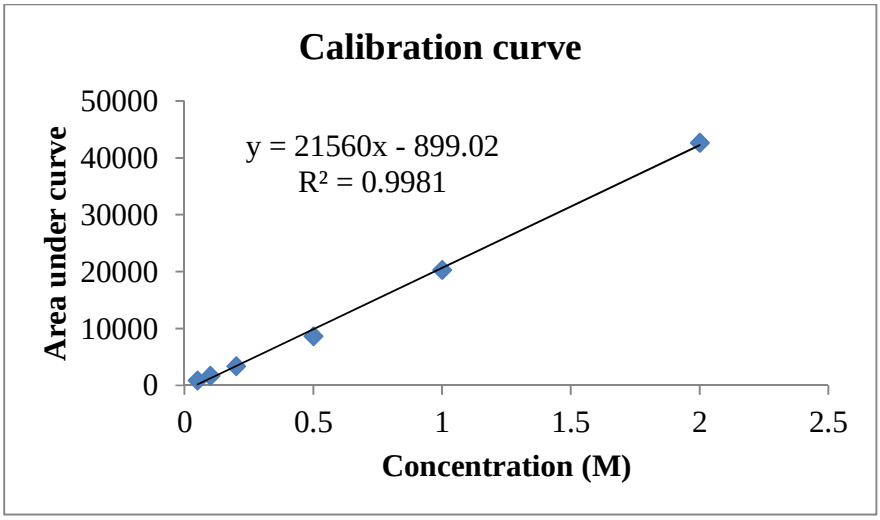

Figure 6.1 Calibration curve for estimation of BzOH concentration

(D7.) Data Processing and Plotting

The goodness of the calibration curve is evaluated by its R^2-value and this equation below can be used to estimate the amount of BzOH present in each sample:

$$Conc.(ppm), present = \frac{(Area\ under\ curve) + (899.02)}{21560}$$

$$Conc_{feed}(M) = \frac{Conc_{stock}(M) * V_{stock}(ml)}{V_{feed}(ml)}$$

$$Conc_{feed}(ppm) = \frac{(9.47M) * (10\ ml)}{(100\ ml)} = 0.947\ M$$

This means that 10 ml of stock BzOH needs to be diluted with solvent (toluene) to make 100 ml such that the concentration of BzOH in each reaction feed is *ca.* 0.95 M.

$$\%\ BzOH\ conversion = \frac{(0.95 - Conc_{present}) * 100}{0.95}$$

Table 6.2 Calculation of BzOH conversion for sample CBV720-Parent.

Time-on-stream (min)	Retention Time (min)	Area under curve	BzOH Concentration present (M)	% BzOH Concentration converted
0	-	-	0.95	0
30	8.86	13268.55	0.657	30.83
35	8.82	8661.628	0.443	53.32
40	8.82	8538.341	0.438	53.92
50	8.82	8379.692	0.430	54.70
60	8.81	7993.451	0.412	56.58
70	8.80	7261.757	0.379	60.16
90	8.80	7318.997	0.381	59.88
120	8.81	7547.027	0.392	58.76
150	8.80	7363.135	0.383	59.66
180	8.80	7307.658	0.381	59.93

Afterwards, a plot of % BzOH against time-on-stream is made for each of the catalyst for comparison.

References

[1] Bodek, I; Lyman, W.J.; Reehl, W.F.; Rosenblatt, D.H. *Environmental Inorganic Chemistry: Properties, Processes and Estimation Methods*, Pergamon Press, New York, **1998.**

[2] Goyer, R.A.; Chisolon, I.J. *Lead,* Academic Press, London, **1972.**

[3] Manahan, S. *Environmental Chemistry*, Brooks/Colei, CA, **1984.**

[4] Wase, J; Forster, C. *Biosorbents for Metal Ions*, Taylor & Francis, London, **1997.**

[5] Inglezakis, V.J.; Loizidou, M.D.; Grigoropoulou, H.P. *J. Colloid Interface Sci.*, **2003**, *261*, 49.

[6] World Health Organization, *Guidelines for Drinking-Water Quality*, **1984**.

[7] Environmental Protection Agency, *National Primary Drinking Water Regulation*, Washington, **2002**.

[8] Huang, C.P.; Blankenship, D.W. *Water Res.*, **1984**, *18*, 37.

[9] Panday, K.K.; Parsed, G.; Singh, V.N. *Water Res.*, **1985**, *19*, 869.

[10] Inglezakis, V.J.; Loizidou, M.M. *J. Colloid Interface Sci.*, **2004**, *275*, 570-576.

[11] Querol, X.; Moreno, N.; Umana, J.C.; Alastuey, A.; Hernández, E.; López-Soler, A.; Plana F. *International Journal of Coal Geology*, **2002**, *50(1)*, 413-423.

[12] EnDyna,I. Potential Nano-Enabled Environmental Application of Radionuclides. EPA/402/R-09/002, Washington, DC 20460, January **2009**.

[13] Rajec, P.; Domianová, K. *Journal of Radioanalytical and Nuclear Chemistry*, **2008**, *275(3)*, 503-508.

[14] Dyer, A. *An introduction to zeolite molecular sieves*, Wiley, **1988.**

[15] Perez-Ramirez, J.; Abello, S.; Bonilla, A.; Groen, J.C. *J. Adv. Funct. Mater*, **2009**, *19*, 164-172.

[16] Chang, L.L.Y. *Industrial Mineralogy: Materials, Processes, and Uses.* Upper Saddle River, NJ: Prentice Hall. **2002**.

[17] Cornelis, K. *Manual of Mineral Science,* 22nd edition. New York: Wiley, **2001**.

[18] Mumpton, F.A. ed. *Mineralogy and Geology of the Natural Zeolites.* Mineralogical Society of America Reviews in Mineralogy, vol. 4. Washington, DC: Mineralogical Society of America. **1977**.

[19] Breck, D.W. *Zeolite Molecular Sieves: Structure, Chemistry and Use*. John Wiley & Sons, New York, USA, **1974.**

[20] Baerlocher, C.; Meier, W.M.; Olson, D.H. *Atlas of Zeolite Framework Types*. 5th ed.; Elsevier: London, **2001**.

[21] Bekkum, H.V. *Introduction to Zeolite Science and Practice*, Elsevier Science Limited, Vol.137, **2001**.

[22] Armbruster, T.; Gunter, M.E. Crystal Structures of Natural Zeolites. In D.L. Bish and D.W. Ming (eds) *Natural Zeolites: Occurrence, Properties, Applications*. Rev. in Mineral and Geochem. vol. **45**, Washington, D.C., 1-67, **2001**.

[23] Deer, W.A.; Howie, R.A.; Zussman, J. *An Introduction to the Rock Forming Minerals*, 2nd ed., Longman, Harlow, London, 696pp, **1992**.

[24] Baerlocher, C.; McCusker, L.B. *Database of Zeolite Structures*, http://www.izastructure.org/databases.

[25] Meier, W.M.; Olson, D.H.; Baerlocher, C. *Atlas of Zeolite Structure Types.* Zeolites, 1996, *17*, 1-230.

[26] Gottardi, G.; Galli, E. *Natural Zeolites*. Minerals and Rocks Series vol. 18. xii + 409 pp. Berlin, Heidelberg, New York, Tokyo: Springer-Verlag. **1985.**

[27] Rajec, P; Domianová, K. *Journal of Radioanalytical and Nuclear Chemistry*, **2008**, *275(3)*, 503-508.

[28] Wi, B.D. Zeolite Molecular Sieves: Structure, Chemistry, and Use. John Wiley-Interscience, New York, **1974**.

[29] Zeolites (natural), USGS Mineral Commodity Summaries, **2011.**

[30] Robert, L. Virta Zeolites, USGS 2009 Minerals Yearbook, October, 2010.

[31] Ng, E.P.; Mintova, S. *Microporous and Mesoporous Materials*, **2008**, *114(1)*, 1-26.

[32] Rios, C.A.; Williams, C.D.; Fullen, M.A. *Applied Clay Science*, **2009**, *43(2)*, 228-237.

[33] Lin, D. C.; Xu, X.W.; Zuo, F.; Long, Y.C. *Microporous and Mesoporous Materials*, **2004**, *70(1)*, 63-70.

[34] Katović, A.; Subotić, B.; Šmit, I.; Despotović, L. *Zeolites*, **1989**, *9(1)*, 45-53.

[35] http://www.tobias-weisenberger.de/5Zeolites.html Jan, 2015.

[36] http://chemelab.ucsd.edu/methanol/memos/ZSM-5.html. Feb, 2015.

[37] http://en.wikipedia.org/wiki/File:Zeolite-ZSM-5-3D-vdW.png Feb,2015.

[38] Bekkum, H.V. E.M.F.; Jansen, J.C. (Eds.), *Stud. Surf. Sci. Catal.*, **1991,** *58*, 531.

[39] Duan, T.C.; Nakano, T.; Nozue, Y. *Journal of Magnetism and Magnetic Materials*, **2007**, *310(2)*, 1013-1015.

[40] Byrappa, K.; Yoshimura, M. Handbook of Hydrothermal Technology: A Technology for Crystal Growth and Materials Processing. William Andrew, **2001**.

[41] El-Juhany, L.I. *Australian Journal of Basic and Applied Sciences*, **2010,** *4(8)*, 3998-4010.

[42] Yang, C.S.; Mora-Fonz, J.M.; Catlow, C.R.A. *The Journal of Physical Chemistry C*, **2011**, *115(49)*, 24102-24114.

[43] Auerbach, S.M.; Carrado, K.A.; Dutta P.K., Handbook of Zeolite Science and Technology. CRC Press, **2003**.

[44] http://www.chem1.com/CQ/hardwater.html. March,2015.

[45] Streat, M.; Patrick, J.; Perez, M. *Water Research*, **1995**, *29(2)*, 467-472.

[46] Dulama, M.D.; Pavelescu, N.; Pasre, L. *Rom. J. Physics*, **2009**, *54*, 851-859.

[47] Wang, P.; Shen, B.; Shen, D.; Peng, T.; Gao, *J. Catalysis Communications*, **2007**, *8(10)*, 1452-1456.

[48] Crønsted, A. F. *Akad. Handl. Stockholm*, **1756**, *18*, 120.

[49] Tanabe, K.; Hölderich, W. F. *Appl. Catal. A*, **1999**, *181*, 399.

[50] Vermeiren, W.; Gilson, J.P. *Top. Catal.*, **2009**, *52*, 1131.

[51] Flanigen, E.M.; Broach, R.W.; Wilson, S.T. In: *Zeolites in Industrial Separation and Catalysis* (Ed. S. Kulprathipanja), Wiley-CVH, Weinheim, Germany, **2010**, 1-17pp.

[52] Broach, R.W.; Jan, D.Y.; Lesch, D.A.; Kulprathipanja, S.; Roland, E.; Kleinschmit, P. In: *Zeolites*, from: *Ullmann's Encyclopedia of Industrial Chemistry*, Wiley-CVH, Weinheim, Germany, **2012**, 1-35 pp.

[53] Khouw, C.B.; Davis, M.E. In: *Selectivity in Catalysis* (Eds. M. E. Davis, S. L. Suib), American Chemical Society, Washington, DC, United States, 1993, 206-211pp.

[54] Pérez-Ramírez, J.; Christensen, C.H.; Egeblad, K.; Christensen, C.H.; Groen, J.C. *Chem. Soc. Rev.* **2008**, *37*, 2530.

[55] Egeblad, K; Christensen, C.H.; Kustova, M.; Christensen, C.H. *Chem. Mater.*,**2008**, *20*, 946.

[56] Groen, J.C.; Moulijn, J.A.; Pérez-Ramírez, J. *J. Mater. Chem.,* **2006,** *16*, 2121.

[57] Chal, R.; Gérardin, C.; Bulut, M.; van Donk, S. *ChemCatChem*, **2011**, *3*, 67.

[58] Lopez-Orozco, S.; Inayat, A.; Schwab, A.; Selvam, T.; Schwieger, W. *Adv. Mater.*, **2011**, *23*, 2602.

[59] Ng, E.P.; Chateigner, D.; Bein, T.; Valtchev, V.; Mintova, S. *Science*, **2012**, *335*, 70.

[60] Zhu, K.; Egeblad, K.; Christensen, C.H. *Eur. J. Inorg. Chem.*, **2007**, *39*, 55.

[61] Abelló, S.; Pérez-Ramírez, J. *Phys. Chem. Chem. Phys.* **2009**, *11*, 2959.

[62] Pavel, C.C.; Palkovits, R.; Schüth, F.; Schmidt, W. *J. Catal.*, **2008**, *254*, 84.

[63] Roth, W.J.; Cejka, J. *Catal. Sci. Technol.*, **2011**, *1*, 43.

[64] Corma, A.; Fornes, V.; Pergher, S.B.; Maesen, Th.L.M.; Buglass, J.G. *Nature*, **1998**, *396*, 353.

[65] van Donk, S.; Janssen, A.H.; Bitter, J.H.; de Jong, K.P. *Catal. Rev.-Sci. Eng.* **2003**, *45*, 297.

[66] de Jong, K.P.; Zecevic, J.; Friedrich, H.; de Jongh, P.E.; Bulut, M.; van Donk, S.; Kenmogne, R.; Finiels, A.; Hulea, V.; Fajula, F., *Angew. Chem., Int. Ed.*, **2010**, *49*, 10074.

[67] Groen, J.C.; Moulijn, J.A.; Pérez-Ramírez, J., *Ind. Eng. Chem. Res.*, **2007**, *46*, 4193.

[68] Jiang, J.; Jorda., J.L.; Yu, J.; Baumes, L.A.; Mugnaioli, E.; Diaz-Cabanas, M.J.; Kolb, U.; Corma, A., *Science*, **2011**, *333*, 1131.

[69] Groen, J.C.; Bach, T.; Ziese, U.; Paulaime-van Donk, A.M.; de Jong, K.P.; Moulijn, J.A.; Pérez-Ramírez, J., *J. Am. Chem. Soc.*, **2005**, *127*, 10792.

[70] Holm, M.S.; Taarning, E.; Egeblad, K.; Christensen, C.H., *Catal. Today*, **2011**, *168*, 3.

[71] Le Van Mao, R.; Ramsaran, A.; Xiao, S.; Yao, J.; Semmer, V., *J. Mater. Chem.*, **1995**, *5*, 533.

[72] Groen, J.C.; Peffer, L.A.A; Moulijn, J.A.; Pérez-Ramírez, J., *Colloids Surf. A*, **2004**, *241*, 53.

[73] Cižmek, A.; Subotic, B.; Šmit, I.; Tonejc, A.; Rosario, A.; Crea, F.; Nastro, A., *Microporous Mater.*, **1997**, *8*, 159.

[74] Groen, J.C.; Jansen, J.C.; Moulijn, J.A.; Pérez-Ramírez, J., *J. Phys. Chem. B*, **2004**, *108*, 13062.

[75] Choi, M.; Cho, H.S.; Srivastava, R.; Venkatesan, C.; Choi, D.H.; Ryoo, R., *Nat. Mater.* **2006**, *5*, 718.

[76] Fernandez, C.; Stan, I.; Gilson, J.P.; Thomas, K.; Vicente, A.; Bonilla, A.; Pérez-Ramírez, J., *Chem. Eur. J.*, **2010**, *16*, 6224.

[77] Verboekend, D.; Groen, J.C.; Pérez-Ramírez, J., *Adv. Funct. Mater.*, **2010**, *20*, 1441.

[78] Holm, M.S.; Svelle, S.; Joensen, F.; Beato, P.; Christensen, C.H.; Bordiga, S.; Bjorgen, M., *Appl. Catal. A*, **2009**, *356*, 23.

[79] Pérez-Ramírez, J.; Verboekend, D.; Bonilla, A.; Abelló, S., *Adv. Funct. Mater.*, **2009**, *19*, 3972.

[80] Li, X.; Shantz, D.F., *J. Phys. Chem. C*, **2010**, *114*, 8449.

[81] Verboekend, D. *New Hierarchical Zeolites Catalysts by Post-Synthetic Design*, **2012**, Doctoral Thesis, ETH Zurich, the Netherlands.

[82] Saxena, S.K.; Kumar, M.; Viswanadham, N. *J. Mater Sci*, **2013**, 48, 7949-7959

[83] Verboekend, D.; Vile, G.; Pérez-Ramírez, J., *Adv. Funct. Mater.*, **2012**, *22*, 916-928.

[84] Pansini, M., *Mineralium deposita*, **1996**, *31(6)*, 563-575.

[85] Ahmad, A.; Puasa, S.; Zulkali, M., Desalination, **2006**, 191(1),153-161.

[86] Reynolds, T.; Richards, P., *Unit Operations and Process in Environmental Engineering*, **1996**, PWS Publishing Company.

[87] Richardson, J.M.; Wigg, T.; Spencer, M., *Fundamental and Applied Catalysis: Principle of Catalyst Development.* **1989**, Plenum Press, New York.

[88] Sawyer, C.N.; a.M., P.L., *Chemistry for Environmental Engineering*. McGraw-Hill, New York . **1979**. 23(3rd ed): p. 1161-1165.

[89] Doraiswamy, L.K., *Organic Synthesis Engineering*, Oxford University Press, USA, **2001**.

[90] Zhong, Y., Studies on equilibrium and dynamic characteristics of new adsorption pairs. 2006, University of Warwick.

[91] Centrone, A.; Brambilla, L.; Zerbi, G., *Physical Review B*, **2005**, *71(24)*, 245-406.

[92] Crittenden, J.C.; Trussell, R.R.; Hand., D.W.; Howe, K.J.; Tchobanoglous, G.,*"Water treatment principles and design".* John Wiley and Sons, Inc., 2nd edition, **2005**.

[93] Cooney, D.O., Adsorption design for wastewater treatment, CRC, **1998**.

[94] Saberi, R.; Nilchi, A.; Rasouli-Garmarodi, S.; Zarghami, R., *Journal of Radioanalytical and Nuclear Chemistry*, **2010**, *284(2)*, 461-469.

[95] Belfort, G., *Environmental Science & Technology*, **1981**, *15(5)*, 601-602.

[96] Lucas, S.; Cocero, M.J.; Zetzl, C.; Brunner, G., *Fluid Phase Equilibria*, **2004**, *219(2)*, 171-179.

[97] McKay, G., *Chemical Engineering Journal*, **2001**, *81(1)*, 213-221.

[98] Langmuir, I., *Journal of the American Chemical Society*, **1916**, *38(11)*, 2221-2295.

[99] Sharker, M.; aA., P.K., *Waste Management*, **2006,** *26*, 559-570.

[100] Bhatnagar, A.; Minocha, A.; Sillanpää, M., *Biochemical Engineering Journal*, **2010**, *48(2)*, 181-186.

[101] Hameed, B.; Salman, J.; Ahmad, A. *Journal of Hazardous Materials*, **2009**, *163(1)*, 121-126.

[102] Weber, T.W.; Chakkravorti, P., *AIChEJ*, **1972**, *20*, 228-229.

[103] Freundlich, H., *Phys. Z. Chem. Eng.*, **1907**, *57*, 385-470.

[104] Ho, Y.S.; Chiu, W.T.; Wang C.C., *Bioresource Technology*, **2005**, *96(11)*,1285-1291.

[105] Acharya, J.; Sahu, J.N.; Mohanty, C.R.; Meikap, B.C., *Chemical Engineering Journal*, **2009,** *149(1)*, 249-262.

[106] Idrisa, M.; Ahmada, Z.; Ahmad, M. *International Journal of Basic & Applied Sciences*, **2011**, *11*, 38-43.

[107] Ho, Y.S.; McKay, G., *Can. J. Chem. Eng.*, **1998,** *76*, 822-826.

[108] Kumur, K.V.; Ramamurthi, V.; Sivanesan, S., *J. Colloid Interface Sci.*, **2005**, *284*, 14-21.

[109] Hammed, B.H.; Ahmad, A.L.; Latiff, K.N.A. *Dyes Pigm.*, **2007**, *75*, 143-149.

[110] Allen, S.J.; Gan, Q.; Matthews, R.; Johnson, P.A., *J. Colloid Interface Sci.*, **2005**, *286(1)*, 101-109.

[111] Ho, Y.S. Adsorption of heavy metals from waste streams by peat, PhD Thesis, University of Brimmingham, UK, **1995.**

[112] Hui, K.S.; Chao, C.Y.H.; Kot, S.C., *J. Hazard. Mater.*, **2005**, 127(1-3), 89-101.

[113] Weber, W.J.; Morris, J.M. *J. Sanit. Eng. Div. Am. Soc. Eng.*, **1963**, *89*, 31-39.

[114] A. Corma, *Chem. Rev.* **1995**, 95, 559.

[115] Th. L. M. Maesen, B. Marcus, in: H. van Bekkum, E. M. Flanigen, P.A. Jacobs, J. C. Jansen (Eds), Introduction to Zeolite Science and Practice, second edition, Studies in Surface Science and Catalysis, vol. 137, Elsevier, Amsterdam, **2001**, Chapter 1.

[116] A. Corma, M. J. Diaz-Cabanas, F. Rey, S. Nicolopoulus, K. Boulahyab, *Chem. Commun*. **2004**, 1356.

[117] A. Corma, M. J. Diaz-Cabanas, J. L. Jorda, C. Martinez, M. Moliner, *Nature* **2006**, 443, 842.

[118] M. Hartmann, *Angew. Chem., Int. Ed.* **2004**, 43, 5880.

[119] Y. Tao, H. Kanoh, L. Abrams, K. Kaneko, *Chem. Rev*. **2006**, 106, 896.

[120] B. Vogel, C. Schneider, E. Klemm, *Catal. Lett.* **2002**, 79, 107.

[121] L. Tosheva, V. P. Valtchev, *Chem. Mater*. **2005**, 17, 2494.

[122] S. Wang, T. Dou, Y. Zhang, X. Li, Z. Yan, *Catal. Commun*. **2005**, 6, 97.

[123] J. Cejka, S. Mintova, *Catal. Rev. Sci. Eng*. **2007**, 49, 457.

[124] A. Corma, U. Diaz, M. E. Domine, V. Fornes, *Angew. Chem., Int. Ed.* **2000**, 39, 1499.

[125] W.J. Roth, J. Cejka, *Catal. Sci. Technol*. **2011**, 1, 43.

[126] R. Srivastava, M. Choi, R. Ryoo, *Chem. Commun*. **2006**, 4489.

[127] Z. Yang, Y. Xia, R. Mokaya, *Adv. Mater*. 43, **2004**, 5880

[128] C.J.H. Jacobsen, C. Madsen, J. Houzvicka, I. Schmidt, A. Carlsson, *J. Am. Chem. Soc.* **2000**, 122, 7116.

[129] C.H. Christensen, K. Johannsen, I. Schmidt, C.H. Christensen, *J. Am. Chem. Soc*. **2003**, 125, 13370.

[130] D. Verboekend, J. Perez-Ramirez, *Catal. Sci. Technol*. 2011, 1, 879.

[131] S. Bernasconi, J.A. van Bokhoven, F. Krumeich, G.D. Pirngruber, R. Prins, *Microporous Mesoporous Mater*. **2003,** 66, 21.

[132] R. Giudici, H.W. Kouwenhoven, R. Prins, *Appl. Catal. A* **2000**, 203, 101.

[133] J.C. Groen, L.A.A. Peffer, J.A. Moulijn, J. Pérez-Ramírez, *Microporous Mesoporous Mater.* **2004**, 69, 29.

[134] C.C. Pavel, R. Palkovits, F. Schuth, W. Schmidt, *J. Catal.* **2008**, 254, 84.

[135] J.C. Groen, S. Abello, L.A. Villaescusa, J. Perez-Ramırez, *Microporous Mesoporous Mater.* **2008**, 114, 93.

[136] D. Verboekend, J. Perez-Ramirez , *Chem. Eur. J*. **2011** , 17 , 1137.

[137] Z. Qin, B. Shen, Z. Yu, F. Deng, L. Zhao, S. Zhou, D. Yuan, X. Gao, B. Wang, H. Zhao, H. Liu, *J. Catal*. **2011**, 278, 266.

[138] Z. Qin, B. Shen, X. Gao, F. Lin, B. Wang, C. Xu, J. Catal. 2013, 298, 102.

[139] D. Verboekend, G. Vile, Javier. Perez-Ramirez, *Cryst. Growth Des.* **2012**, 12, 3123.

[140] D. Verboekend, M. Milina, S. Mitchell, J. Perez-Ramirez, Cryst. Growth Des. 2013, 13, 5025.

[141] A. H. Janssen, A. J. Koster, K.P. de Jong, *Angew. Chem.* **2001**,113, 1136; *J. Phys. Chem. B.* 2002, 106, 11905.

[142] B.C. Lippens, J.H. de Boer, *J. Catal*. **1965**, 4, 319.

[143] E.P. Barret, L.J. Joyner, P.H. Halenda, *J. Am. Chem. Soc.* **1951**, 73, 373.

[144] J. Garcia-Martinez, M. Johnson, J. Valla, K. Li, J. Y. Ying, *Catal. Sci. Technol.*, **2012**, 2, 987.

[145] M. Choi, H. S. Cho, R. Srivastava, C. Venkatesan, D. Choi, R. Ryoo, *Nat. Mater*., **2006**, 5, 718.

[146] K. Sadowska, A. Wach, Z. Olejniczak, P. Kustrowski, J. Datka, *Microporous and Mesoporous Mater.,* **2013**, 167, 82.

[147] S. Abello, A. Bonilla, J. Perez-Ramirez, *App. Catal. A.* **2009**, 364, 191.

[148] J. Aguado, D. P. Serrano, in Feedstock Recycling of Plastic Wastes (Ed: J. H. Clark), The Royal Society of Chemistry, Cambridge 1999.

[149] D. W. Park, E. Y. Hwang, J. R. Kim, J. K. Choi, Y. A. Kim, H. C. Woo, *Polym. Degrad. Stab.* **1999**, *65*, 193.

[150] D. P. Serrano, J. Aguado, J. M. Escola, J. M. Rodrı ´guez, J. *Anal. Appl. Pyrolysis* **2005**, 74, 353.

[151] J. Agullo´, N. Kumar, D. Berenguer, D. Kubicka, A. Marcilla, A. Go´mez, T. Salmi, D. Y. Murzin, *Kinet. Catal*. **2007**, *48*, 535.

[152] A. Marcilla, A. Go´mez-Siurana, F. Valde´s, *J. Anal. Appl. Pyrolysis*, **2007**, *79*, 433.

[153] J. Perez-Ramirez, S. Abello, A. Bonilla, J.C. Groen, *Adv. Funct. Mater*. **2009**, 19, 164-172.

[154] Jamshidi, R; Afzali, Z; Afzali, K. *Asian Journal of Chemistry*. **2009**, *21(5)*, 3381-3384.

[155] Jalbani, N; Kazi, T.G.; Jamali, M.K.; Arain, M.B.; Afridi, H.I.; Baloch, A. *J. Food Comp. Anal.,* **2007**, *20*, 226–231.

[156] Arain, M.B.; Kazi, T.G.; Jamali, M.K.; Jalbani, N.; Afridi, H.I.; Baig, J.A. *J. Hazard. Mater.*, **2008**, *154*, 998–1006.

[157] Ansari, R.; Kazi, T.G.; Jamali, M.K.; Arain, M.B.; Sherazi, S.T.; Jalbani, N.; Afridi, H.I. *J. AOAC Int.*, **2008**, *91*, 400–407.

[158] Moradi, S.E.; Baniamerian, M.J. Chemical Industry & chemical Engeneering Quarterly **2011**, *17(4)* 397-408.

[159] Wang, S; Wu, H. *J. Hazard. Mater*. **2006**, *136*, 482–501

[160] Duran, C.; Ozdes, D.; Sahin, D.; Bulut, V. N.; Gundogdu, A.; Soylak, M. *Microchemical Journal*, **2011**, *98(2)*, 317-322 .

[161] Samadi, S; Sereshti, H.; Assadi, Y. *Journal of Chromatography A*, **2012**, *1219*, 61-65.

[162] M. Chamsaz, M; Atarodi, A.; Eftekhari, M.; Asadpour, S.; Adibi, M. *Journal of Advanced Research*, **2013,** *4*, 35-41.

[163] Fritz, J.S. Analytical Solid-Phase Extraction, *John Wiley and Sons Inc*, New York, **1999**, p. 140.

[164] King, J.N.; Fritz, J.S. *Anal. Chem.*, **1985**, *57*, 1016.

[165] Junk, G.A.; Avery, M.J.; Richard, J.J. *Anal. Chem.*, **1988**, *60*, 1347.

[166] Miller, K.G.; Poole, C.F. *J. High Resolution Chrom.*, **1994,** 17, 125.

[167] Sun, J.J.; Fritz, J.S. *J. Chromatogr.*, **1990,** *522*, 95.

[168] Marvin, C.H.; Brindle, I.D.; Hall, C.D.; Chiba, M. *Anal. Chem.*, **1990**, *62*, 1495.

[169] Junk, G.A.; Richard, J.J. *Anal. Chem.*, **1988**, *60*, 451.

[170] Walas, S.; Tobiasz, A.; Gawin, M.; Trzewik, B.; Strojny, M.; Mrowiec, H. *Talanta*, **2008**, *76*, 96-101.

[171] Abollino, O.; Aceto, M.; Sarzanini, C.; Mentasti, E. *Anal. Chim. Acta*, **2000,** *411*, 223–237.

[172] Cesur, H; Bati, B. *Turk. J. Chem.*, **2002**, *26*, 599–606.

[173] Guo, Y.; Din, B.; Liu, Y.; Chang, X.; Meng, S.; Liu, J. *Talanta*, **2004**, *62*, 207-213.

[174] Gustavo Rocha de, C.; Ilton Luiz de, A.; Paulo dos Santos, R. *Mater. Res.,* **2004**, *7*, 329-334.

[175] Gode, F.; Pehlivan, E. *J.Hazard. Mater*., 2006, 136, 330-337.

[176] Saeed, M.M.; Ahmed, R. *J. Radioanal. Nucl. Chem*., **2006**, *267*, 147-153.

[177] Liu, Y.; Liang, P.; Guo, L. *Talanta*, **2007**, *68*, 25–30.

[178] Ngeontae, W.; Aeungmaitrepirom, W.; Tuntulani, T. *Talanta*, **2007**, *71*, 1075–1082.

[179] Fan, J.; Wu, C.; Wei, Y.; Peng, C.; Peng, P. *J. Hazard. Mater*., 2007, 145, 323–330.

[180] de Pena, Y.P.; Rondon, W. *American Journal of Analytical Chemistry,* **2013**, *4*, 387-397.

[181] Qadeer, R.; Hanif, J.; Saleem, M.; Afzal, M. *J. Chem. Soc. Pak.,* **1992,** *14*, 91–96.

[182] Lemos, V.A.; Teixeira, L.S.G.; Bezerra, M.A.; Costa, A.C.S.; Castro, J.T.; Cardoso, L.A.M.; de Jesus, D.S.; Santos, E.S.; Baliza, P.X.; Santos, L.N. *Appl. Spectrosc. Rev*., **2008**, *43*, 303–334.

[183] Daniels, E.A.; Puri, M. *The International Journal of Applied Radiation and Isotopes,* **1985**, *36(2)*, 148-149.

[184] Pokonova, Y.V. *Solid Fuel Chemistry*, **2012**, *46(3)*, 179-184.

[185] Sayed, S.A. *Zeolites*, **1996**, *17*, 261.

[186] Razee, S.; Masujima, T. *Anal. Chim. Acta*, **2002**, *464*, 1.

[187] Corma, A.; Lois, F.P.; Viruela, P.; Ziovich-Wilson, C. *J. Am. Soc*., **1994**, *116*, 134.

[188] Potdar, A.; Shukla, A.; Kumar, A. *J. Membrane Sci.*, **2002,** *210*, 209.

[189] Basheer, C.; Alnedhary, A.A.; Madhava, B.S.; Valliyaveettil, S.; Lee, H.K. *Anal. Chem.*, **2006,** *78*, 2853

[190] Ge, D.; Lee, H.K. *J. Chrmatogr. A* , **2012**, *1251*, 27.

[191] Basheer, C.; Alnedhary, A.A.; Madhava, B.S.; Lee, H.K. *J. Chromatogr. A.* **2009,** *1216*, 211.

[192] Verbeokend, D.; Keller, T.C.; Mitchell, S.; Perez-Ramirez, J. *J. Adv. Funct. Mater*, **2013**, *23*, 1923-1934.

[193] Janssen, A.H.; Koster, A.J; de Jong, K.P. *J. Phys. Chem. B.*, **2002**, *106*, 11905.

[194] Auerbach, S.M.; Carrado, K.A.; Dutta P.K. *Handbook of Zeolite Science and Technology*, CRC Press, **2003**.

[195] Ghaedi, M.; Montazerozohori, M.; Soylak, M. *Journal of Hazardous Materials*, **2007**, *142(1-2)*, 368-373.

[196] Narin, I.; Kars, A.; Soylak, M. *Journal of Hazardous Materials*, **2008**, *150(2)*, 453-458.

[197] Okiemen, F.E.; Maya, A.O.; Oriakhi, C.O. *International Journal of Environmental Analytical Chemistry*, **1987**, *32*, 23-27.

[198] Horsfall, M.J.; Spiff, A.I. *African Journal of Biotechnology*, **2005a**, *4(2)*, 191-196.

[199] K.V. Kumur, K.V.; Ramamurthi, V.; Sivanesan, S. *J. Colloid Interface Sci.*, **2005**, *284*, 14-21.

[200] McKay, G.; Ho, Y.S. *Water Res.*. **1999,** *33*, 585-587.

[201] McKay, G.; Ho, Y.S. *Process Biochem*, **1999**, *34*, 451-460.

[202] Cunha, G; Romao, L.; Santos, M.; Araujo, B.; Navickiene, S.; Padua, V. *Bioresour Technol.*, **2010**, *101*, 3345-3354.

[203] Baker, F.S.; Miller, C.E.; Repik, A.J.; Tolles, E.D. Kirk-othmer Encyclopedia of Chemical Technology. **1992**.

[204] Bhatnagar, A.; Minocha, A.; Sillanpää, M. *Biochemical Engineering Journal*, **2010**, *48(2)*, 181-186.

[205] Acharya, J.; Sahu, J.N.; Mohanty, C.R; Meikap, B.C. *Chemical Engineering Journal*, **2009**, *149(1)*, 249-262.

[206] Mohan, D; Sing, K.P. *Water Res.* **2002**, *36*, 2304-2318.

Vitae

Name :Kazeem Oludare Sulaiman

Nationality :Nigerian

Date of Birth :5/11/1983

Email :kosulaiman@yahoo.com

Address :Lagos, Nigeria

Academic Background :

2015: King Fahd University of Petroleum and Minerals (KFUPM), Dhahran, KSA.

M.Sc. Chemistry; CGPA= 3.75/4.

2008: Obafemi Awolowo University (OAU), Ile-Ife, Nigeria.

B.Sc. Chemistry; CGPA= 4.01/5.

Personal/Technical Skills

- Ability to work comfortably in the laboratory with passion and determination of achieving the desired results using modern analytical and spectroscopic instruments such as XRD, BET surface analyzer, NMR, FTIR, SEM, ICP-OES, 2D-GC-MS, etc.
- Capability to learn very fast and familiarity with the knowledge of quality assurance and regulatory policies and standards, and standard laboratory safety practices.
- Proficient working knowledge of drawing and data processing software like CHEMDRAW, SPSS, STATA and ORIGIN.
- Strong problem solving, numerical and analytical skill as a clear thinker, who can work under pressure with little or no supervision, and possesses team spirit.

Professional Affliations

- Chemical Society of Nigeria (CSN);
- Materials Research Society (MRS);
- American Chemical Society (ACS);
- Saudi Arabian International Chemical Sciences Chapter of American Chemical Society (SAICSC-ACS).

Conference Papers/ Thesis Works

A1 N. Al-Yassir, **K. Sulaiman**, K. Alhooshani, A. Aitani, A. Sayari. Design of hierarchical dealuminated FAU-type zeolites having trimodal porosity structure by treatment in mono- and binary tetraalkylammonium hydroxides. Poster presentation at Fourth International Conference on Multifunctional, Hybrid and Nanomaterials tagged Hybrid Materials 2015, 9-13 March, 2015, Sitges (near Barcelona), Spain.

A2 **K. Sulaiman**, K. Alhooshani, N. Al-Yassir. The chemistry of intracrystalline mesoporosity in superdealuminated ultrastable Y zeolites upon quaternary ammonium hydroxides mediated alkaline treatment. Poster presentation at 2014 Materials Research Society (MRS) Fall Meetings and Exhibit held at Sheraton Boston Hotel and Hynes Convention Center, Boston, Massachusetts, USA. November, 30 - December 5, 2014.

A3 **K. Sulaiman**, K. Alhooshani, N. Al-Yassir. Synthesis of hierarchical ultrastable Y zeolite by alkaline treatment using novel mesopore directing agents for upgrading heavy petroleum fraction. Poster presentation at 3rd International Conference and Exhibition on Laboratory Technology (LabTech 2014) held at Gulf International Convention Center, Gulf Hotel, Manama, Kingdom of Bahrain, October 28-30, 2014.

A4 **K. Sulaiman**, K. Alhooshani, N. Al-Yassir. The role of intracrystalline mesoporosity on the hydrogenation of polynuclear aromatics in diesel fuels on noble metal/mesoporous HY zeolite catalysts. Oral presentation at 23rd Canadian Symposium on Catalysis (CSC) held at Westin Hotel, Edmonton, Alberta, Canada, May 11-14, 2014.

B1 **K. Sulaiman**. Synthesis, characterization, and evaluation of hierarchical dealuminated FAU-type Y zeolites in catalytic and heavy metal ion adsorption studies. M.Sc. Thesis at KFUPM, May, 2015.

B2 **K. Sulaiman.** Theoretical approach to computation of molar heat capacities of simple organic heterocyclic compounds in gaseous phase. B. Sc. Thesis at Obafemi Awolowo University, Ile-Ife, Nigeria. December, 2008.

Honor & Award

- ✓ KFUPM Graduate (M. Sc.) Full Scholarship Awardee
- ✓ Second Best Poster Award Recipient at 3rd International Conference and Exhibition on Laboratory Technology (LabTech 2014) held at Gulf International Convention Center, Gulf Hotel, Manama, Kingdom of Bahrain, October 28-30, 2014.